Using reactive transport modeling to link hydrologic flux and root zone geochemistry at Second Creek, a sulfate enriched wild rice stream in northeastern Minnesota

A Thesis
SUBMITTED TO THE FACULTY OF
UNIVERSITY OF MINNESOTA
BY

Amanda R. Yourd

IN PARTIAL FULFILLMENT OF THE REQUIREMENTS
FOR THE DEGREE OF
MASTER OF SCIENCE

Gene-Hua Crystal Ng

February 2017

Acknowledgements

I would like to acknowledge the Minnesota Pollution Control Agency, Clean Water, Land, and Legacy Amendment, U.S. Geological Survey, and the University of Minnesota Department of Earth Sciences for providing financial support for this project. Invaluable conversations and edits were provided by Gene-Hua Crystal Ng, Amy Myrbo, Edward Swain, and William Seyfried. Field, modeling and lab support was provided by Scott Alexander, Hoai-Nam Bui, Ryan Conway, Chip Gehring, Amy Myrbo, Patrick O'Hara, Wes Rutelonis, Andy Wickert, Bill Seyfried, Peter Scheuermann, LacCore, UMN Stable Isotope Lab, St. Croix Watershed Research Station, and the Minnesota Geological Survey. I would also like to thank my friends and family for their support over the past two years.

Dedication

This thesis is dedicated to Gene-Hua Crystal Ng in honor of her support and patience throughout this project.

Abstract

Wild rice (*Zizania palustris*) is an economically, culturally, and ecologically important aquatic plant species in Minnesota. In northeastern Minnesota, iron ore and taconite mining have led to elevated surface water sulfate concentrations, which has raised concern about the potential of sulfate negatively impacting wild rice populations. Recent studies have shown that elevated sulfide concentrations in the wild rice root zone (sediment porewater) is more closely correlated with lower occurrence of wild rice than surface water sulfate. This toxic porewater sulfide can be attenuated by precipitation of iron sulfide minerals if dissolved ferrous iron is locally available. Although these geochemical reactions occur in the sediment porewater, or hyporheic zone, where groundwater and surface water mix, the effect of groundwater flux and geochemistry on geochemical processes within the hyporheic zone has not been examined in the context of wild rice and sulfate. Here, we use physical and geochemical field data collected from surface water, porewater, and groundwater to inform a reactive transport model of Second Creek, a mining impacted wild rice stream in northeastern Minnesota. The model is implemented for different hydrologic flux regimes in different locations at Second Creek to examine the geochemical response of the sediment porewater to changes in both physical and geochemical conditions. We show that porewater sulfide concentrations can are dependent on hydrologic flux direction and magnitude, as well as on concentrations of surface water sulfate, sediment organic carbon, and porewater iron. This work emphasizes the importance of constraining groundwater flux and geochemistry when examining processes at the groundwater-surface water interface.

Table of Contents

List of Tables

List of Figures

Introduction

Surface water chemistry has been a primary focus of state and federal water regulation bodies in the United States since the passage of the Clean Water Act of 1972. The standards set by federal or state agencies regarding surface water quality has prompted research on surface water hydrology, geochemistry, and ecology. However, this focus on surface water has also perpetuated the idea that surface water quality issues can be treated as separate from groundwater quality, even though these two water regions frequently mix at the sediment-water interface, also known as the sediment porewater or hyporheic zone.

The mixing of groundwater and surface water in the hyporheic zone makes it a hot spot of biological activity and oxidation-reduction reactions (Winter et al. 1998). Hyporheic zones can have particular influence on aquatic plants, as they are commonly rooted within this geochemically complex area (Hayashi & Rosenberry 2002; Kurtz et al. 2007). However, hyporheic process are difficult to measure, especially in stream settings, due to the numerous factors affecting hyporheic exchange, including stream meanders, pool-riffle sequences, flow velocity, and hydraulic conductivity of stream sediments (D'Angelo et al. 1993; Harvey & Bencala 1993; Morrice et al. 1997; Wroblicky et al. 1998). There have been numerous efforts to examine physical hyporheic exchange in streams using both field tracer experiments (Bencala & Walter 1983; Morrice et al. 1997; Stream Solute Workshop 1990) and groundwater modeling techniques (Harvey & Wagner 2000; Storey et al. 2003; Lautz & Siegel 2006). However,

there have been fewer efforts to model physical and geochemical hyporheic processes together (Runkel and Kimball 2002; Bardini et al. 2012; Zarnetske et al. 2012), especially in high sulfate freshwater systems.

In Minnesota, the concern that high concentrations of mining derived surface water sulfate (SO_4) levels may negatively impact wild rice growth has prompted in-depth examinations of the geochemical interactions within freshwater aquatic ecosystems (Pastor et al. 2017; Myrbo et al., in review, a; Myrbo et al., in review, b). These studies have primarily focused on surface water and hyporheic zone (porewater) geochemistry, but have not quantitatively examined the influence of hydrologic flux condition or groundwater geochemistry on porewater geochemistry. To address this gap in understanding, we conducted an intensive, 6-month field survey at Second Creek, a high SO_4 concentration, mining impacted wild rice stream in northeastern Minnesota. To examine the link between hydrologic flux conditions and geochemistry in the hyporheic zone, we use physical hydrologic and geochemical data from three different zones (groundwater, porewater, surface water) to inform a reactive transport model implementation of Second Creek. This model can be used to assess the simultaneous physical and geochemical processes, involving both local and regional scale conditions, that influence wild rice stream beds. It can also provide insights on the long term impact of a hydrologic regime on wild rice root zone geochemistry.

2. Background and Previous Work

a. Wild Rice Ecology and Cultural Significance

Ecology

Northern wild rice (*Zizania palustris*) is an annual aquatic grass that grows in lakes and slow flowing rivers underlain with glacial sediment. The genus, *Zizania*, describes four species of wild rice native to North America and China (*aquatica, palustris, texana, latifolia*). In Minnesota, both *aquatica* and *palustris* are found, but *palustris* is most common through much of the state, especially in northern regions (Myrbo et al., *in review* b). In the 1950s, a domestic cultivar of wild rice, colloquially known as paddy rice, was developed for large-scale agricultural use in rice paddies in Minnesota and California. For the purposes of this study, the term "wild rice" is in reference to naturally occurring northern wild rice, rather than the domestic variety.

The life cycle of wild rice is highly dependent on water depth and turbidity, with ideal depth between 0.3 and 0.6 m (Aiken et al. 1988; Myrbo et al., in review, b). During the autumn months, mature wild rice seeds fall from the plant, and sink to the sediment water interface, where they remain dormant through the winter. In the spring, the seeds germinate and grow into seedlings. Once the seedlings grow tall enough to reach the surface in June or early July, the plant enters the floating leaf stage, where leaves float on the surface of the water in long, thin strands. During this stage, the plant is particularly susceptible to water level changes (Aiken 1986; Vennum 1988). Due to the plant's shallow root system (10 cm maximum depth), even relatively minor water level increases

can uproot the plants if the changes occur quickly enough. Once the plant is large enough to grow above the water surface, it enters the "emergent" stage. To minimize self-pollination, the female flowers emerge first at the tip of the stem, where they are wind-pollinated before the male flower emerges. By late August and early September, wild rice seeds are mature enough to harvest for human consumption (Kjerland 2015).

Abundance

In the U.S. wild rice currently grows in the northern Midwest, from North Dakota to Michigan. Jenks (1900) defined the 'wild rice district' as the glaciated regions of the Midwest where bedrock is covered by thick layers of glacial sediment that provide a muddy aquatic substrate to support the shallow root systems of wild rice. Historical evidence has pointed to a much greater prevalence of wild rice than is observed today, with thick stands growing throughout the eastern United States (Jenks 1900). It has been estimated that there has been a 32% decline in watersheds with wild rice in Minnesota and Wisconsin since 1900, and today, the only remaining thick and extensive stands are found in isolated areas of the northern Minnesota, Wisconsin, and Ontario, Canada (Drewes & Silbernagel 2012).

Historical and Cultural Significance

Wild rice has been an important cultural, economic, and food resource for several Native American tribes for more than one thousand years (Jenks, 1900). In more recent history, wild rice has been important to the Ojibwe, Dakota, and Ho-Chunk people of the Upper Midwest and Canada. Wild rice plays a central role in the Ojibwe migration story from the eastern United States to the shores of Lake Superior in the early 17th century,

where the people migrated to a land where "food grows on the water." Since the Ojibwe arrived in the Midwest, wild rice, or *manoomin* (Ojibwe word for wild rice, with a literal translation to "good berry") has been considered a sacred gift from the creator and continues to play a central role Ojibwe life and identity (LaDuke 2003; LaDuke 2005).

Prior to European colonization, wild rice was one of the primary food sources for the Ojibwe and Dakota people of Minnesota. Elders, or older members of the community respected for their knowledge and wisdom, would examine the rice in the late summer and determine when it was ready to harvest. Harvesting tools included a canoe, push pole, and wooden knockers. One person would push the canoe into a wild rice stand, while another person would knock the seeds off the plant into the bottom of the canoe for collection. On shore, the rice was then dried, parched, and winnowed at a wild rice camp. Oral tradition reports show that wild rice camps would last for several weeks until the harvesting season was over, and were a celebratory time for groups to come together and prepare for winter (Jenks, 1900). Traditional harvesting continues in this manner today, although European colonization of the upper Midwest resulted in a decrease of wild rice abundance, which had a profoundly negative impact on Native American tribes in Minnesota.

European Colonization and Wild Rice

In the mid 19th century, European colonization spurred the growth of the agriculture and logging industries, resulted in wetland drainage to establish crops and buildings, and dam installation to transport timber and power saw mills. Due to the

sensitivity of wild rice to water level changes, these major alterations to hydrology had a significant negative impact on wild rice (Jenks 1900; Meeker 1996; Rogosin 1954).

This industrialization also coincided with U.S. government treaties with Native American tribes, which resulted in the restriction of local Ojibwe tribes to small, remote areas of the state (Walker & Doerfler 2007). The U.S.-Dakota War of 1862 resulted in the forced removal of most of the Dakota people from Minnesota (with the exception of the Mdewakanton Sioux) to modern day North and South Dakota. This war ended with the public hanging of 38 Dakota people, the largest mass execution in U.S. history. The combination of the decline of wild rice population, war with the U.S. government, and the formation of the Indian Reservation system in Minnesota was catastrophic for indigenous people (Anderson & Woolworth 1988).

Treaty Rights and Wild Rice Harvest

When the Ojibwe ceded their land through treaties with the U.S. government in the 1850s and 60s, they retained the right to hunt, fish, and gather on these lands (Gilbert et al. 1854). In certain treaty areas, these rights have been tested and upheld in federal court (Walker 2007). In recent years, the Minnesota state government has opted for settlement before these cases reach the federal level. In 2016, Minnesota Governor Mark Dayton proposed a bill that would allow all tribal members carrying a tribal identification card to harvest wild rice on any state water body at any time of the year (Associated Press 2016).

Current Uses

Today, wild rice is harvested by both Native and non-Native residents of the upper Midwest, although Native harvesters still outnumber non-native harvesters in Minnesota and Wisconsin (Drewes & Silbernagel 2012). Harvester surveys in Minnesota have shown that the number of harvesters is decreasing and the average age of harvesters in increasing, which has raised concern about the preservation of traditional harvesting in future generations (Drewes & Silbernagel 2012). Methods of rice harvesting by Native and non-Native people closely resembles tradition Ojibwe harvesting techniques. Traditionally harvested wild rice is an important part of the economy in northern Minnesota; it has a different taste and visual appearance than paddy rice, and thus sells for higher prices. Wild rice has become a symbol of Minnesota wild foods as the Minnesota state grain, and has become an important cultural symbol of Minnesota as a whole. However, gathering and consumption of wild rice is still the most prevalent in Ojibwe communities. Approximately 50% of Ojibwe members on reservations in Minnesota engage in wild food harvest and consumption (DeGonzague et al. 1999).

2b. Wild Rice and Sulfate

Early Research

Historically, surface water with high SO_4 concentrations have been linked with lower wild rice populations (Moyle 1944). SO_4 is a water soluble, oxidized form of sulfur that is usually derived from the local geologic substrates. In the late 19th century, iron mining began in northeastern Minnesota and proved to be such a lucrative business for the area that the region became known as the Iron Range. In the majority of historic and current mines on the Iron Range, iron ore or taconite is extracted and the crushed sulfide bearing

waster rock is left in tailings piles or basins. When the fresh surfaces of the iron sulfide minerals react with oxygen and water, the reduced iron and sulfide are oxidized into Fe^{3+} and SO_4^{2-}. The Fe^{3+} is quickly immobilized via precipitation of Fe^{3+} oxides and oxyhydroxides, but the aqueous SO_4^{2-} is more readily dissolved in the surface water (Equation 1).

$$FeS_2 + 3.5O_2 + H_2O = Fe^{2+} + 2\ SO_4^{2-} + 2H^+ \qquad \text{(Equation 1)}$$

Most mine tailings basins are not completely isolated from the surrounding hydrologic systems, so sulfate enriched tailings water is transported to natural surface water bodies through surface runoff, surface seeps, or regional groundwater flow. This has resulted in elevated sulfate concentrations of many of the surface water bodies in the Iron Range (Myrbo et al., in review, b).

In response to the concern that these high sulfate levels were negatively impacting wild rice populations, Dr. John Moyle, a research scientist for the Department of Conservation, the precursor to the Department of Natural Resources, conducted a field survey of wild rice lakes in the late 1930s and early 40s. Moyle observed that "No large stands of rice occur in water having sulfate above 10 ppm [mg/L]." This information was reported to the state, but was largely ignored in a regulatory sense.

In 1972, the passage of the Clean Water Act and the formation of the Environmental Protection Agency (EPA) prompted many states to adopt their own surface water standards. In 1973, Minnesota adopted Moyle's 10 mg/L (0.1 mM) SO_4 recommendation for wild rice waters. This recommendation was reexamined in 2010 when the NorthMet PolyMet copper nickel mine was proposed in the central region of the

Iron Range. While reviewing the environmental impact statement for this proposed mine, the EPA took note of the 10 mg/L SO_4 standard and required the state of Minnesota to adhere to the 1973 recommendation. As the SO_4 standard garnered more public attention from wild rice harvesters, Native American tribes, and mining companies, the scientific efficacy of the standard was brought into question. In particular, Moyle's recommendation was questioned because his study did not investigate the specific mechanism by which SO_4 negatively impacted wile rice. Additionally, since Moyle's study, SO_4 toxicity studies have shown that plants are more sensitive to the reduced form of SO_4, sulfide, rather than sulfate in the surface water (Koch et al. 1990; Berthelin et al. 1991; Lamers et al. 2002).

Recent Studies

The controversy surrounding the 10 mg/L SO_4 standard prompted the Minnesota Pollution Control Agency (MPCA) to undertake an intensive field study (Myrbo et al. in review, b; Pollman et al. in review), mesocosm (outdoor tank) experiment (Pastor et al. 2017; Myrbo et al. in review, a), and laboratory hydroponic experiment (Pastor et al. 2017) to analyze the scientific relationship between surface water SO_4 and wild rice growth. The two-year field study was conducted on 93 lakes, 32 stream sites, and 7 rice paddies throughout Minnesota, and more than 75 chemical and physical parameters were characterized at each site. Spearman correlation analysis of results showed that wild rice cover was not negatively correlated with surface water sulfate, but rather with sulfide in the sediment porewater (Myrbo et al, in review, b). This porewater sulfide had a weak, non-linear correlation with surface water SO_4 and a strong negative correlation with

porewater Fe. High porewater sulfide concentrations were only observed where porewater Fe was low. This is due to the tendency of sulfide to immediately react with ferrous iron in the porewater to precipitate iron sulfide (FeS) minerals via the following reaction:

$$Fe(II) + HS^- \leftrightarrow FeS + H^+ \qquad \text{(Equation 2)}$$

Structural equation modeling (SEM), a regression based statistical approach, of the field data also showed that porewater sulfide and Fe production are both dependent on concentrations of electron donors in the sediment, present as various forms of organic carbon, while dissolved Fe is also dependent on a source of sediment iron (Pollman et al., in review). The SEM showed equal contribution of sediment organic carbon, sediment Fe, and surface water sulfate to porewater sulfide production.

Mesocosm and hydroponic experiments corroborated the findings of Myrbo et al. (in review, b), but further indicated that wild rice seedling emergence, seedling survival, biomass growth, seed production, and seed mass were all negatively impacted by porewater sulfide (Pastor et al. 2017). Hydroponic experiments showed significant reductions in seedling growth at sulfide concentrations or about 320 µg/L (9.68 µM).

Based on the findings in the field, mesocosm, and hydroponic studies, the MPCA concluded that concentrations less than 120 µg/L sulfide (3.63 µM HS^-) in 10-cm integrated porewater samples would protect wild rice (MPCA 2016). Several environmental factors can impact sulfide accumulation in porewater, but the most important factors are sediment total organic carbon (TOC) and iron concentrations. TOC in the sediment stimulates sulfate and iron reduction, while sulfide and reduced iron for

iron sulfide minerals. Since porewater iron is produced through the biological reduction of iron minerals in the sediment to water soluble iron, the amount of iron is controlled by the total amount of sediment iron. Because of these relationships and the variability between wild rice waters throughout the state, the MPCA concluded that no single surface water sulfate standard was sufficient to protect wild rice. Instead, they proposed a site specific standard based on TOC and sediment concentrations (MPCA 2016) (Equation 3). This equation was derived using the field data and the structural equation model in Pollman et al. (in review).

$$SO_4 = 1.21 \times 10^{-5} \times TOC^{-1.197} \times \text{Sediment Iron}^{1.923} \qquad \text{(Equation 3)}$$

3. Problem and Approach

Statement of the Problem

The MPCA study and analysis quantified major relationships between sulfate, iron, organic carbon, and sulfide in sulfate impacted wild rice waters. However, there are some significant considerations that are not quantitatively accounted for in the MPCA model, including groundwater flux and geochemistry. Because the geochemistry in the MPCA model occurs in the hyporheic zone, where groundwater and surface water mix, groundwater flux and geochemistry could have a profound impact on root zone geochemistry. In particular, if a water body was primarily fed by groundwater (here termed a "gaining system"), porewater geochemistry could be dominated by groundwater. If groundwater has a different sulfate concentration than surface water, but only surface water is measured as part of the analysis, the predicted level of sulfide in the

porewater could be incorrect. Streams in Minnesota are commonly groundwater fed, so groundwater could be even more influential in wild rice streams than in lakes.

The complex geochemistry and physical hydrology of stream hyporheic zones make this area particularly difficult to directly study. Organic carbon concentrations are commonly high in wild rice waters, producing anoxic conditions that make it necessary to conduct geochemical sampling in an oxygen free environment in the field to preserve the redox state of the analytes. Physical parameters, such as hydraulic head and head gradient are also difficult to measure in the hyporheic zone. Hydraulic head gradients are often so small that they are within the error of existing measurement tools. Tools such as seepage meters, temperature probes, and piezometers can provide quantitative flux information, but are especially prone to error in stream settings (Rosenberry & Labaugh 2008). Additionally, stream hyporheic zones can be extremely heterogeneous over varying spatial and temporal scales, so continuous and extensive monitoring is needed.

Because the hyporheic zone is dynamic and difficult to observe directly, it is useful to construct numerical models to examine geochemical and hydrologic flux conditions. Chemistry and hydraulic conditions are easier to measure in groundwater and surface water than in the hyporheic zone. Because the hyporheic zone is a mix of groundwater and surface water, groundwater and surface water can be used as boundary conditions to numerically simulate processes in the hyporheic zone. In particular, reactive transport models (RTMs) have been shown to be useful when studying hyporheic zones (Runkel and Kimball 2002; Lautz and Siegel 2006). A reactive transport model uses physical aquifer properties for solute transport with the groundwater flow equation, and pairs this

physical information with geochemical processes, allowing for the analysis of geochemical and physical conditions over different spatial and temporal scales. RTMs have been developed to examine chemical transport in a variety of contexts, and can be used to:

1. Constrain variables that are especially dynamic or difficult to field measure.
2. Test for interactions between variables.
3. Develop long term projections about changes in geochemistry over time.
4. Quickly and relatively easily test the long term impacts of different scenarios.
5. Broadly translate problems to similar environmental settings.

Because the proposed sulfate and wild rice standard is site-specific, it will require manual measurement of geochemical parameters in every wild rice water body (MPCA 2015). The new standard does not require the measurement of physical parameters, such as hydraulic head gradients. A RTM could be used to examine the relative importance of physical hydrologic properties in wild rice settings.

Approach

We address the lack of physical hydrology measurements in the MPCA sulfate and wild rice study by using physical and geochemical data collected during an intensive field campaign to inform a reactive transport model of Second Creek, a mining impacted wild rice stream in northeastern Minnesota with high sulfate concentrations (3.15-8.72 mM (Myrbo 2013)). We use physical and geochemical field data collected from three different zones (groundwater, porewater, surface water) to inform and constrain a reactive transport model with four main questions about Second Creek in mind:

1. How do regional and local groundwater flux and chemistry affect wild rice root zone geochemistry?
2. How do hydrologic and geochemical fluxes change during the course of a summer?
3. Does hydrologic flux direction impact porewater geochemistry?
4. How can physical hydrologic parameters be incorporated with the geochemical understanding put forth by the MPCA studies to inform water policy?

4. Study Area and Field Methods

Study Area

This research was conducted at Second Creek, a small stream catchment with wild rice in the St. Louis River watershed in northeastern Minnesota (Figure 1). Just downstream of the area of focus, the creek discharges into the Partridge River, an important wild rice stream and tributary to the St. Louis River, which flows into Lake Superior. Second Creek is underlain by Quaternary glacial outwash and till sourced from the Superior lobe, and flows through a low-relief glacial outwash channel. The main channel of the stream is relatively narrow (2-3 m) and shallow (1-2 m), and is flanked by 20-30 meters of wetlands (Figure 2). During the summer months, wild rice and submergent macrophytes grow in the main channel of the stream, and the densely vegetated wetlands contain grasses, sedges, and shrubs. Surface water sources to Second Creek include mine tailings basin discharge from the north and northeast, which causes elevated sulfate levels in the main channel (>8 mM). Sediment porewater iron levels are also unusually high (~40 mg/L), while porewater sulfide levels are low (~0.1 μM HS^-)

compared to >30 μM HS^- in other sites surveyed in Myrbo et al. (in review, b). Prior to this study, little was known about regional groundwater flow or chemistry in the area.

Field Methods

We collected physical and geochemical data from Second Creek from May through October, 2015. The goal of the physical hydrology measurements was to constrain regional groundwater flow and local groundwater-surface water interaction in the wetland and main channel. In early June, six water table groundwater wells with depths of approximately 4-7 meters were drilled and equipped with pressure transducers with 10-minute recording intervals (Figure 3). Four piezometers were hand installed in the wetlands adjacent to Second Creek, with three in the west wetland and one in the east wetland (Figure 3). Pressure transducers were also installed in the piezometers and a stream gauge in the main channel in order to track local differences in head between surface water and shallow groundwater. Three vertical temperature probes were used in conjunction with mini piezometer data to infer streambed flux in the main channel and wetlands. The temperature probes were constructed using 1-inch diameter PVC tubing with a series of 6-8 thermistors affixed with epoxy. The probes were inserted into the stream or wetland sediment such that the top thermistor was approximately at the sediment-water interface, and the bottom thermistor was located at approximately 30-40 cm depth below the sediment-water interface, with most sensors clustered within the top 10 cm, which corresponds to the wild rice root zone. Temperature readings were logged at 1 minute to 15 minute intervals to capture diurnal variability over each 24-48 deployment, which occurred five times over the summer. Seepage meters were also

installed three times over the summer, each time for 24-48 hours in the main channel and/or west wetland to directly measure flux direction (Figure 3).

Geochemical samples methods follow those established by Myrbo et al. (in review, b) and Johnson (2013). Approximately monthly sampling was carried out using methods by Myrbo et al. (in review, b). Monthly aqueous geochemical data was collected from groundwater, surface water, and sediment porewater. Monthly samples for sediment geochemistry were collected from various locations throughout the main channel and wetlands. Groundwater and surface water data types included major cations and anions, alkalinity, pH, specific conductivity, and dissolved oxygen. Porewater data included cations, anions, alkalinity, sulfide, pH, and oxidation reduction potential. Groundwater wells were sampled after three well volumes were pumped out of the well. Porewater samples were collected from the main channel and the wetland using an HTH sediment gravity corer (Pylonex, Sweden) and 7 cm diameter polycarbonate tubing. On shore, plastic wrap was placed on the top of the core to avoid oxygen intrusion; 10-cm Rhizon™ filters (pore size 0.12-0.18 μm) (Rhizosphere.com, Netherlands; Shotbolt 2010) were then inserted vertically into the top of the sediment core and attached to an evacuated serum bottle to collect the porewater sample. Since the Rhizon filters were 10 cm, all porewater core data represents integrated concentrations over 10 cm intervals. Sediment samples were similarly collected from the stream channel and wetland using the gravity corer. In late August, passive porewater equilibrators ("peepers") were also used to sample porewater. Peepers allow for diffusion of porewater into wells spaced at 1.56 cm intervals, producing high vertical resolution geochemical profiles in the redox-

sensitive porewater zone (Teasdale et al. 1995). Peepers were installed 2-3 week prior to collection to allow for adequate equilibration with surrounding porewater (U.S. EPA 2001), and they were sampled for pH, cations, anions, sulfide, and methane under a nitrogen atmosphere.

Cation samples (Al, Ba, Ca, Fe, K, Li, Mg, Mn, Na, P, Si, Sr) were acidified with one drop of trace metal grade 6 N HCl, and measured using a Thermo Scientific iCAP 6500 dual view ICP-OES (inductively coupled plasma - optical emission spectrometer) at the University of Minnesota, Twin Cities. Anion samples (fluoride, acetate, formate, chloride, nitrate, bromide, sulfate) were kept cool and out of sunlight in opaque bottles and measured using Thermo Dionex ICS 5000+ ion chromatography system at the University of Minnesota, Twin Cities. In addition to the standard anion analysis, samples were also collected for porewater sulfide; these were kept anoxic, preserved with 0.2 mL of 2.0 N ZnAc and 0.5 mL of 15 M NaOH, and analyzed colorimetrically using a Lachat Autoanalyzer following in-line acid distillation and NaOH trapping at the St. Croix Watershed Research Station. Surface water and groundwater alkalinity samples were collected in bottles with no headspace and were analyzed within 48 hours using colorimetric acid titration. Porewater alkalinity samples were analyzed using the same method, but were preserved under a nitrogen atmosphere. Other parameters, such as pH, dissolved oxygen (DO), oxidation-reduction potential (ORP), and conductivity were measured directly in the field using a Thermo Scientific Orion STAR A329.

Sediment samples collected from the main channel and wetland were analyzed for total carbon (TC) and acid volatile sulfide (AVS). AVS samples were collected under a

nitrogen atmosphere, preserved with 2.0 N ZnAc, and frozen immediately upon collection. The samples were then analyzed using a weak acid extraction (0.5 N HCl) and measured with a volt meter at the University of Minnesota, Duluth. Sediment from the wetlands and main channel was collected from cores three times during the summer from multiple depths and locations (approximate locations shown in Figure 3) for TC analysis. Before analysis, samples were freeze dried and a portion was removed and tested for reactivity with 6 N HCl. Of the 17 samples tested, two samples (both from the main channel) reacted with the acid, indicating the presence of carbonates. The samples were then analyzed on the Costech 4010 Elemental Analyzer (EA) at the University of Minnesota Stable Isotope Lab. Because 15 of the 17 samples did not react with HCl, TC is used as a proxy for total organic carbon.

5. Field Data Results and Discussion

Physical Hydrology

The physical hydrology at Second Creek from May through October of 2015 was defined by a period of flooding from mid-July through late September. In mid-July, heavy rains washed out beaver dams on the creek upstream of our study area, carrying debris towards to the outlet and blocking the deteriorating culverts (Figure 2) directly downstream of the study area. This led to flooding and the uprooting of wild rice growing in the stream. The stream returned to lower water level when a backhoe was used to clear the material blocking the culvert. The midsummer flood effectively divided the season into three hydrologically distinct periods: (1), non-flood water levels from

May to mid-July, (2) flooded water levels from mid-July until late September, and (3) return to non-flood water levels from late September until mid-October (Figure 4, 5).

Although the unexpectedly high flood water washed out wild rice and significantly impaired geochemical and physical data collection from the main channel, it provided a unique situation in which to examine porewater geochemical response to changes in surface water hydrology. In particular, the high flood waters could be used to examine the response of streambed porewater geochemistry to a large and sudden influx of mine water due to an active pumping event or breach in an upstream pit lake. Additionally, the flooding of the wetlands created hydrologic conditions analogous to a lake, where organic rich sediment is overlain by still or slowly moving water. This made it possible to evaluate geochemical processes under the lake-like conditions, compared to both low and high surface water stream conditions.

Aquifer Sediment

Aquifer sediment was collected during well installation for texture analysis. Figure 6 shows fractions of sand, silt, clay, and gravel for the aquifers on the west and east side of Second Creek. The west aquifer sediment is primarily composed of coarse sand and silt with smaller fractions of clay and gravel. This relatively high of degree sediment heterogeneity is characteristic of a medial glacial outwash margin, where both glacial till and outwash sediment are observed (Anderson 1989). The east well sediment is dominated by very coarse sand and gravel, with trace levels of silt and clay. The well-sorted eastern aquifer sediment is likely indicative of a more distal glacial outwash margin, or an outwash channel within the margin.

Groundwater Wells

Pressure transducers installed in the stream gauge and five water table groundwater wells show highest groundwater head in the most westerly groundwater wells, moderate surface water head in the main channel, and lowest head in the east groundwater well (Figure 5). This trend indicates that, on a regional scale, Second Creek is primarily a flow-through stream, with general groundwater flow from west to east towards the Partridge River. The highly permeable sediment observed in the east aquifer also likely facilitates flow from Second Creek surface water through aquifer sediment into the Partridge River. During the period of rapid stream water level rise in late July and early August, which coincided with rainfall events, surface water head levels occasionally rose above groundwater head levels in the east well (E1) and two of the west wells (A2, B1) located nearest to the stream bank: this created a temporary, local-scale reversals of hydrologic gradient on the west side.

Wetland Piezometers

Hand-installed piezometers in the shallow wetland groundwater adjacent to the stream show smaller spatial scale head differences between the surface water and shallow groundwater in the wetland (Figure 7). Local head fluctuations recorded by tools such as hand-installed piezometers provide hydrologic information that is more closely related to the wild rice root zone in the top 10 cm of the streambed than groundwater wells in the upslope locations. However, head differences between surface water and shallow groundwater recorded by mini piezometers adjacent to the stream channel (PZI, PZO, PZE) are very small, making head gradients during most periods throughout the summer

difficult to establish. Also, wetland piezometers are informative about vertical flux in the wetland during the flooded period when there is standing surface water in the wetland, but during the non-flooded period, wetland piezometers only convey information about lateral flux between the stream channel and wetland.

As indicated in Figure 7, there are periods during the summer when head differences between shallow groundwater and surface water are negligible, and times when they are distinct enough to infer a hydrologic gradient. During non-flood surface water conditions in early summer (late June through mid-July), heads recorded by hand-installed piezometers in the west wetland are similar to, or slightly less than, surface water head. During the initial stages of rapid stream water level rise in mid-July to early August, when surface water head is higher than piezometer head for the majority of the time, surface water head is notably higher than head in the wetland piezometers, confidently indicating that overall flow is from surface water to shallow wetland groundwater (downward flux; losing stream situation). From mid-August until late September, surface water flooded the wetland piezometers, causing head level measurements in the piezometers to perfectly match the surface water level. After the culverts were cleared, surface water head declined rapidly, briefly falling below the head recorded by one wetland piezometer (PZO). From this we can infer that lateral flow was from the wetland groundwater to surface water during the late summer (upward flux). Although we did not directly measure flux at the stream bed, we can use the higher wetland piezometer head levels to estimate a gaining stream situation during this time.

Temperature Probes and Seepage Meters

Since piezometers alone are not sufficient to determine small hydraulic gradients at Second Creek, temperature probes and seepage meters were used to further quantify flux direction and magnitude in the streambed and wetlands. Temperature probes were deployed at multiple locations throughout the west wetland and main channel six different times during the summer for a period of 24-48 hours per deployment. Due to installation complications imposed by high water in the main channel during the flood event, most temperature probe data is from the west wetland. Flux values were obtained through the calibration of a heat transport model, VS2DH (Healy & Ronan 1996), to the observed flux profile time series, making use of the shift and attenuation of diurnal temperature variability in surface water (Stonestrom & Constantz 2003).

Temperature probe results and qualitative and quantitative model uncertainty are shown in Table 1. During the early summer, non-flooded period, different temperature probes indicated upward and downward flux in the main channel. During the flooded period, data from the west wetland indicates upward flux in August, and both upward and downward flux in September. In October, during the non-flood flow, two of the three temperature probes indicate upward flux in the main channel. Since Second Creek sediment is heterogeneous, and temperature probes only capture data from small spatial and temporal windows, some discrepancy is expected. The result of upward flux in the west wetland at two sampling periods during the flooded period is contrary to the hypothesis of overall downward hydrologic flux during high water events. The two temperature probe deployment dates in August coincide with local drops in stream level, which could have temporarily reversed the hydraulic gradient in the wetland (Figures 5,

7). Additionally, qualitative confidence from the optimization analysis showed that flux direction from this period is the least well-constrained, so the upward groundwater flux could be the result of uncertainty in the calibration. In combination with the results from the rest of the summer, these unexpected results highlight the transient nature of hyporheic processes as well as the sensitivity of temperature probes to spatial heterogeneity and small scale changes in hydraulic gradient.

Seepage meters allow for the direct quantification of flux magnitude and direction and were deployed at several locations in the west wetland and main channel at three different times during the summer. Seepage meters indicated upward flux during the non-flood period in June, and downward flux during the flooded period in August and September (Table 1). Calculated seepage meter flux quantities vary by an order of magnitude, even between seepage meters in similar locations, and are several orders of magnitude different than temperature probe flux estimates. This is likely due to the multiple sources of error associated with seepage meter data collection, including improper seal, faulty hose/bag attachment, and accumulation of trapped gas (Rosenberry & Labaugh 2008). The latter error source seems particularly likely at Second Creek, as there was visible accumulation of gas in the seepage meter chambers. Additionally, the large degree of spatial heterogeneity at Second Creek (Figure 8) affects the interpretation of the measurements. Due to these factors, the specific flux measurements recorded by the seepage meters are likely to be less reliable than temperature probe flux magnitude estimates. However, seepage meter errors are less likely to affect the measured flux direction, and the consistency of flux direction during the sampling periods suggests that

seepage meters, if not robust enough to provide reliable flux magnitudes, can be used as a qualitative indicator of flux direction.

Hydrologic Regime Delineation from Physical Data

While groundwater wells clearly indicate that Second Creek is a flow through stream with regional flow is from west to east, local flux conditions in the streambed are more difficult to elucidate. For evaluating processes affecting the wild rice root zone, local flux changes in the streambed are of primary concern. Because no physical measurement method alone adequately constrained this flux over the entire summer, we use data from groundwater wells, wetland piezometers, temperature probes, and seepage meters, in combination with physical observation of surface water level changes, to qualitatively divide the summer into three periods of distinct local hydrologic flux regimes.

In the early summer, we infer from seepage meters and temperature probes that flux magnitude in the main channel is very low and direction is either inconclusive or slightly upward. During the flooded period in mid-summer, when the surface water level is elevated above nearby groundwater levels, flux is likely downward in the main channel. The wetland piezometer data supports this the most clearly, and seepage meter data shows downward flux in the main channel and west wetland during this period. After the flood recedes, there is a clear indication of upward flux in the main channel recorded by two of the three temperature probes, and flow from shallow wetland groundwater to surface water is indicated by wetland piezometer data. Dividing the summer into these three periods oversimplifies the complexity of hyporheic processes in

natural stream settings, but it clearly delineates distinct hydrologic regimes for which to examine groundwater influence on porewater geochemistry on SO_4 impacted wild rice waters.

Geochemistry

Sediment

Sediment carbon content is higher in the wetlands than in the main channel (Figure 9). Solid phase concentrations were converted to moles per liter water using a porosity of 0.39 and bulk density of 1864 g/L for both wetland and channel samples, which are within the typical ranges for glacial material (Manger 1963; Kresic 2007). No significant differences were observed with changes in sample depth or sample month, and concentrations are similar in the east and west wetlands. Since inorganic carbon was not removed prior to measurement on the EA, carbon content measurements likely include some amount of inorganic carbon (Schumacher 2002); the extracted organic component also likely includes less labile organic forms (Smith et al. 2013). Thus, actual concentrations of readily degradable organic carbon are likely lower than these data, which also means that smaller magnitude variations within these concentrations may be difficult to detect.

Sediment samples collected from wetland and channel sediment during May-July and September trips were also analyzed for acid volatile sulfide (AVS) content, and results are shown in Figure 10. There is significant spread within the main channel samples, and no notable difference between shallow (~0-10 cm) and deep (~15-25 cm) channel samples. Wetland AVS data are not numerous enough to indicate any notable

trends, but the single measurement from the east wetland is higher than the west wetland and main channel samples. There are also no notable trends in the main channel samples throughout the summer. This suggests that the portion of sulfide mineralization that occurs over one season is either (1) not detectable with the AVS extraction method used, or (2) not significant enough to change the overall AVS pool on a monthly scale.

Aqueous Data

Aqueous geochemical data was collected from the surface water, porewater, and groundwater six times throughout the summer (Figure 5). Additionally, peepers were deployed to obtain geochemical profiles representing time-averaged conditions from 8/13/2015 through 9/1/2015. Results for pH, alkalinity, and selected cations and anions for surface water, groundwater, and porewater are shown in Figure 11. Data from the four west groundwater wells are well clustered, so an arithmetic mean for the data from each sampling event is. Replicate porewater samples display higher variability than surface water and groundwater, so all porewater data are shown individually instead of as averages.

i. Surface Water

Second Creek surface water chemistry serves as the upper boundary condition affecting streambed geochemical conditions. The most notable trend in surface water is the high SO_4 concentrations resulting from discharge from upstream mining pit-lakes (Figure 11). The highest SO_4 concentration of 10.34 mM is observed in August and the lowest concentration of 2.76 mM is observed in May. The temporal fluctuations in SO_4 are likely due to proximity of sampling date to rainfall event or spring snow melt, when

the low SO_4 precipitation dilutes the concentrated SO_4 in surface water (Figure 5). Concentration of the conservative tracer, Cl, in surface water is higher than west groundwater, and concentrations increase slightly over time.

ii. Groundwater

Since physical data indicate that Second Creek is a regionally flow-through stream from west to east, we consider west groundwater chemistry to be a lower boundary condition for streambed geochemistry. In the west wells, groundwater cations and anions, pH, and alkalinity are lower than surface water and porewater values. SO_4 concentrations are ~0.3 mM in the west groundwater, which is significantly lower than surface water SO_4, although still slightly above the initial surface water sulfate SO_4 recommendation of 0.1 mM by the MPCA. Cl is also significantly lower in west groundwater than in surface water.

In contrast, groundwater cations and anions from the east well are significantly higher than west wells and more closely match surface water concentrations. In particular, east groundwater and surface water SO_4 concentrations are nearly identical during June, August, and July sampling events. Since west groundwater SO_4 is low, and surface water is high, we infer that the elevated SO_4 concentration in the east groundwater must be sourced from surface water, confirming that Second Creek is a flow through stream. Cl in east groundwater exceeds surface water concentrations during the early summer. The water table is at least 0.6 m closer to the ground surface on the east side, so groundwater is more easily accessible to plant roots, which has the effect of concentrating conservative anions on the east side.

iii. Porewater (streambed core)

In general, porewater cation and anion concentrations either fall between surface water and west groundwater data, or are above surface water concentrations. Cation and anion concentrations tend to be higher in the wetland porewater than in the main channel porewater, especially for dissolved Fe and Cl. The higher C concentrations could be due to the effect of evapotranspiration by aquatic plants in the wetland and main channel. The wetlands, especially the east wetland, are more vegetated than the main channel, so conservative anions are expected to be higher. Non-conservative porewater sulfide concentrations are similar between the wetland and main channel, although sulfide is higher in the shallow (0-10 cm) channel samples than in the deeper (10-20 cm) samples (Figure 11).

Comparison of west and east porewater iron data observations illustrates some possible trends in iron-sulfide dynamics. Because Second Creek is a flow-through stream from west to east, the west wetland does receive as much high SO_4 surface water input as the east wetland. As a result, west wetland sulfide production and FeS precipitation are likely less prominent than in the east. Less removal of porewater dissolved Fe with FeS precipitation could explain the observed higher concentrations of porewater Fe in the west wetland relative to the east, where Fe concentrations are lower and the single east wetland AVS level is higher. The difference in the wetland porewater dissolved Fe and AVS data indicate that in the east wetland, Fe reduction is less significant and/or FeS precipitation is more significant than in the west wetland. This highlights the importance of coupled iron sulfide interaction in controlling streambed geochemistry, and it

demonstrates that even in systems naturally enriched in iron relative to sulfide, iron may become depleted as a results of iron sulfide precipitation.

iv. Porewater (peeper)

Peeper geochemical profiles show that porewater concentrations of sulfide, Fe, and CH_4 are higher in the wetland than in the main channel, and wetland Fe and CH_4 also increase with depth (Figure 12). This increase indicates that during the flood period in late August, the wetland, especially at depth, is a more reducing environment than the main channel. Three of the four sulfide profiles show discrete peaks in sulfide, all at slightly different depths. This is notable for two reasons: (1) the zone of sulfide accumulation is on a scale of 2-4 cm; a resolution that the 10-cm resolution porewater core sulfide results cannot capture, and (2) this zone can vary in depth within 50 cm laterally, which highlights the heterogeneity at Second Creek.

Porewater SO_4 recorded by peepers is higher in the channel than in the wetland. This could reflect higher downward flux in the main channel, which would allow high SO_4 surface water to penetrate further into the porewater under losing stream conditions, and/or lower sediment organic carbon content in the main channel, leading to less SO_4 reduction than in the highly reducing wetland. There is a slight increase in SO_4 at ~30 cm in the deeper main channel peeper that coincides with a decline in main channel iron. This could indicate a zone of less reducing sediment at depth (e.g. a gravel lens with low organic content) or an interface with water of a different chemistry (e.g. groundwater). Again, the differences in SO4 profiles for the two channel peepers highlights the heterogeneity of channel sediment.

Taken together, the field data reveal several interesting trends over time (Figure 11). First, main channel porewater SO_4 peaks during the flooded period in September. Similarly, porewater Cl concentrations in the main channel increase from approximately west groundwater levels in the early summer, to near surface water levels in September and October. The anion peaks during September align with the hypothesis of downward hydrologic flux during this period, with advection of high SO_4 and Cl surface water into porewater. These results indicate a possible connection between hydrologic flux and porewater geochemistry.

6. Model Methods

a. Background

Field-based, experimental, and modeling studies involving microbial SO_4 and Fe reduction kinetics and thermodynamics have revealed complex and overlapping processes involving redox zonation, microbial respiration rates, organic carbon degradation, and other environmental constraints (McGuire et al. 2002; Curtis 2003; Jin & Bethke 2005; Pallud & Van Cappellen 2006; Tarpgaard et al. 2011; Laverman et al. 2012). Reduction of terminal electron acceptors (TEAs) in groundwater and sediment porewater is often described and modeled using a Monod or dual-Monod approach, which represents preferential reduction of TEAs from high reduction potential to low reduction potential (Van Cappellen & Gaillard 1996; Hunter et al. 1998; Schäfer et al. 1998; Gwo et al. 2001; Mayer et al. 2001). In many natural environments, common TEAs, such as O_2, NO_3, Mn(VI), Fe(III), SO_4 and CO_2, are expected to be consumed in that order (Claypool & Kaplan 1974; Champ et al. 1979; Froelich et al. 1979; Stumm &

Morgan 1996). In Monod kinetics, a TEA with a higher reduction potential inhibits the reduction of a TEA with a lower energy yield. The approach assumes that these reactions are irreversible and cannot occur simultaneously.

However, this redox zonation does not always occur in the order of reduction potential, and there have been many cases of observed overlapping zones and reverse gradients of TEA reduction (Jakobsen & Postma 1996; Ludvigsen et al. 1998; McGuire et al. 2002; Laverman et al. 2012; Hansel et al. 2015). Furthermore, the irreversible nature of the reactions in Monod kinetics can cause thermodynamically infeasible reactions to occur, which can cause large, unrealistic fluctuations in pH (Curtis 2003). In addition to problems associated with using Monod kinetics in models, there are several other factors that influence TEA reduction that make quantification with a model difficult.

In the case of SO_4 reduction, the numerous efforts to quantify factors that affect SO_4 reduction rate (SRR) have shown that environment type, microbial strain, TEA competition, and trophic status have varying degrees of influence on SRR (see references in Table 2). A review of literature SRR show a variation from 0.5-2233 nmol SO_4 cm^{-3} d^{-1} (Table 2). This broad range of rates reflects the experimental biases associated with SRR field and laboratory studies (outlined by Pallud and Van Cappellen 2006) as well as the difficulty in quantifying the complex interactions between organic carbon, SO_4, and microbes in natural environments. For example, Pallud et al. (2007) found that SO_4 availability affects rates below concentrations of 1 mM SO4, while Tarpgaard and Jorgensen (2011) found high reduction rates at SO_4 concentrations of 1-100 μM. Holmer and Storkhorn (2001) found that freshwater trophic status also influences SRR, with

eutrophic lakes commonly have higher rates than oligotrophic lakes due to higher SO_4 and organic matter concentrations. Different strains of SRB also prefer different forms of organic carbon (Detmers et al. 2001), so the thermodynamic properties and biological availability of different forms of organic carbon can also affect SO_4 reduction rate (Larowe & Van Cappellen 2011). Other microbe-specific factors that affects rates include cell physiology (Bradley et al. 2016), SO_4 uptake capacity (Pallud & Van Cappellen 2006; Tarpgaard et al. 2011), sediment C:N ratios, and sulfide concentrations (Okabe et al. 1992). Additionally, competition between other TEAs, such as NO_3, can inhibit SRR of some microbial strains, but this inhibition is highly microbe and environment specific, and is not well constrained (Laverman et al. 2012).

Fe reduction is similarly difficult to model due to the challenges in quantifying diverse microbial processes. Unlike SO_4, oxidized forms of Fe are either sediment bound or chelated to organic compounds. Additionally, Fe redox processes frequently occur in microaerobic environments preferred by microbes, where rapid, meter-decimeter scale Fe-redox cycling can occur both biologically and abiotically (Groffman & Crossey 1999; Sobolev & Roden 2002; Roden 2012). The temporally and spatially transient nature of these processes can produce a large suite of concomitant minerals and complexes, including Fe(III) oxides, (oxy)hydroxides, Fe(II)/Fe(III) compounds, and chelated Fe(III) compounds, all of which are sensitive to changes in pH, alkalinity, acidity, and exposure time to the surrounding aqueous solution (Rickard & Luther 2007). Abiotic reduction rates can be estimated for these minerals and complexes based on thermodynamic and mineral properties, such as crystal structure and total surface area (Hering & Stumm

1990). However, sorption and/or precipitation of Fe(II) onto the surface of Fe(III)-reducing bacterial cells or Fe(II)/Fe(III) minerals and compounds used as TEAs by microbes has been found to be a major limitation to biological Fe(III) reduction rates (Roden 2006). This suggests that modeling Fe(III) reduction should include parameters related to cell density and surface area of Fe(III) minerals that is available to reduction (i.e. free of sorbed/precipitated Fe(II)), rather than total mineral surface area and crystal structure (Roden 2006). NO_3 has also been shown to drive anaerobic Fe-redox cycling (Weber et al. 2006), which would add further complication to Fe-redox models.

In wild rice waters, where SO_4 and Fe geochemistry in wild rice root zone is the focus, redox processes are also affected by the organic-rich and microaerobic region around the roots of aquatic plants, known as the rhizosphere. Aquatic plants exude both oxygen and organic substrates from their roots into the surrounding sediment, creating a microenvironment ideal for microbial life (Armstrong 1964; Grayston, Vaughan, and Jones 1997; Bais et al. 2004; Bruijn 2013). The microaerobic environment of the rhizosphere creates a redox boundary that is chemically similar to what is found at the sediment water interface. In densely vegetated aquatic areas, the surface area of plant roots can be greater than the horizontal surface area of the sediment-water interface, which suggests that the rhizosphere could actually have greater influence on total biogeochemical processes in wetlands than the cycling that occurs at the sediment-water interface (Neori et al. 2000; Weiss et al. 2004). The microaerobic environment of the rhizosphere allows for the biotic oxidation of certain metals, while the nearby anaerobic zone allows for the binding and immbolization of these metals (Hammer 1988;

Kosolapov et al. 2004). In some cases, the presence of dense vegetation has been found to inhibit SO_4 reduction (Holmer et al. 1998), decrease pH and Fe(II), but increase redox potential in the surrounding sediment (Yang et al. 2012). Seasonal fluctuation in plant community distribution, nutrient levels, and oxygen content in the rhizosphere can cause weekly to monthly scale changes in the locations and areas of redox boundaries (Jacob and Otte 2003; Figure 13).

b. Model Formulation

We use the reactive transport mode, PHT3D (Prommer et al. 2003), to examine geochemical response to hydrologic fluxes over the summer of 2015 at Second Creek. PHT3D couples the numerically robust transport algorithms from MT3DMS (Zheng & Wang 1999) with the geochemical model PHREEQC-2 (Parkhurst & Appelo 1999). The transport component uses groundwater flow fields produced with MODFLOW (Harbaugh 2005). The standard PHT3D/PHREEQC-2 geochemical database is used for equilibrium constants for aqueous species reactions.

In PHT3D, we implement the partial equilibrium approach of Jakobsen and Potsma (1999), where redox reactions are controlled by the availability of electron donors, which are generically represented here as labile organic carbon with the stoichiometry of CH_2O. This leads to the following coupled reaction involving SO_4 reduction, Fe reduction, and methanogenesis:

$$2(CH_2O) + SO_4^{2-} \rightarrow 2(HCO_3^-) + H_2S \quad \text{(Equation 4)}$$

$$4Fe(OH)_3 + CH_2O + 7H^+ \rightarrow 4Fe^{2+} + HCO_3^- + 10H_2O \quad \text{(Equation 5)}$$

$$2CH_2O \rightarrow CH_4 + CO_2 \quad \text{(Equation 6)}$$

Following this approach, the oxidation half of the redox reaction (organic carbon degradation) is kinetic, while the reduction half of the reaction is assumed to be at or near equilibrium. In other words, organic carbon oxidation is assumed to be the limiting factor, while SO_4 and Fe reduction are assumed to occur quickly.

To implement the partial equilibrium approach in the model, we use the first-order rate equation for organic carbon, with decay parameter k':

$$d[OC]/dt = -k'[OC] \qquad \text{(Equation 7)}$$

where SO_4 and Fe reduction rates are dependent upon the initial concentration of organic carbon [OC] and the magnitude of the decay parameter, k'. Ideally, this rate equation proposed by Berner (1964) would use a known initial concentration of organic carbon and kinetic rate *constant*, k. However, this rate 'constant' has been shown to vary by orders of magnitude, as described in the above literature review, there are significant complexities associated with accurately quantifying kinetic rate parameters and labile organic carbon concentrations. Additionally, there are other factors, such as lability of organic carbon and organic carbon concentration that affect the decay of organic carbon (Henrichs & Doyle 1986; Emerson & Hedges 1988; Dale et al. 2008). Organic carbon concentration and other kinetic constrains are unknown at Second Creek. We therefore use the existing physical and geochemical surface water, porewater, and groundwater data at Second Creek to calibrate organic carbon concentration and decay parameter, k'. We use k' instead of the rate constant, k, to account for the uncertainties associated with organic carbon oxidation and SO_4 and Fe reduction in natural environments outlined above. Other kinetic rate equations that incorporate some of these complexities have

been proposed, (Li et al. 2010; Curtis 2003; Jin & Bethke 2002; Jin & Bethke 2005), but they require information, such as microbe-specific knowledge, organic carbon stoichiometry, and/or mineral properties, that is not available at Second Creek. Although these factors remain unquantified at Second Creek, the calibration of decay parameter, k', to existing field data, can incorporate these uncertainties without adding complexity to the model. Furthermore, the high concentrations of surface water SO_4 (3.15 – 8.72 mM) indicate that organic carbon availability is likely the most significant limiting factor in SO_4 reduction (Holmer & Storkholm 2001).

Domain and Flow Model

To model vertical profiles in the hyporheic zone, we established 1D domains discretized in 1.5 cm thick layers. The top of the domain is the sediment water interface. Although our study focuses on geochemical changes in the dynamic top 0.5 m of the streambed sediments (our estimation of the average hyporheic zone depth), the model domain bottom was further extended to 3 m depth for a deep lower boundary condition representing groundwater conditions. To simplify the model based on our approximately monthly sampling intervals, we divide the summer into 30-day periods of steady-state flux conditions for both the wetland and stream channel. During these periods, we impose constant groundwater upwelling or downwelling. Flux values are first based on physical hydrology field data from the temperature probes, seepage meters, and piezometers, and are then further calibrated until PHT3D simulation match observed porewater geochemistry.

Geochemical Model

The geochemical domain in PHREEQC-2 is divided into three zones, (1) surface water, (2) sediment porewater in the streambed/wetland, and (3) groundwater, based on observed variations between these three zones in the field data. Surface water and groundwater chemistry are used as constant concentration upper and lower boundary conditions, respectively. Aqueous components in the model include inorganic C (alkalinity), CH_4, dissolved O_2, Al, Ba, Ca, Cl, Fe(II), HS, K, Mg, Mn (II), Na, O, P, Si, SO_4, pH, pe, and organic carbon. Fe^{2+} is used to represent the entire pool of modeled dissolved Fe, when in reality, Fe^{3+} can also be functionally dissolved in water when chelated to organic compounds (Rickard & Luther 2007). The model also includes cation exchange for H^+, Fe^{2+}, Mn^{2+}, Ca^{2+}, and Mg^{2+}. A cation exchange capacity (CEC) of 0.02 mol/L produced results matching observed major cation concentrations and falls within the general range for sediments (Stumm & Morgan 1996). Based on the model by Ng et al. (2015), for a glacial outwash aquifer in northern Minnesota, we used an equilibrium constant, logK, of -4.03 to model exchange for all divalent cations. Initial solution chemistry for each zone is based on observed monthly water chemistry data and further charge balanced and equilibrated using PHREEQC-2.

Solid phase processes include $Fe(OH)_3$, which reduces to provide an Fe source for FeS precipitation, which is a sink for sulfide and Fe^{2+}. Elevated concentrations of dissolved Fe^{2+} at Second Creek indicate a plentiful Fe supply, so we initialize the entire model domain with an arbitrarily high concentration of $Fe(OH)_3$. Since AVS has been observed at Second Creek (Myrbo et al., in review, b), FeS precipitation is allowed in the

model, but each simulation time period is initialized without FeS to help track accumulated FeS precipitates over a given simulation. Both FeS and $Fe(OH)_3$ are represented as equilibrium phase minerals in the model, but similar to the organic carbon decay parameter, k', we use adjusted thermodynamic equilibrium parameters (shown here as logK*) that are calibrated to geochemical porewater data to incorporate complex processes related to SO_4 and Fe dynamics. For example, specific sediment mineralogy is unknown at Second Creek, and it is likely that there are a variety of Fe(III) oxides, (oxy)hydroxides, and mixed Fe(III)/Fe(II) compounds at Second Creek (Rickard & Luther 2007), for which $Fe(OH)_3$ with a calibrated equilibrium parameter provide an approximation. FeS forms ranging from less stable precipitates to more crystalline (ex. mackinawite) cover a range of logK constants (-2.9 to -4.648 (Berner 1967; Helgeson 1978; Morse et al. 1987; Davison 1991; Chen & Liu 2005)). A logK value corresponding to more soluble phases would likely be most appropriate for our simulations over a short 30-day time period. The reactions for $Fe(OH)_3$ ("Fe(OH)3(a)" in the PHT3D database) and FeS ("FeS(ppt)" in the PHT3D database) are shown with database values (logK) and calibrated values (logK*) in Table 3. Our calibrated logK* of 3.15 for FeS corresponds well with the suggested revision of logK = -3.00 in the PHREEQC database based on field data by Chen and Liu (2005).

Model Scenarios

Based on the observed and quantifiable differences between channel and wetland sediment and the three periods of distinct hydrologic flux inferred from field data, we test three different scenarios using the model. Simulation A models upward flux in the main

channel from June-July, Simulation B models downward flux in the main channel from July-September, and Simulation C models downward flux in the west wetland from July-August. Length of simulation time was dependent on field data availability, because geochemical porewater field data were used for both geochemical model initialization and calibration targets at simulation end, while surface water and groundwater geochemistry were used for upper and lower boundary conditions. The calibrated mineral thermodynamic parameters (logK*) were the same for all simulations, while the initial organic carbon concentration and decay parameter (k') were increased in Simulation C, based on observable differences in carbon content between the wetland and main channel (Figure 9). Each simulation has different hydrologic flux values; flux direction was inferred using physical data and flux magnitude was calibrated using porewater geochemistry data as calibration targets.

7. Model Simulation Results and Discussion

Simulations A and B are both from the main channel under downward (A) and upward (B) hydrologic flux regimes. Simulation C shows results for the west wetland during a downward flux scenario, which is used as an analogue for a lake setting (described further below). Based on availability of field data, simulations A and C are run for 30-day periods, and simulation B is run for a 60-day period.

Simulation A: Main channel June-July

Model results for select geochemical species from the non-flood water level period of June-July show changes in porewater geochemistry in only the top ~5 cm of the sediment profiles (Figure 14). Vertical water flux within the main channel streambed

was difficult to constrain using physical measurements alone, but the combination of field observations and physical data (piezometer, temperature probe, seepage meter) suggest a slight upward flux during this period (Figure 7, Table 1). The upward flux used was calibrated to porewater geochemical observations, as was the organic carbon concentration and kinetic rate parameter (Table 4). Although simulated porewater results match the July calibration targets relatively well, it should be noted that the constant surface water head boundary at the top likely influences the results. For example, surface water SO_4 concentration increases from June to July, but the initial June concentration is used for the entire, 30-day simulation period. This contributes to the lower modeled sulfide concentrations compared to field sulfide concentrations.

The simulation profiles in Figure 14 show that in this upward flux scenario, high SO_4 surface water does not penetrate to depths greater than ~5 cm below the sediment water interface. Conservative tracer Cl reaches a greater depth (~7.5 cm) than SO4, indicating that organic carbon degradation coupled to SO_4 reduction within the top 5 cm of the domain prevents deeper penetration of SO_4. However, as mentioned previously, porewater SO_4 concentration may be higher if the lower June SO_4 concentration was not used as a constant upper boundary condition. Simulated porewater sulfide results from the reduction of SO_4 that infiltrates into the sediment, but concentrations are below the protective concentration identified (MPCA 2016). The July model results show that a slight peak in sulfide production is associated with the highest concentration of SO_4 in the sediment, at ~2 cm, while a slight decrease in dissolved Fe is associated with this peak. The modeled sulfide peak is lower in concentrations than the July sulfide shallow

porewater field data. This could again be due to the relatively lower June SO_4 input that was used as constant boundary for the entire simulation. Similarly, simulated porewater alkalinity in July is lower than field values, again possibly due to the constant application of lower June surface water concentrations at the upper boundary condition. Alternatively, since organic carbon degradation increases alkalinity, lower simulated alkalinity indicates less reduction in the model than in the field.

Neither observations nor simulations show an increase in dissolved Fe over time. Instead, there is an overall decrease in simulated dissolved Fe throughout the top 10 cm. Although a high concentration of $Fe(OH)_3$ was put into the model as a source for reduced Fe, trace amounts of surface water oxygen diffuse into the top ~2 cm of the simulation profile, oxidizing some of the initialized reduced Fe to precipitate additional $Fe(OH)_3$ (shown as difference between simulated result concentration and simulated initial concentration in the simulation profiles). There is also a slight peak in FeS precipitation in the top 4 cm, indicating that both FeS and $Fe(OH)_3$ precipitate at shallow depths an in approximately equal concentrations in this simulation. This slight peak in simulated FeS precipitation also coincides with a small peak in simulated sulfide, suggesting that even with little sulfide produced during periods of upward flux, FeS precipitation plays a role in limiting dissolved sulfide concentrations. Deeper than ~4 cm $Fe(OH)_3$ begins to reduce, generating reduced Fe to precipitate FeS at depth. The sulfide used for FeS at depth in the model likely results from the reduction of initial SO_4 in the model, rather than sulfide produced from diffusing surface water SO_4 during the simulation period, so

the peak in FeS in the top 10 cm represents the amount of precipitation with freshly reduced sulfide.

Other major aqueous components include pH, Ca, and Mg, all of which are affected by cation exchange. The favorable match between simulated and observed pH lends confidence in the overall geochemical model implementation, because pH reflects the combined influence of various redox, acid/base, mineral phase, and cation exchange reaction. Cation exchange results show a dominance of Mg sorption over sorption of other cations. Surface water Mg concentrations are high at Second Creek due to the weathering of Mg-rich tailings associated with sulfide tailings deposits (Berndt & Bavin 2009). The high Mg surface water enters the shallow (top ~2 cm) porewater, where simulations indicate that it sorbs to sediment in the stream channel, and causes calcium and other cations (including H^+) to desorb. Simulated cations and pH at 30 days correspond well with target data, and demonstrate the importance of sorption in controlling water chemistry.

Simulation B: Main Channel, July-September (flood)

Sixty-day simulation representing the main channel for the flooded period of July through September are shown much greater solute penetration into sediment porewater than in Simulation A (Figure 15). Although flooded conditions during mid-summer made flux measurements in the stream channel difficult, downward flux in the main channel seemed likely due to the much elevated surface stream head. Calibration to water chemistry data corroborated this, with the best model fits to data incorporating the

calibrated downward flux and organic carbon values (Table 4). Note that initial calibrated organic carbon and kinetic rate parameter are the same as in Simulation A.

Downward advection into sediment porewater causes high SO_4 surface water to penetrate farther into porewater than during the gaining stream situation of the early summer (Figure 15). At simulation end in September, porewater SO_4 concentrations are elevated above initial concentrations within the top ~40 cm of the sediment. The September simulated SO_4 profile matches well with the deep September field SO_4 data. The constant top boundary condition of initial surface water chemistry has an especially strong effect on the profiles during a losing stream situation where surface water has a greater impact on porewater chemistry. Downward advection is also observed in the simulation results for conservative tracer Cl. Cl was used for charge balance adjustment so surface water levels using the model are one order of magnitude higher than levels observed in the field. In spite of this discrepancy, the simulated Cl profiles bears striking similarity to the SO_4 profile in attenuation depth. This indicates that although SO_4 reduction is occurring in the model, reduction rate is not fast enough to appreciably slow the solute front moving down into the sediment at this flux rate. In contrast, in Simulation A, there is a more discernable lag between SO_4 and Cl fronts, indicating that SO4 reduction is more significant here.

The greatest simulated dissolved sulfide accumulation occurs just below the surface at 2 to 10 cm depth, where SO_4 concentrations are highest. Although sulfide concentrations are still below the state's recommended porewater sulfide limit for wild rice (3.75 μM), concentrations in this downward flux scenario are much greater than in

Simulation A. Field data for sulfide was not available in September to provide a calibration target for sulfide. Field porewater sulfide data are available in July, but concentrations are initialized at a lower concentration to avoid unrealistically high sulfide concentrations near the bottom of the profile. At simulation end after 60 days (September), sulfide levels increase to concentrations similar to observations in the top 0-10 cm (indicated with the circle at the mean depth of 5 cm) during the initial (July) time, which is also similar to the other 0-10 cm measurements in the late summer (Figure 11). Relatively stable sulfide concentrations may be controlled by FeS precipitation in the active region of SO_4 reduction. Dissolved Fe concentrations in the top ~8 cm decrease from higher initial condition levels to near zero levels in September. This coincides with a peak in FeS precipitate in simulations, indicating that the Fe at that depth is removed via mineral precipitation.

In this simulation, dissolved Fe levels are sufficient to prevent sulfide concentrations from exceeding the proposed sulfide concentration of 3.75 μM to protect wild rice through FeS precipitation. However, it should be noted that under this downward flux (losing stream) scenario, the model shows significant decrease in dissolved Fe in the top 5 cm over the 60-day simulation period. As in Simulation A, there is a large reservoir of $Fe(OH)_3$ in the sediment to provide reduced Fe, and again, $Fe(OH)_3$ concentration first increases near the surface due to precipitation with initial porewater concentrations of dissolved Fe that are oxidized by trace amounts of surface water oxygen. Below ~10 cm when the trace surface water oxygen levels are reduced, the large reservoir of $Fe(OH)_3$ begins to reduce and supply dissolved Fe. The decrease in

dissolved Fe indicates that some dissolved Fe is being both oxidized and precipitating as $Fe(OH)_3$ while some is precipitating as FeS. The simulation profiles for both mineral phases show that FeS and $Fe(OH)_3$ are precipitating in approximately equal concentrations. Although the flooded conditions at Second Creek were temporary during the summer of 2015, results suggest that if flooding were to persist beyond 60 days, and downward flux was maintained, the $Fe(OH)_3$ reservoir of available Fe for FeS precipitation could become depleted in the wild rice root zone. This depletion could slow FeS precipitation, potentially allowing dissolved sulfide concentrations to exceed the state's recommended limit in the top 10 cm.

As in Simulation A, Mg sorption dominates over sorption of other cations in the sediment. Because flux is downward, surface water high in Mg penetrates further into the porewater, so sorbed Mg reaches to greater depths in this simulation. Additionally, there is a notable increase in simulated Ca at ~20 cm to levels above surface water Ca due to Ca desorbing as Mg sorption increases. There is a similar increase in dissolved Fe between 20 and 30 cm in the model that could result from desorption and/or Fe reduction. The decrease in pH at this depth can also be attributed to the desorbing of H^+ with increased Mg sorption. The close match between modeled and measured pH values again lend confidence to the geochemical model in this simulation.

Simulation C: West Wetland July – August (flood)

Field data and 30-day model simulation results are shown in Figure 16 for the west wetland during the flooded period of July through August. Consistent with more compact sediment with higher organic content in the wetland compared to the main

channel (Figure 8, 9), the calibrated hydrologic flux is an order of magnitude lower, organic carbon concentration is an order of magnitude higher, and the first order kinetic rate parameter is higher in the wetland compared to the main channel (Table 4). The rate parameter, k', includes many different kinetic factors that are not explicitly accounted for in the model, so an increase in this parameter approximates the changes in microbial communities and organic carbon accessibility in the wetland compared to the main channel.

At the end of the 30-day simulation, modeled porewater SO_4 and Fe match well with field data, while the modeled sulfide and alkalinity profiles are less than the field measured value. Dissolved CH_4 peeper data, shown along with simulated CH_4 in Figure 16, represents average conditions over August 13 through September 1, 2015 during which the peepers were deployed. Because the reduction half of redox reactions is thermodynamically controlled in the model, energetically low methanogenesis cannot occur until after SO_4 and Fe reduction. Therefore, simulated CH_4 does not begin to increase until ~18 cm, below the depth where other redox reactions have already occurred. The peeper data shows a more gradual increase in CH_4, which could be indicative of the complexities of overlapping redox zones in natural environments, or CH_4 produced at depth in the sediment column moving upward via molecular diffusion to shallower depths (Dale et al., 2008).

Although effective wetland hydrologic flux is downward as it is in Simulation B, the flux is lower magnitude, and SO_4 does not penetrate as far into the sediment column in the wetland. At simulation end, modeled SO_4 concentrations are depleted above a

depth of 15 cm, compared with ~25 cm by 30 days in Simulation B. This is due at least in part to lower wetland hydrologic flux; increased SO_4 reduction in Simulation C is another possible cause. There is a slight peak in simulated dissolved sulfide in the top ~5 cm, but concentrations are overall much lower than in Simulation B. Dissolved porewater Fe concentrations are significantly higher than in the previous simulations (A and B), and September concentrations exceed initial June concentrations between 15 and 50 cm. The high dissolved Fe concentrations are likely responsible for the lower sulfide concentrations, because it readily leads to equilibrium FeS precipitation, which can be seen to be greater in this wetland simulation than the channel simulations. Interestingly, this means that more sulfide is produced in the wetland compared to channel during the flood period, even though wetland dissolved sulfide concentrations are lower. The higher dissolved Fe concentrations that are responsible for this low sulfide do not arise from differences in mineralogy, but from differences in redox activity. The greater FeS precipitation, Fe(OH)3 decrease, and high dissolved CH4 levels indicate that the west wetland is a highly reducing environment relative to the main channel. The model calibration suggests this difference is primarily due to the significantly higher sediment organic carbon concentrations calibrated in the wetland. A larger pool of initial organic carbon would stimulate more reduction and generate the high alkalinity observed in model and field results. In combination with the slower influx of oxygenated surface water, this creates an environment conducive to rapid reduction.

The cation exchange model again predicts Mg sorption to dominate, producing aqueous concentrations that correspond well with observations.

Model assumptions and uncertainties in kinetic degradation

A major source of uncertainty lies in the model representation of kinetic degradation, which drives all redox processes. Using the partial equilibrium approach with organic carbon oxidation as the limiting redox half reaction (Jakobsen & Postma 1999) is likely a reasonable assumption for Second Creek, because TEA (SO_4) concentrations are very high and not likely limiting in the wild rice root zone. Kinetic oxidation rates are estimated by manually calibrating organic carbon concentrations and the first order decay parameter, both of which lack reliable direct constraints. Observed total sediment carbon fractions are useful for inferring higher concentrations in the wetland than in the main channel, but actual concentrations are difficult to quantify, because readily labile forms (those used by microbes over the monthly to seasonal time scale considered in this study) could differ significantly from total amounts measured (Schumacher 2002). The adjusted decay parameter, k', used in the first-order organic carbon degradation equation (Equation 7), encompasses a wide variety of complex processes that have not been incorporated into the model, such as microbial metabolic processes, competition between microbes, sediment surface area, form of organic carbon, and surface complexation.

To assess our manually calibrated initial organic carbon concentration and decay rate parameter, we compare the resulting degradation rates from these two model inputs with literature microbial SO_4 reduction rates. Literature SO_4 reduction rates are commonly reported as moles per volume per time, where the volume is the total porewater where sulfate reduction occurs. In laboratory incubation studies, the reduction

rates apply to batch reactions in closed systems, and the volume is the experiment container. In field studies and flow-through experiments, the rates are also affected by flux and other geochemical conditions, and the volume is the depth to which sulfate reduction is observed. We use two approaches for calculating simulated SO_4 reduction rates to compare to these literature values. First, to generate estimates comparable to batch-reaction experiments, the first order kinetic rate equation for organic carbon (Equation 7) was applied for the different simulations (Table 4) to calculate average organic decay rates over a 30-day simulation period; these ranged from -100.45 nmol cm^{-3} d^{-1} in the wetland to -12.32 nmol cm^{-3} d^{-1} in the main channel (Table 5), which correspond to SO_4 reduction rates of 50.22 nmol cm^{-3} d^{-1} in the wetland and 6.16 nmol cm^{-3} d^{-1} in the main channel when adjusted for stoichiometry in Equation 4. These estimates for the model may be high, because some organic carbon oxidizes using other terminal acceptors than SO_4, such as Fe(OH)3 and inorganic carbon for methanogenesis. The second approach for estimating simulated rates emulates the field measurements; total moles of reduced SO_4 are taken from model mass balance results, and these are normalized by the approximate depth of the SO_4 profiles and divided by the simulation times (Table 5).

Due to site-specific microbial, geochemical, hydrological, and measurement method factors, a wide range of microbial SO_4 reduction rates have been obtained via field measurements and laboratory experiments Table 2. Our estimated rates from the model fall within the broad range. Based on environmental setting and measurement approach, the most conceptually consistent comparison is likely between our depth-

normalized estimates for the model and field studies in sulfate-enriched, eutrophic (for wetland simulation), and oligotrophic (for channel simulation) lakes (Steenbergen et al. 1993; Holmer & Storkholm 2001). Our modeled rates are consistent with this smaller subset of studies, with the lower channel rate corresponding to the oligotrophic (nutrient-limited) lake results. Our spread in channel estimates during the flood and non-flood times demonstrates the sensitivity of reduction rate measurements on hydrological factors, and hence the difficulty of measuring model kinetic parameters.

Other model assumptions/uncertainties include the constant upper and lower geochemistry boundary conditions of surface water and ground water, implementation of $Fe(OH)_3$ as the sole source of Fe, equilibrium mineral dissolution and precipitation (which lack representation of mineral surface area affects), and propagation of field data error. The constant geochemical boundary conditions have a large impact on the porewater simulation results, especially in Simulation B, where flux is downward. Sediment solid-phase Fe data was not collected, so the specific Fe mineral(s) that provide porewater Fe are not known. We use $Fe(OH)_3$ as the sediment Fe source in the model due to the prevalence of the mineral in low temperature settings (Rickard & Luther 2007), but other Fe(III) or Fe(II) (e.g., siderite) minerals could also be providing a source for dissolved Fe. Furthermore, the surface area of these minerals is unknown.

8. Conclusions

This study demonstrates how both groundwater and surface water quality can impact hyporheic zone geochemistry in mining impacted stream settings. This work is important in that it characterizes processes at multiple temporal and spatial scales and

domains, but all with the focus on how these different aspects affect the wild rice root zone. We examine changes in stream dynamics over a wild rice growing season, and use a combination of field data and model simulations to examine the porewater geochemical response to these changes in a high SO_4 system. When examined together, model simulations and field results in this study provide insight into three different factors that are important to porewater sulfide and Fe dynamics in the wild rice root zone, which ultimately affect wild rice growth: (1) surface water and groundwater chemistry, (2) streambed sediment geochemistry, and (3) direction and magnitude of hydrologic flux. Because the effects of these factors are interconnected in natural systems, it is difficult to determine the relevance of each one through field observations alone, but the model simulations help elucidate the relative importance of each factor at Second Creek over the study period of summer 2015.

In all model simulations and field data, porewater sulfide levels are orders of magnitude lower than dissolved Fe concentrations. Relationships between porewater Fe, sulfide, FeS, and other water chemistry are difficult to examine using field data alone. In simulations, the effect of FeS precipitation on dissolved Fe and sulfide is notable from the significant accumulation of FeS within the top 5-10 cm, where dissolved sulfide concentrations are low (compared to precipitated concentrations) and dissolved Fe concentrations decrease over time. When sulfide concentration is sufficiently high, this indicates a potential for depleting Fe in shallow porewater sediments, limiting its availability for precipitating sulfide. This scenario is most clearly illustrated in Simulation C during the flooded period in the wetland. This simulation shows the

greatest precipitation of FeS (about an order of magnitude higher concentration than in Simulation A during the non-flooded period), indicating the highest potential for a finite source of available Fe in the sediment (generically represented as $Fe(OH)_3$ in the model) to be eventually depleted. However, both the highest peak in sulfide and the lowest concentrations of Fe occur in Simulation B during the flooded period in the channel, indicating that factors other than Fe sediment availability may be a factor for sulfide levels. Simulation B has the greatest downward flux of higher pH surface water, which limits $Fe(OH)_3$ reduction (see Equation 5) to likely contribute to the lower Fe2+ concentrations and correspondingly higher sulfide concentrations. Although high pH surface water also advects into the sediment in simulation C, the rate is lower, and the more reducing wetland conditions intensify Fe reduction rates; subsequent high rates of FeS precipitation in Simulation C also release H^+ (Equation 2), further enhancing Fe reduction. These results indicate that sulfide sensitivity to Fe may occur over different time scales, with local aqueous geochemical conditions controlling shorter time scales, and overall Fe sediment reservoirs controlling longer time scales.

Comparison of channel and wetland simulations during the flooded period highlights how geochemical and physical sediment properties have an important impact on porewater geochemistry. Sediment organic carbon content is clearly a driving force in redox reactions, as evidenced by the strikingly higher porewater Fe and CH_4 concentrations in the wetland compared to the main channel (calibrated sediment organic carbon is 10x higher in the wetland). Our study shows that models can be useful for evaluating important variables that are difficult to measure directly in the field, such as

actual labile organic carbon concentrations and decay rates. Additionally, the model shows that changes in organic carbon content can occur over relatively small (meter scale) spatial scales, and that these changes can have a considerable impact on porewater geochemistry. The pool of sediment Fe, present in the model as Fe(OH)3, is similarly important in the model as the source of porewater Fe to attenuate sulfide.

The geochemical relationships demonstrated with the model corroborate the findings of Pollman et al. (in review) that sulfide accumulation in porewater depends on Fe and organic carbon levels, but our results further indicate that hydrologic flux plays a significant role in porewater geochemistry. This is especially clear through comparison of the two main channel simulations (A and B). In Simulation A, where there is upward groundwater flux, SO4 transport from the surface water into the sediment by dispersion is relatively limited. When the hydraulic gradient is reversed in Simulation B, surface water flows into sediment porewater, and SO4 penetration and sulfide generation are much more significant. This is an important result because it shows that, in an Fe-rich environment like Second Creek, porewater sulfide concentrations may only become high when the high SO4 surface water advects into the porewater where it can be reduced. If downward flux is sustained long enough for Fe depletion to occur, sulfide concentrations could exceed the proposed protective concentration for wild rice. This project highlights both the utility of a model in estimating geochemically important but difficult-to-measure variables, and the importance of incorporating hydrologic information from surface water and groundwater when examining hyporheic zone geochemistry.

9. Ongoing Work and Future Directions

A major limitation on the field-based aspects of the 2015 study was insufficient data from the main channel of the streambed and lack of reliable physical data constraints on hydrologic flux. Thus, in the following 2016 field campaign, we focused on the main stream channel and improved our physical instrumentation installations. In 2015, local changes in hydraulic flux proved difficult to measure using seepage meters, temperature probes, and wetland piezometers alone, as measurement uncertainties were often significant compared actual flux, and 24-48 hour deployments of some instruments could not be readily extrapolated due to significant daily flux fluctuations in the field. During the summer of 2016, piezometers and season-long deployments of temperature probes were collocated within the main channel streambed and west wetland, with the expectation that obtaining continuous fine-scale measurement of hydrologic flux gradient using multiple techniques would reduce errors. The two main improvements over the 2015 campaign were: (1) continuously recording temperature probes over three months (they were deployed for only 24-48 hours in 2015), and (2) installation of main channel piezometers at multiple depths in the stream to obtain hydraulic gradient in the main channel (main channel piezometer measurements were absent from the 2015 data).

Porewater peepers and sediment cores analyzed for microbial DNA were also collocated with piezometers and temperature probes in the wetland and main channel twice during the summer of 2016 to evaluate interactions between microbial activity and geochemical processes in a hydrologically dynamic hyporheic setting such as Second Creek. The ~1.5 cm-scale peeper geochemistry measurements are more relevant to

highly heterogeneous microbial activity and pair more naturally to the model simulation profiles than the 10 cm resolution porewater core geochemistry. Using peeper data as calibration targets for the model will lead to the refinement of the unknown parameters in the model. The collocated sediment cores were sampled at ~5cm intervals (or at intervals corresponding to observable changes in sediment characteristics, such as color, texture, and grain size) for microbial DNA. Microbial communities have not been studied in-depth at Second Creek, even though redox reactions are likely primarily microbially driven, so this data will fill an important gap in our understanding. Specifically, the microbial data could be useful in either refining existing kinetic parameters in the model, or informing the use of a different another kinetic model for redox reactions. This paired hydrogeochemical and microbial analysis will also provide insights into how physical factors influence microbiological activity.

In addition to the new data collected in 2016, we hope to collect additional sediment samples for geochemical analysis. Neither organic carbon nor sediment Fe concentrations or form are well-constrained from direct field measurements and were instead estimated or calibrated in the 2015 study. Considering the importance of these variables in porewater geochemistry, there would be much greater confidence in model results if reliable concentrations of these variables were also measured. Specifically, speciated sediment Fe concentrations would be useful in understanding Fe sources at Second Creek and would help with the refinement of kinetic parameters. Additionally, 2015 and 2016 sediment collection was not extensive enough to determine the lower extent of the hyporheic zone, where groundwater chemistry is dominant. Although the

depth of the hyporheic zone changes with changes in head levels and stream flow, constraining sediment properties (e.g., grain-size) in the stream bed would allow for more accurate estimation of the approximate depth.

This additional field data will serve to improve the current reactive transport model. Additional future changes to the model should include better constraints on kinetic parameters (using the field measurements discussed above), a variable upper boundary condition to match the monthly changes in surface water chemistry, increasing simulation time to examine longer term changes, and running simulations for the east wetland.

10. Tables

Method	Flux	*PRE-FLOOD*	*FLOOD*	*POST-FLOOD*
Main Channel — **Temp. Probe**	Direction	⇧ ⇧ ⇩		⇧ ⇩ ⇧
	Magnitude [µm/s]	1.26 1.23E-6 -9.88E-6		1.31 -.417 7.09E-6
	RMSE	0.011 0.225 0.229		0.029 0.019 1.447
	Date	6/6-6/7 6/26-6/27		10/16-10/17
Main Channel — **Seepage Meter**	Direction	⇧ ⇧ ⇩ ⇩		
	Magnitude [µm/s]	8.31e-3 1.82e-3	-7.72e-3 -.0167	
	Date	6/25-6/26	8/31-9/1	
West Wetland — **Temp. Probe**	Direction		⇧ ⇧ ⇧ ⇧ ⇧ ⇧	
	Magnitude [µm/s]		4.79 .591 1.50 9.67 9.88 6.62	
	RMSE		0.023 0.025 0.101 0.041 0.044 0.135	
	date		8/13-8/14 8/31-9/1	
West Wetland — **Seepage Meter**	Direction		⇩ ⇩ ⇩ ⇩ ⇩	
	Magnitude [µm/s]		-2.20E-3 -4.14E-3 -3.50E-3 -2.95E-3 -5.53E-3	
	date		8/31-9/1 9/18-9/19	

Table 1. Temperature probe and seepage meter data from the main channel (top) and the wetland (bottom) for pre-flood, flood, and post flood conditions. Direction of arrows indicates groundwater flux direction. For qualitative confidence measurements of flux direction, black arrows represent data with the most confidence, gray arrows are moderately confident, and white arrows are data with the least confidence. Quantitative confidence estimates for temperature probes were determined from root-mean-square-error (RMSE) of simulated compared to observed temperature (°C) over depth. Qualitative confidence measures were determined by the shape of the flux versus RMSE plot (described in text). Qualitative seepage meter confidence was determined through field observations (described in text).

SO4 reduction rate	location (environment type)	rate measurement method	source
[nmol SO4/cm3/d]			
5-25	Lake Klagard, Denmark (oligotrophic)	AVS recovery	Holmer and Storkholm, 2001; Holmer et al., 1998
175-500	Lake Holmsjon, Finland (SO4 enriched)	AVS recovery	Holmer and Storkholm, 2001
40-60	Lake Vechten, Netherlands (eutrophic)	AVS recovery	Holmer and Storkholm, 2001; Steenbergen et al., 1993
240	Scheldt Estuary, Belgium and Netherlands (freshwater)	flow through reactor	Pallud and Van Cappellen, 2006
700	Scheldt Estuary, Belgium and Netherlands (saline)	flow through reactor	Pallud and Van Cappellen, 2006
2-17	Skagerrak, Norwegian Sea	35S isotope tracer	Dale et al., 2008
0.5	Southern Ocean Weddell Sea	Sediment incubation, 35S isotope tracer	Robador et al., 2015
2233	Arctic Ocean	Sediment incubation, 35S isotope tracer	Robador et al., 2015
161	Arctic Ocean	Sediment incubation, 35S isotope tracer	Robador et al., 2015
518	North Sea	Sediment incubation, 35S isotope tracer	Robador et al., 2015
236	Baltic Sea	Sediment incubation, 35S isotope tracer	Robador et al., 2015
55	Arabian Sea	Sediment incubation, 35S isotope tracer	Robador et al., 2015
21	Arabian Sea	Sediment incubation, 35S isotope tracer	Robador et al., 2015
316	Andaman Sea	Sediment incubation, 35S isotope tracer	Robador et al., 2015
25	South China Sea	Sediment incubation, 35S isotope tracer	Robador et al., 2015
242	Mono Lake boat launch, US (hypersaline)	flow through reactor	Laverman et al., 2012
600	Mono Lake Black Point, US (hypersaline)	flow through reactor	Laverman et al., 2012
1226	Elkhorn Slough marsh, US (brackish estuary)	flow through reactor	Laverman et al., 2012
643	Elkhorn Slough, US (brackish estuary)	flow through reactor	Laverman et al., 2012
674	Waarde, Netherlands (brackish estuary)	flow through reactor	Laverman et al., 2012
554	Tresmes, France (river)	flow through reactor	Laverman et al., 2012
2186	Rattekaaim, Netherlands (saline estuary)	flow through reactor	Laverman et al., 2012
1690	Baylands, US (salt marsh)	flow through reactor	Laverman et al., 2012
1687	Pescadero , US (estuary)	flow through reactor	Laverman et al., 2012
960	Créteil, France (freshwater lake)	flow through reactor	Laverman et al., 2012
991	Hourdel salt marsh, France (saline estuary)	flow through reactor	Laverman et al., 2012
646	Hourdel port, France (saline estuary)	flow through reactor	Laverman et al., 2012
554	North CA Coast , US (marine)	flow through reactor	Laverman et al., 2012
614	Humboldt Bay (US) (marine)	flow through reactor	Laverman et al., 2012

Table 2. Literature SO_4 reduction rates from a variety of settings. See source reference for details on methodology and uncertainties.

Reaction	**logK (database)**	**logK* (calibrated)**
$Fe(OH)_3 + 3H^+ \leftrightarrow Fe^{3+} + 3H_2O$	4.89	1.50
$FeS + H^+ \leftrightarrow Fe^{2+} + HS^-$	-3.915	-3.15

Table 3. Solid phase reactions used in the model with database and calibrated parameters.

	Hydrologic flux	OC Concentration	OC rate parameter (k')	Cation Exchange Capacity
	[m/s]	[mmol/L]	[s^{-1}]	[mol/L]
Simulation A	7.00E-08	2.09E-01	7.50E-08	0.02
Simulation B	-2.00E-08	2.09E-01	7.50E-08	0.02
simulation C	-8.00E-09	2.09	6.00E-08	0.02

Table 4. Calibrated parameters for the three model simulations. OC = organic carbon. A positive value for hydrologic flux means upward flow of groundwater. Rate parameter k' was adjusted to account for processes occurring in natural setting that are unquantified in the model (e.x. surface complexation, microbial metabolism, mineral surface area, OC form).

		a.) based on kinetic rate law		b.) based on sulfate front depth and model sulfate	
Simulation	**location**	**OrgC oxidation rate (30 day average)**	**SO4 reduction rate using redox equation**	**Approx. SO4 front depth**	**rate**
		[nmol OC/cm3/d]	[nmol SO4/cm3/d]	[m]	[nmol/cm3/d]
A	**channel**	-12.32	**6.16**	0.04	**153.40**
B	**channel**	-12.32	**6.16**	0.40	**14.28**
C	**wetland**	-100.45	**50.22**	0.16	**193.09**

Table 5. Organic carbon oxidation and SO_4 reduction rates for the model simulations. In column a, values from Table 4 were used in Equation 6 to calculate rates, while column b rates were calculated based on modeled SO_4 balance and depth of front.

11. Figures

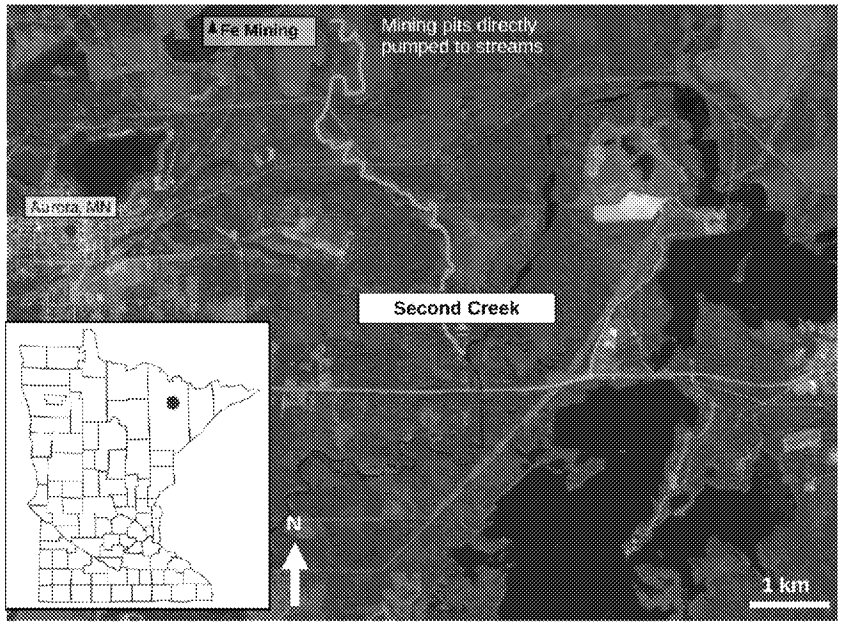

Figure 1. Regional setting with study area denoted by the box. Note mine tailings basins to the north and west of the site.

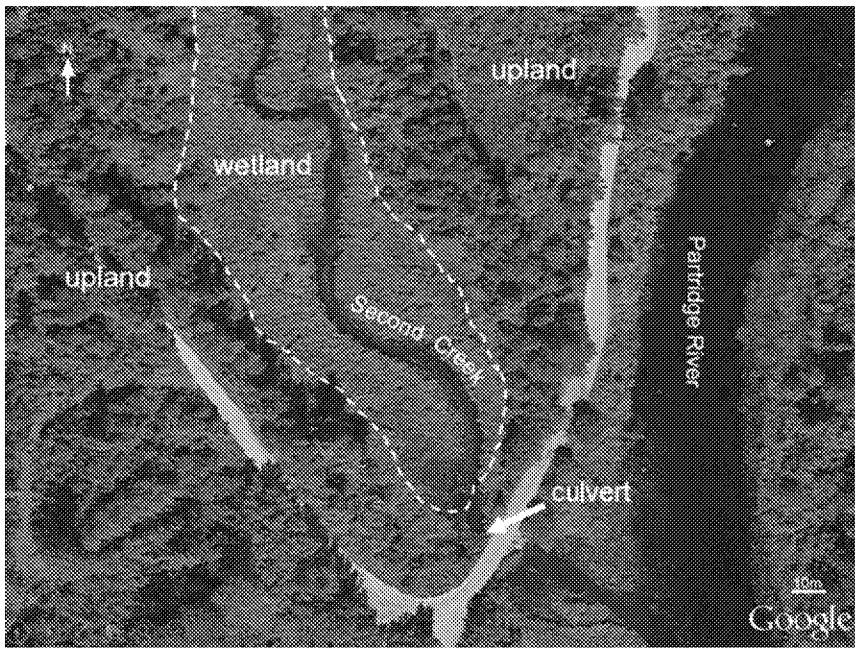

Figure 2. Zoom in of study are outlined in Figure 1. Dashed lines show approximate wetland delineation. Note that Second Creek flows through a culvert just upstream the confluence with the Partridge River.

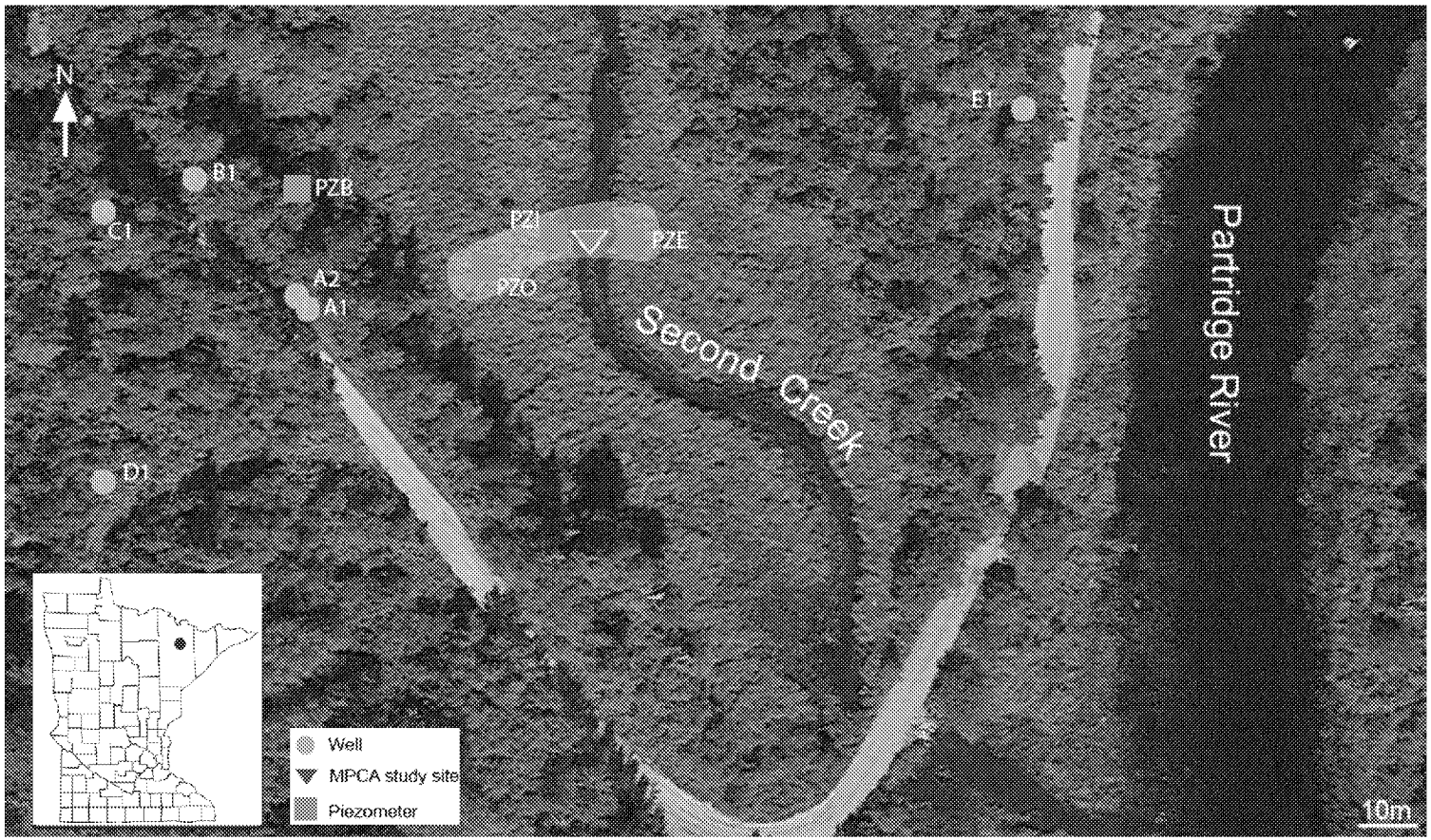

Figure 3. Location of groundwater wells (circles), piezometers (squares), and MPCA study site location (triangle) at Second Creek. Shaded area indicates area of focus of the temporary installations (temperature probes, seepage meters) and geochemical sampling locations.

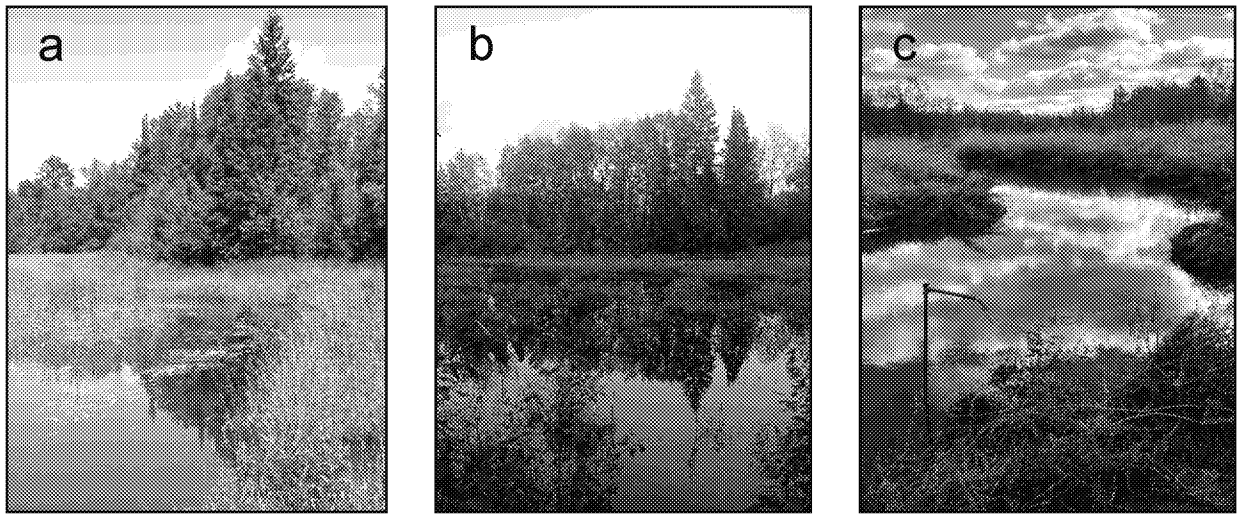

Figure 4. Second Creek surface water during the non-flooded period in late June (a), the flooded period in mid-September (b), and the non-flooded period in mid-October (c). Note wild rice in the floating leaf stage growing in June.

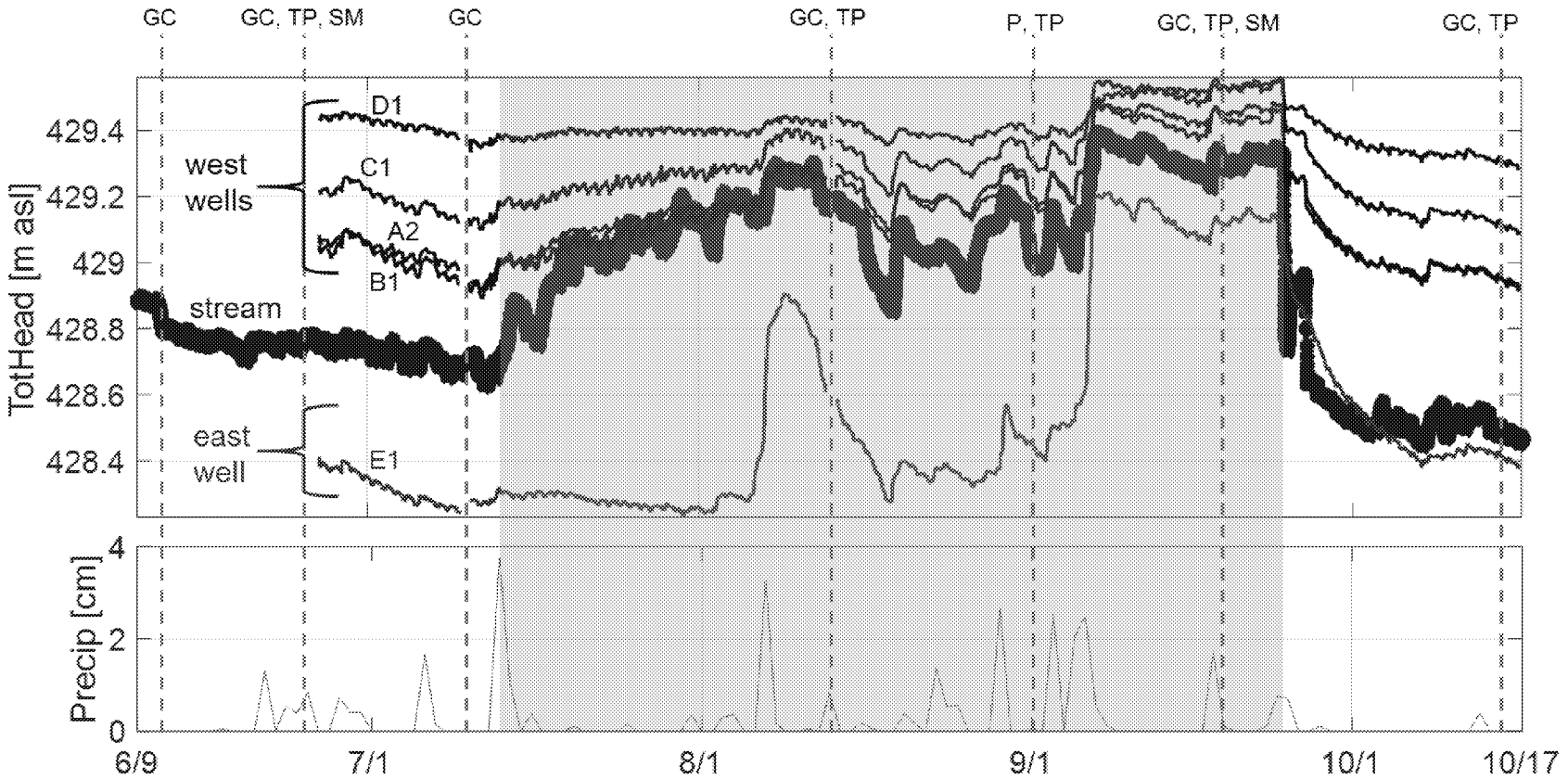

Figure 5. Daily precipitation and hydraulic head plot showing head levels for west groundwater wells (top), stream surface water (thick middle line), and east groundwater wells (bottom) during the sampling period in 2015. Mid-summer flood event is indicated by the shaded area from mid-July through late September. Sample dates are shown by dashed vertical lines with sample type indicated by codes above (GC=geochemistry sample; TP=temperature probe collection date; SM=seepage meter collection date). In general, groundwater head levels decrease from west to east, with surface water head falling in between west and east head, indicating that, regionally, Second Creek is a flow through stream from west to east.

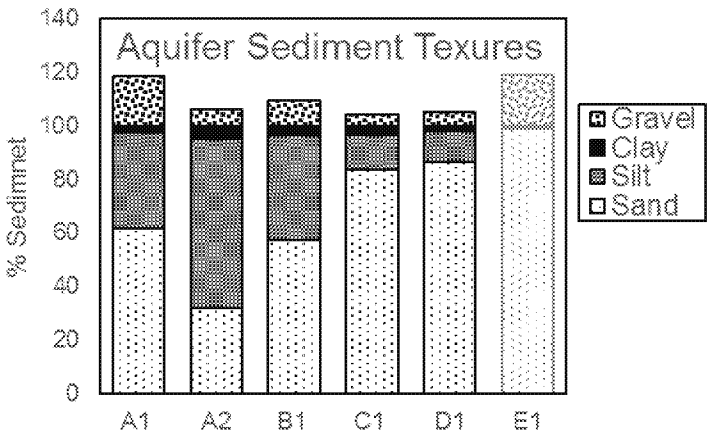

Figure 6. Fractions of sand, silt, clay, and gravel for the west aquifer (A1-D1) and the east aquifer (E1). Aquifer samples were collected during well installation in June. In cases where multiple aquifer samples were analyzed, the arithmetic mean is shown. While both aquifers are primarily sand, the east aquifer is primarily sand and gravel, while the west aquifer sediment has higher fractions of silt and clay.

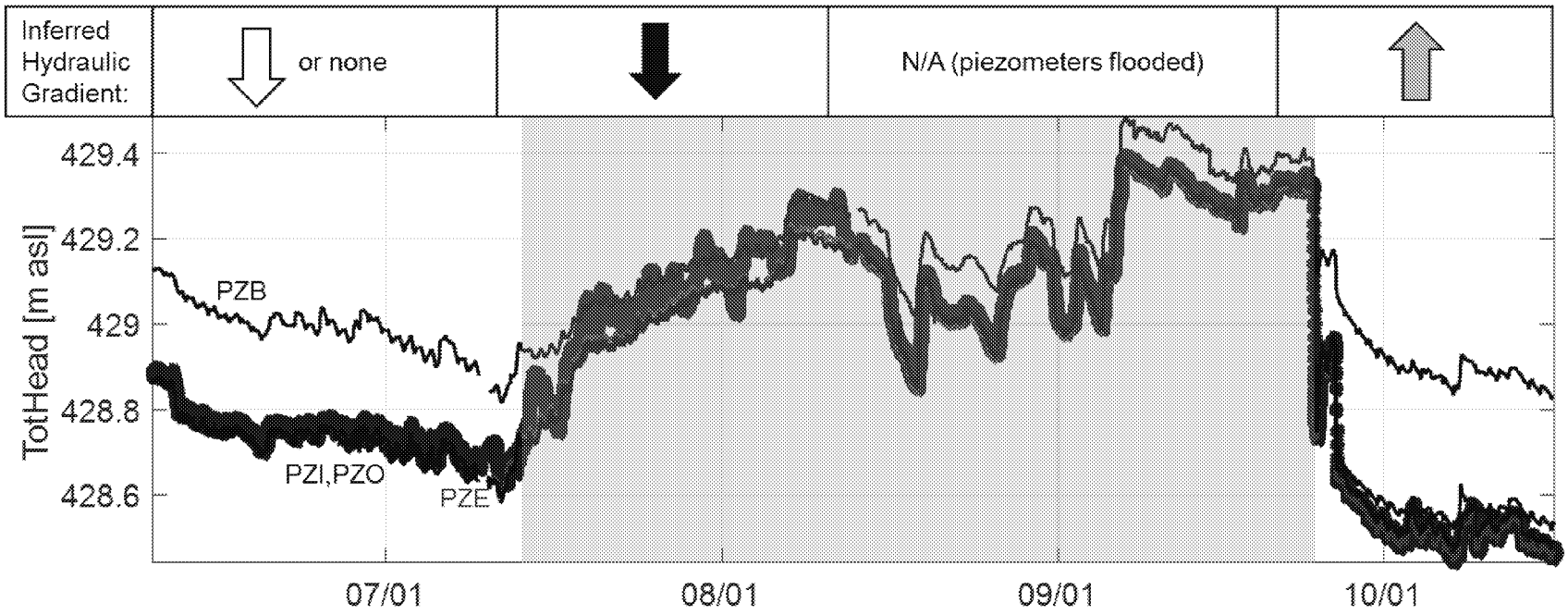

Figure 7. Hydraulic head plot for surface water (thick middle nice), piezometers in the west and east wetland during summer of 2015 with the flooded period indicated by the shaded region. In general, heads recorded by mini piezometers adjacent to the stream channel (PZI, PZO, PZE) are too similar to surface water heads to establish a clear hydraulic gradient. Qualitative confidence measurements of flux direction are shown with black arrows represent data with the most confidence, gray arrows are moderately confident, and white arrows are data with the least confidence.

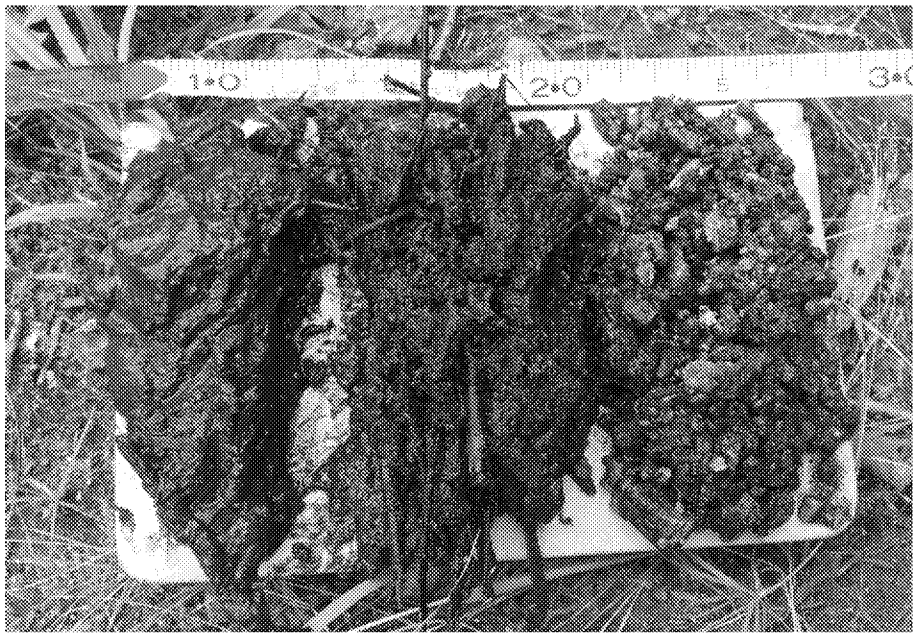

Figure 8. Sediment from the sediment water interface of the wetland (left) and two adjacent locations in main channel (center and right). Main channel sediment illustrated the high degree of sediment heterogeneity found laterally on the streambed of Second Creek.

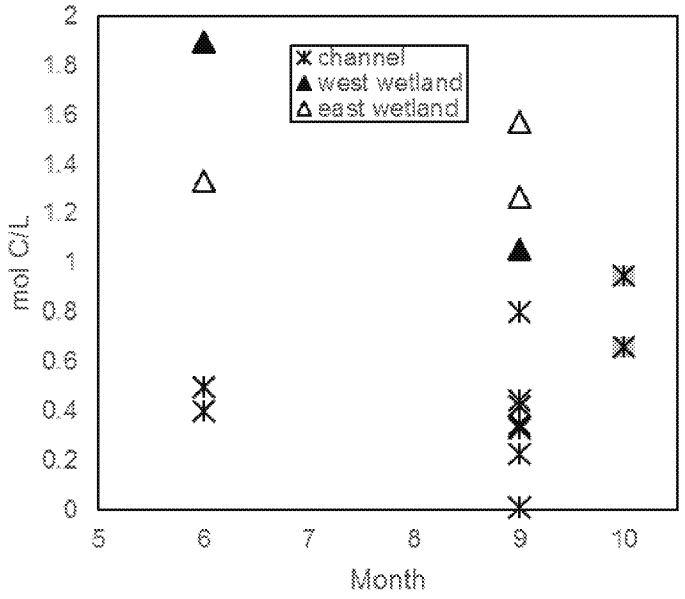

Figure 9. Total carbon concentration (moles per liter of water) for channel and wetland sediment. Samples are from July, September, and October. Squares indicate the only samples that reacted with the addition of HCl, so the total carbon fraction of the other samples is assumed to be primarily organic carbon. Sediment organic content is higher in the wetlands than in the main channel. There is no correlation between sample depth and organic content.

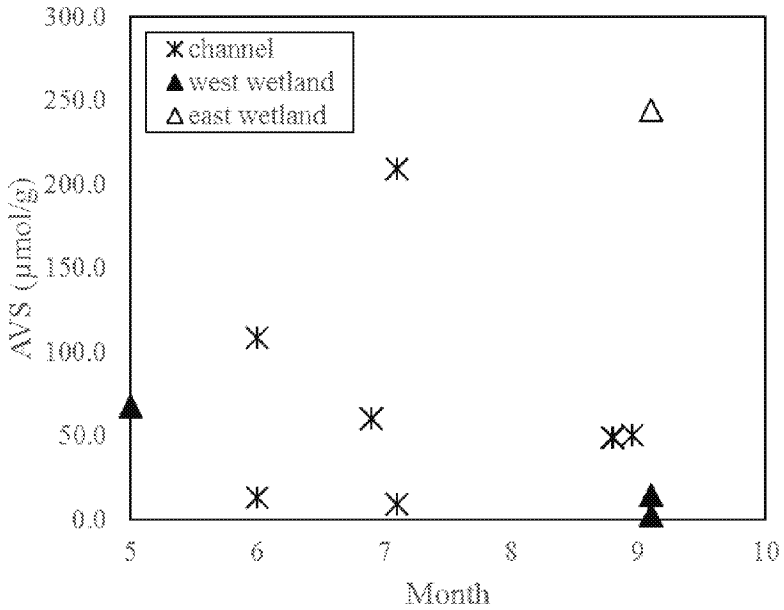

Figure 10. Sediment Acid Volatile Sulfide (AVS) concentrations for channel and wetland sediment using 0.5 N HCl extraction. There are no trends between samples depth and AVS concentrations, but the east wetland has higher AVS than the main channel and west wetland.

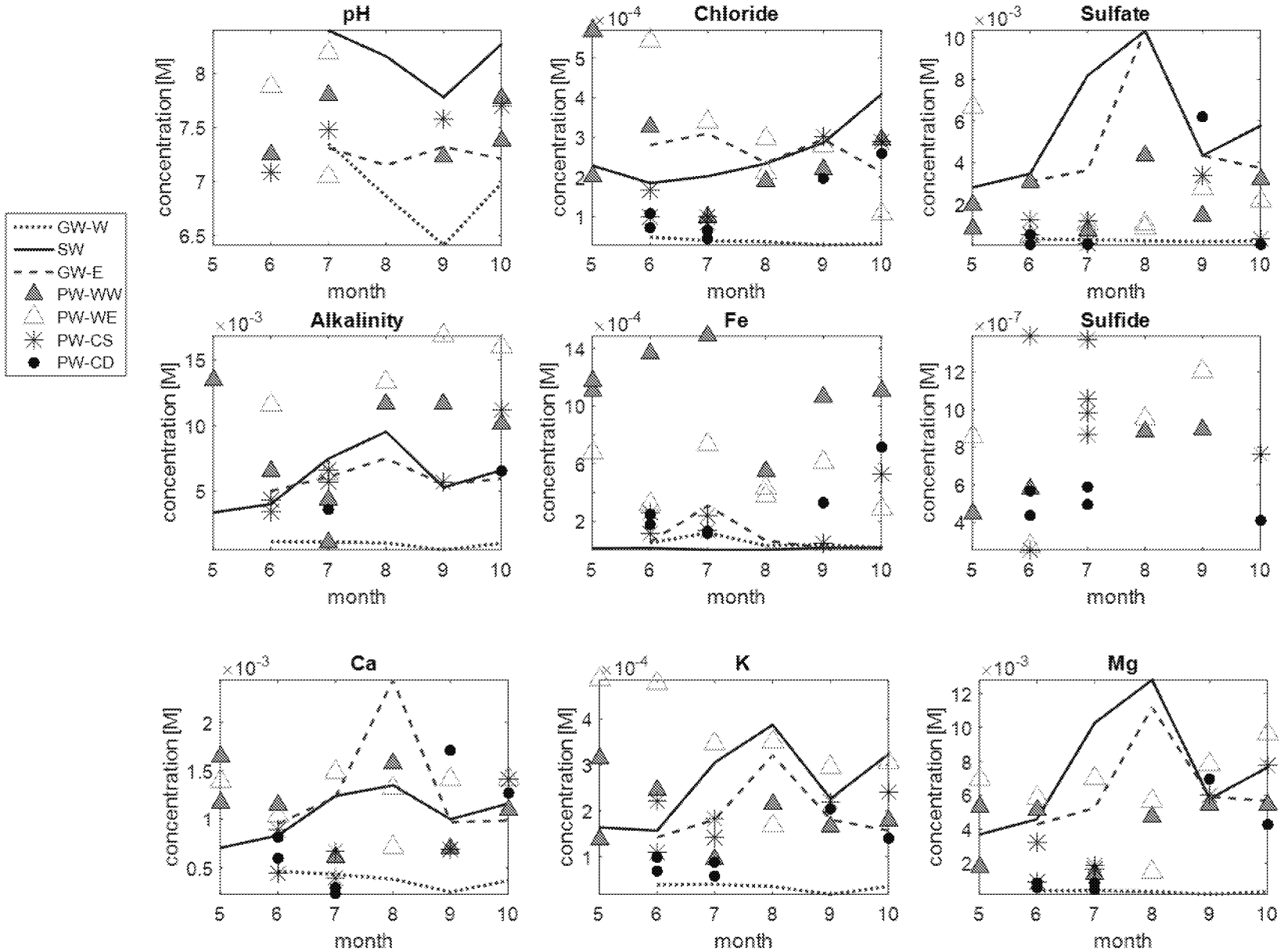
GW-W
SW
GW-E
PW-WW
PW-WE
PW-CS
PW-CD
pH
Chloride
Sulfate
Alkalinity
Fe
Sulfide
Ca
K
Mg
concentration [M]
month

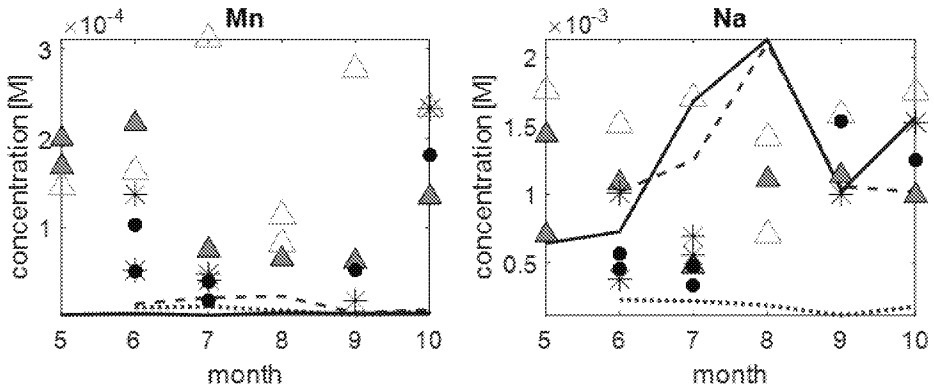

Figure 11. Selected geochemistry results for surface water (solid line), west groundwater (dotted line showing arithmetic mean of wells A2, B1, C1, D1), east groundwater (dashed line), west wetland porewater (filled triangle), east wetland porewater (open triangle), shallow (~0-10 cm) main channel porewater (asterisk), and deep (~10-20cm) main channel porewater (filled circle).

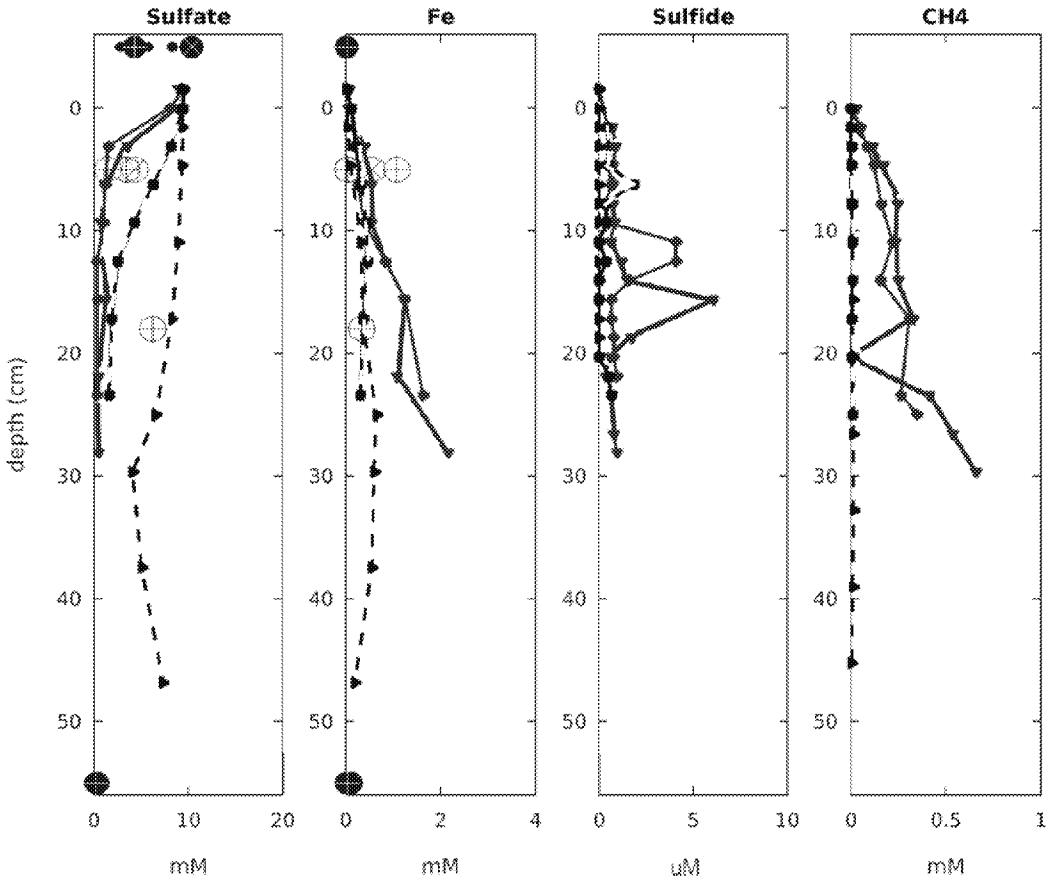

Figure 12. Selected geochemistry results from porewater peepers installed in the main channel (dashed lines) and the west wetland (solid lines). Porewater core data are shown in crossed open circles for the west wetland and main channel. Surface water and west groundwater data are superimposed onto the porewater profile, and are shown at the top and bottom of the profile, respectively. West groundwater data was collected from wells, so the depth shown on this plot is approximate, as deep groundwater from directly below the main channel and wetlands was not sampled.

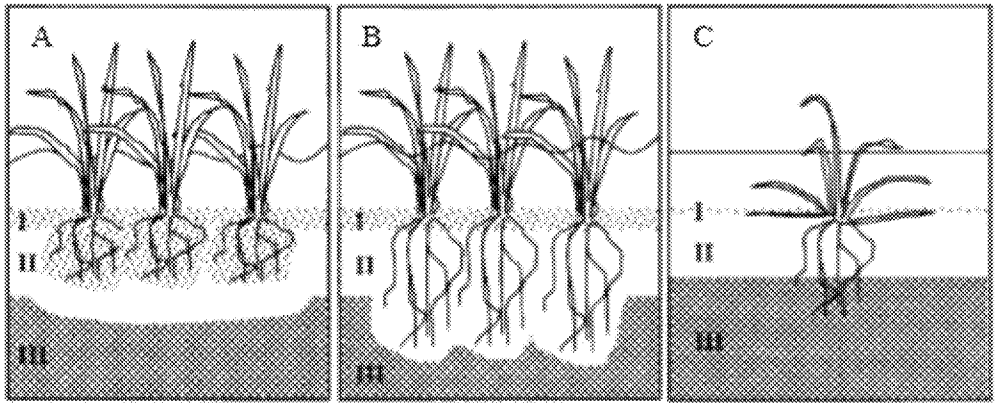

Figure 13. Conceptual model of seasonal fluctuation and spatial distribution redox conditions created by the rhizosphere of wetland plants. Shading indicates different layers of sediment redox conditions. Layer I is the oxidized surface sediment, Layer II represents moderately reduced, microaerobic sediments, and Layer III contains highly reduced sediments. When a plant is young, or has shallow root systems, Layer I into Layer II (A). As the plant matures and the root zone deepens, Layer II will extend into Layer III, increasing total microaerobic area in a wetland (B). When the plant dies, the aerobic stratification returns to unvegetated conditions (C). Modified from Jacob and Otte, 2004.

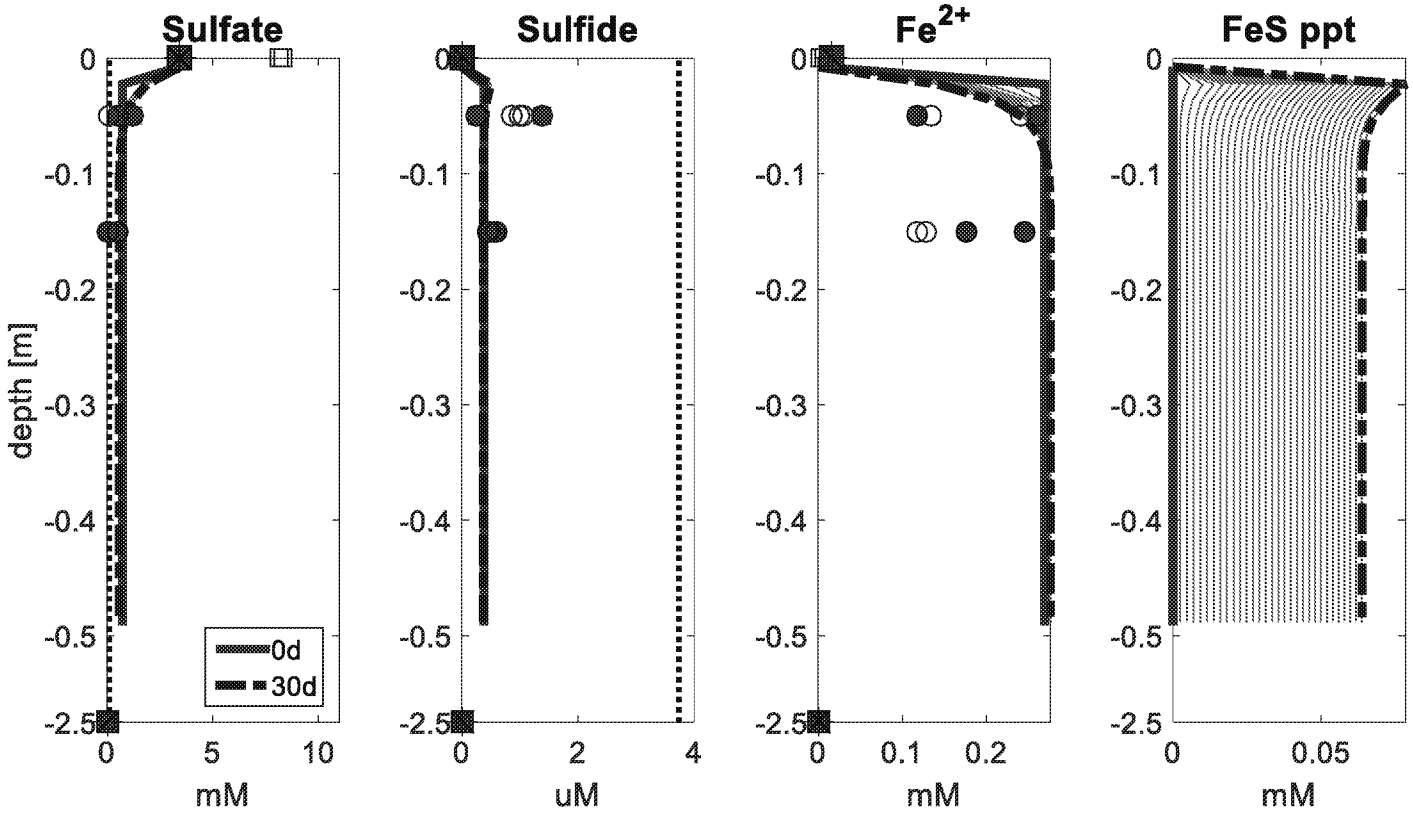
Sulfate
Sulfide
Fe2+
FeS ppt
depth [m]
0
-0.1
-0.2
-0.3
-0.4
-0.5
-2.5
0d
30d
0
5
10
mM
0
2
4
uM
0
0.1
0.2
mM
0
0.05
mM

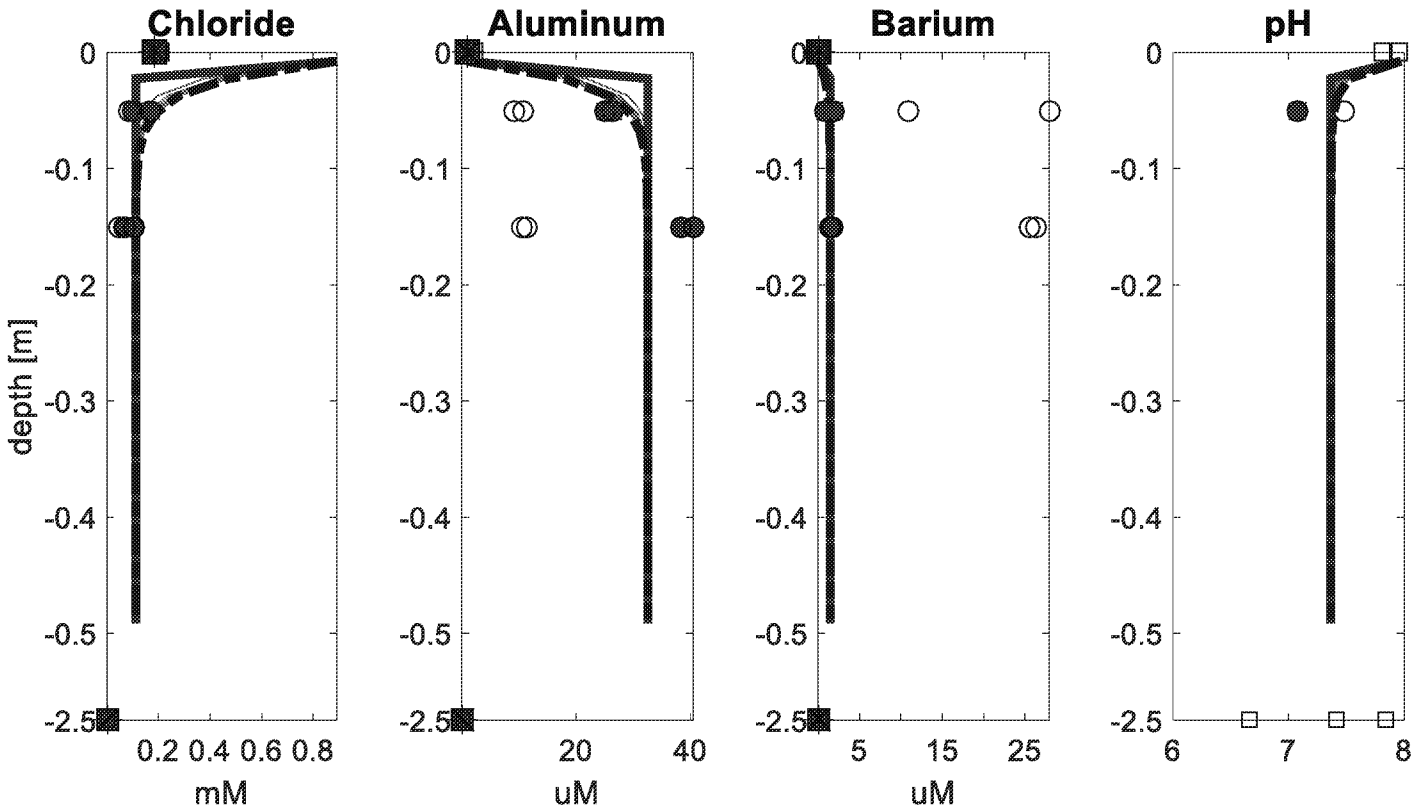
Chloride
Aluminum
Barium
pH
depth [m]
0
-0.1
-0.2
-0.3
-0.4
-0.5
-2.5
0.2 0.4 0.6 0.8
mM
20
40
uM
5
15
25
uM
6
7
8

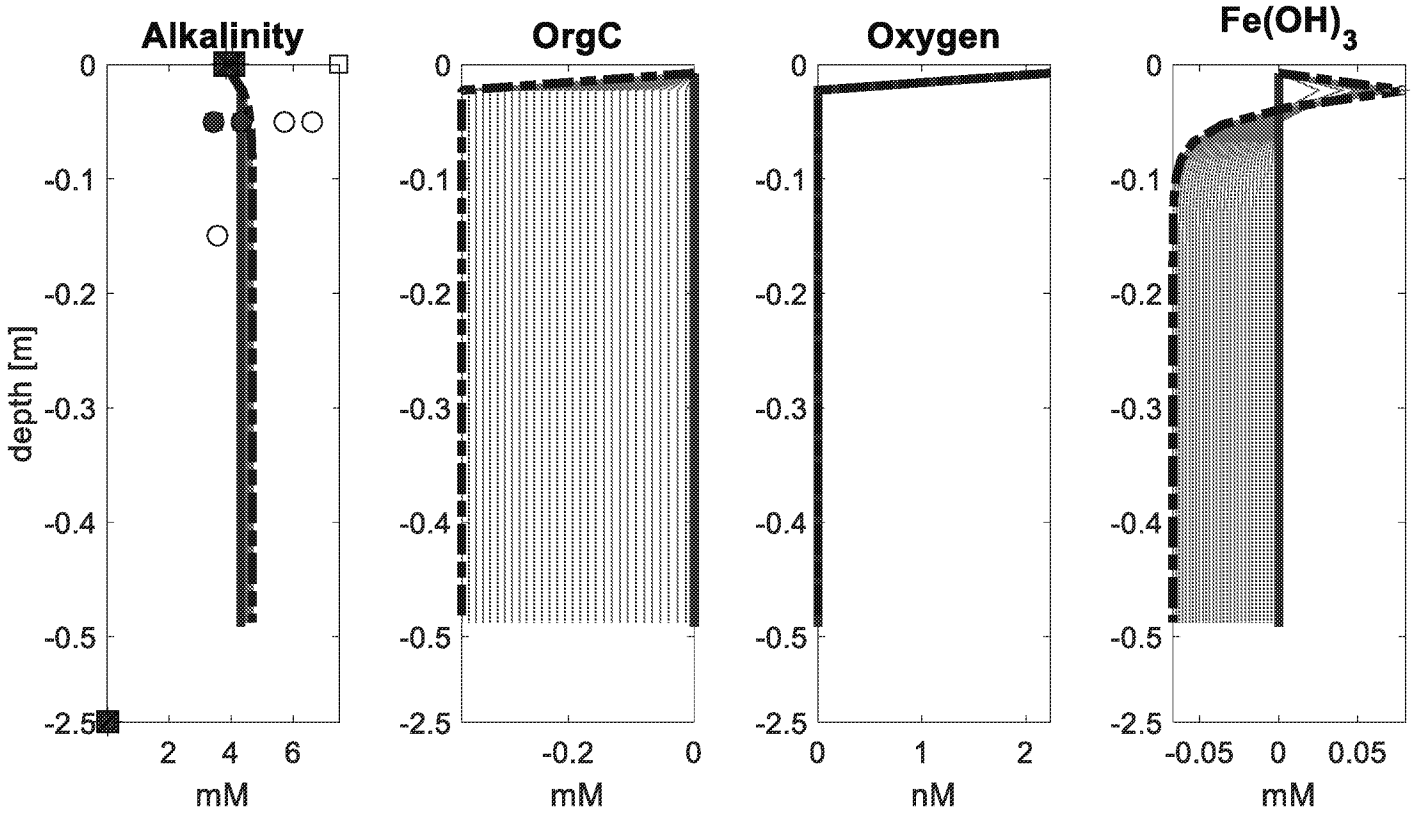
Alkalinity
OrgC
Oxygen
Fe(OH)3
depth [m]
0
-0.1
-0.2
-0.3
-0.4
-0.5
-2.5
2
4
6
-0.2
0
1
2
-0.05
0.05
mM
nM

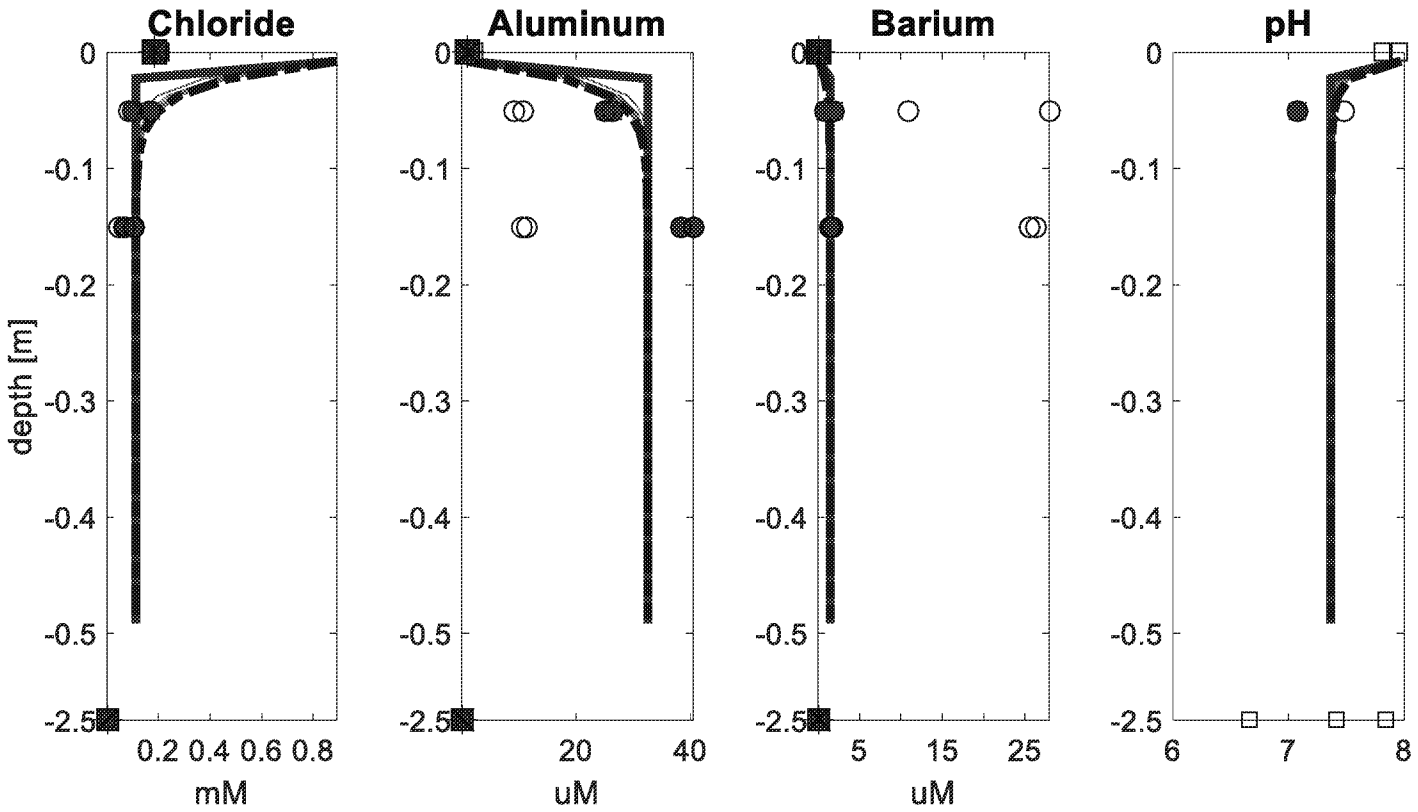
Chloride
Aluminum
Barium
pH
depth [m]
0
-0.1
-0.2
-0.3
-0.4
-0.5
-2.5
0.2 0.4 0.6 0.8
mM
20
40
uM
5
15
25
uM
6
7
8

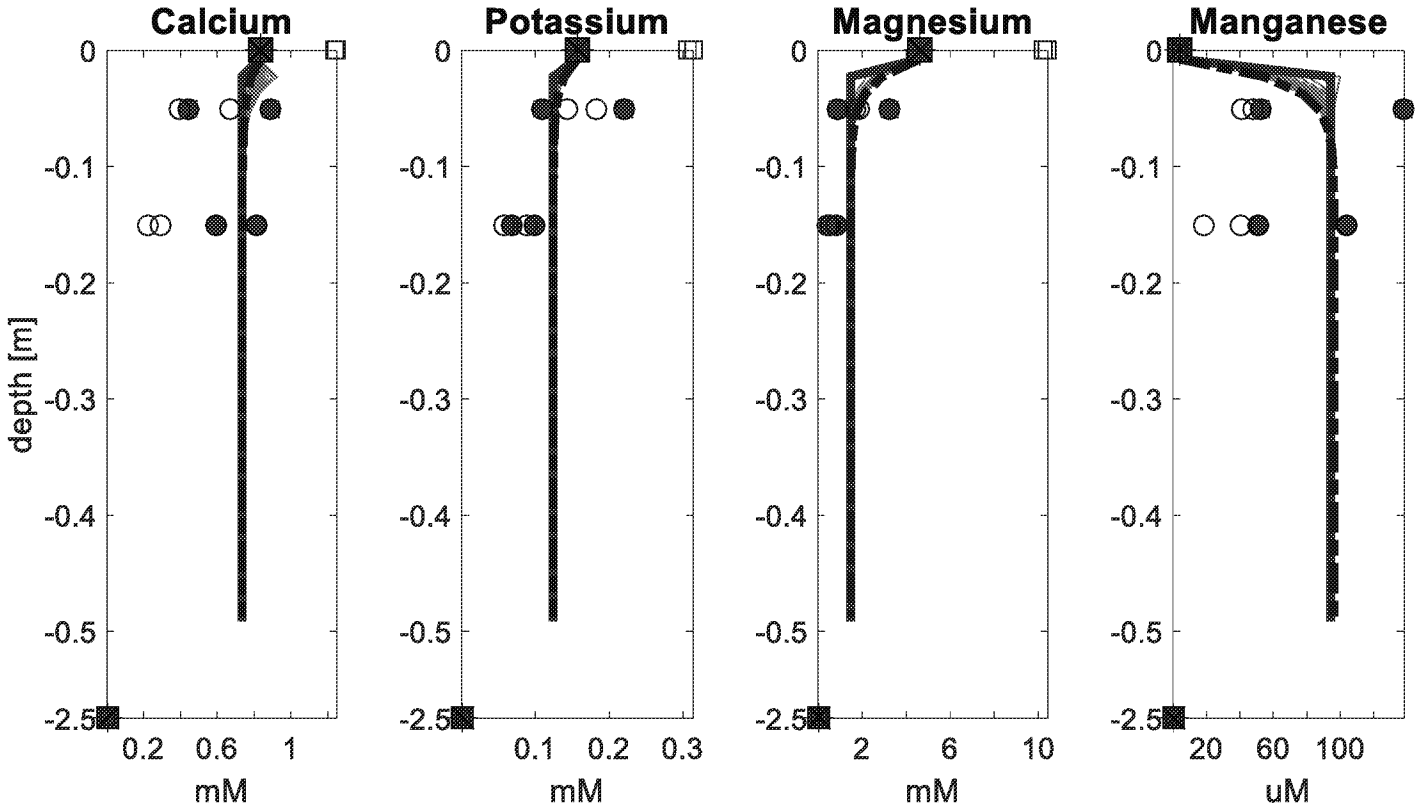
Calcium
Potassium
Magnesium
Manganese
depth [m]
0
-0.1
-0.2
-0.3
-0.4
-0.5
-2.5
0.2
0.6
1
0.1
0.2
0.3
2
6
10
20
60
100
mM
mM
mM
uM

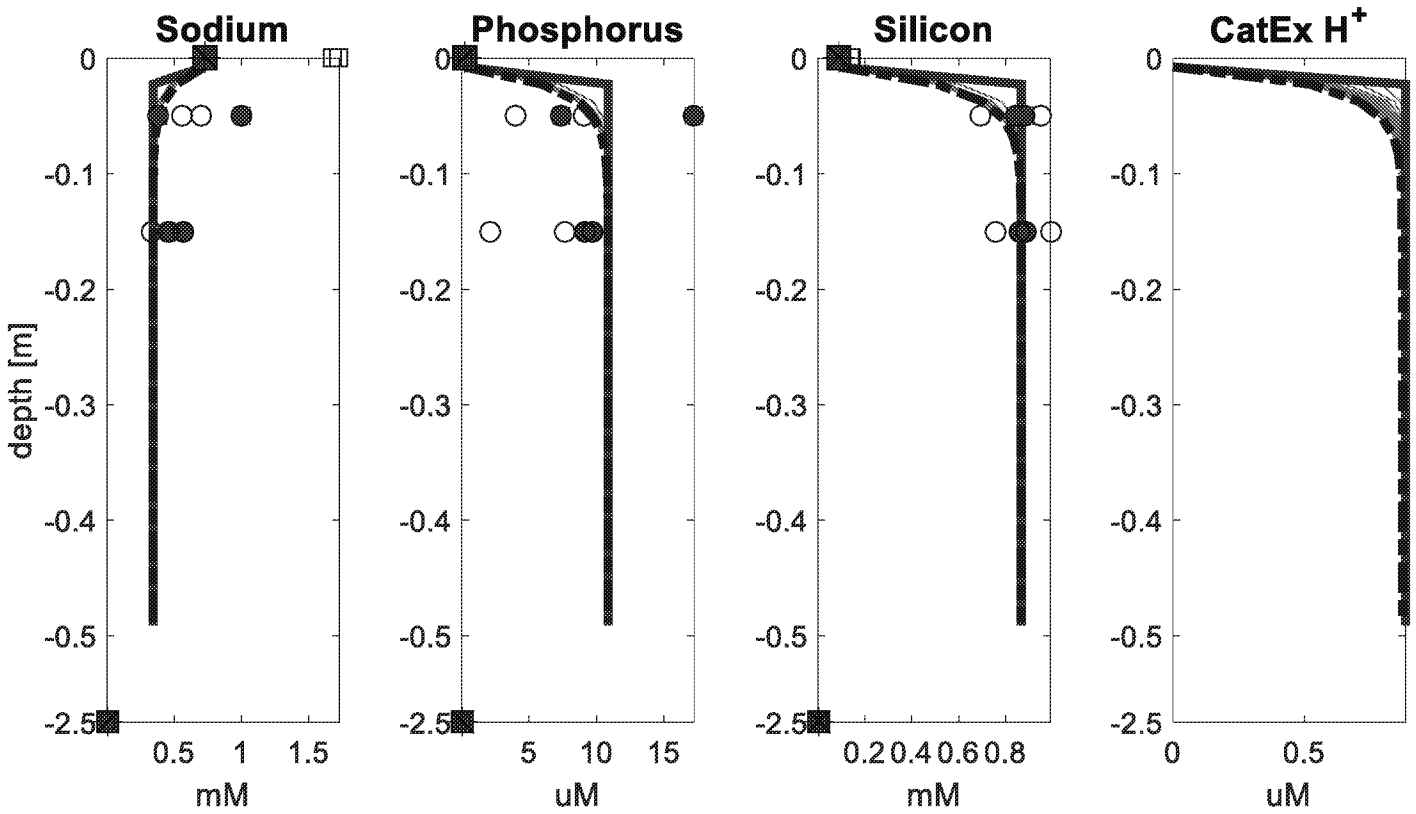
Sodium
Phosphorus
Silicon
CatEx H+
depth [m]
0
-0.1
-0.2
-0.3
-0.4
-0.5
-2.5
0.5
1
1.5
mM
5
10
15
uM
0.2
0.4
0.6
0.8
mM
0
0.5
uM

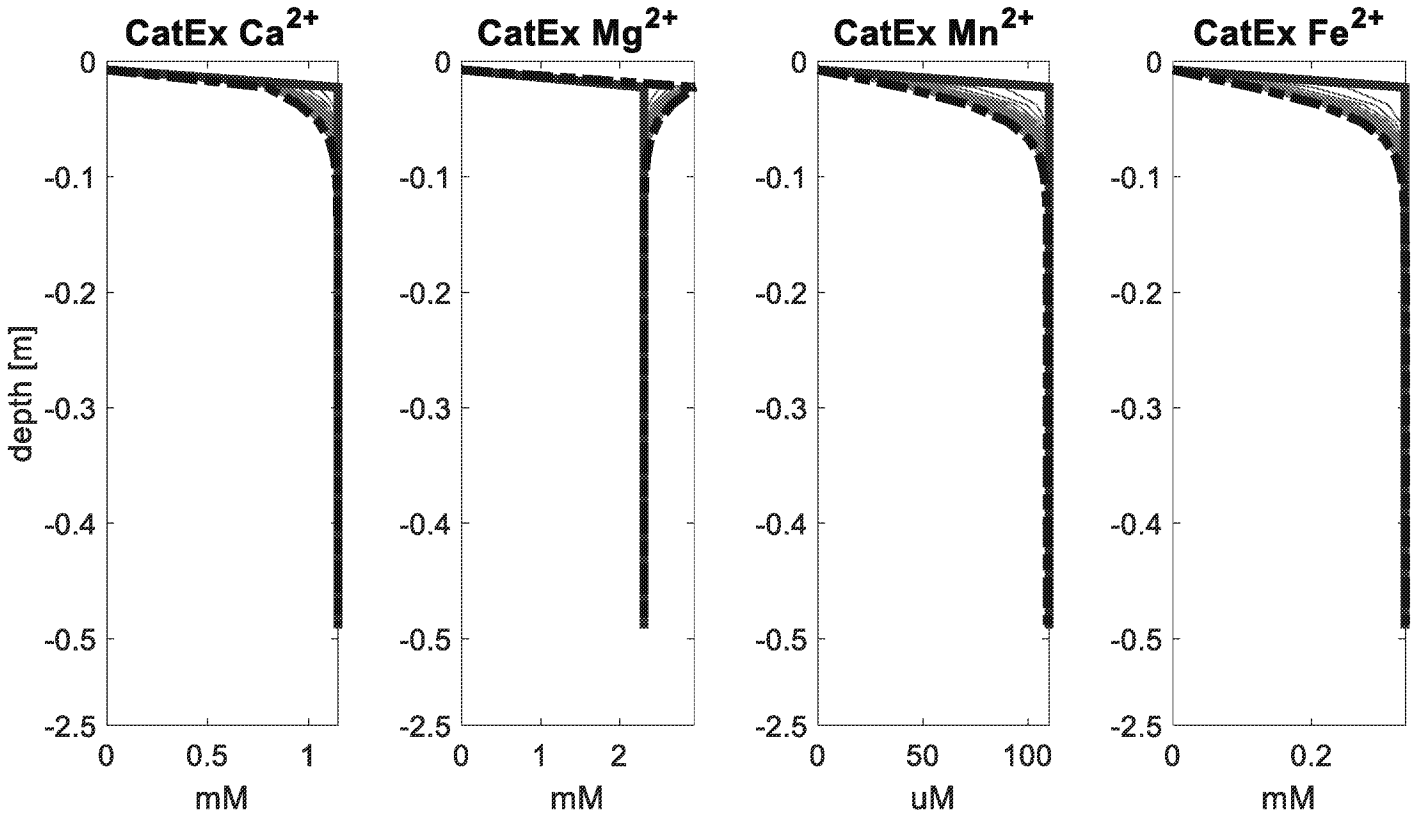

Figure 14. One dimensional model profiles for Simulation A. Simulation initial condition is indicated by the solid line, and simulation end profile is shown in dashed line, while daily time steps are shown by the thin lines between initial and final conditions. Porewater field data points represent the mean of the sample depth, with the upper data point at 5 cm to represent a 0-10 cm sample interval, and the lower points at 15 cm to represent a 10-20 cm sample interval. Initial porewater field data are samples were collected on June 11, 2015 (closed circles), and data used for calibration targets were collected on July 9, 2015 (open circles). Groundwater and surface water initial (closed square) and final (open square) are also shown. $Fe(OH)_3$ is shown as difference in concentration from initial conditions (simulation lines = result concentration-initial concentration).

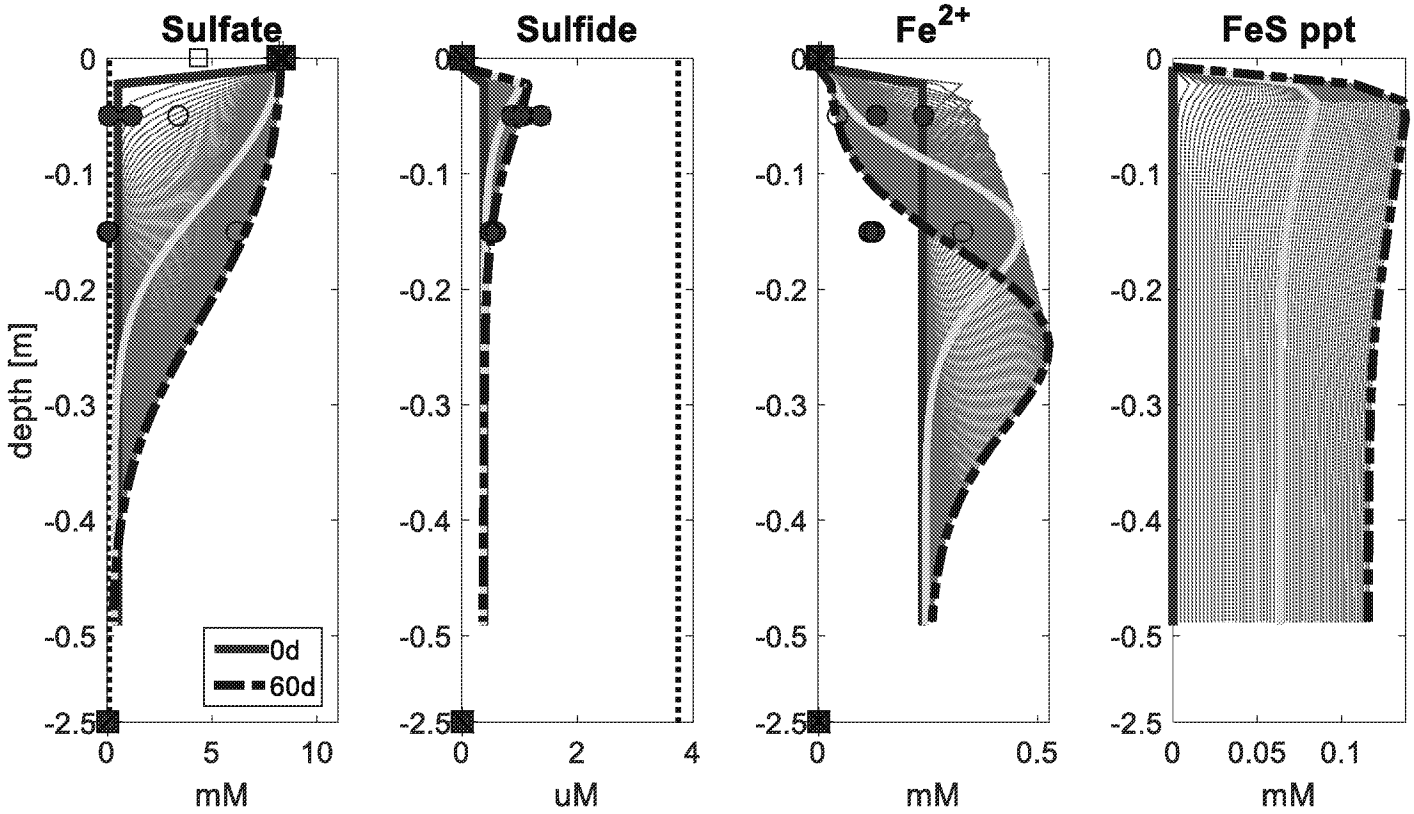
Sulfate
Sulfide
Fe2+
FeS ppt
depth [m]
0
-0.1
-0.2
-0.3
-0.4
-0.5
-2.5
0d
60d
0
5
10
mM
0
2
4
uM
0
0.5
mM
0
0.05
0.1
mM

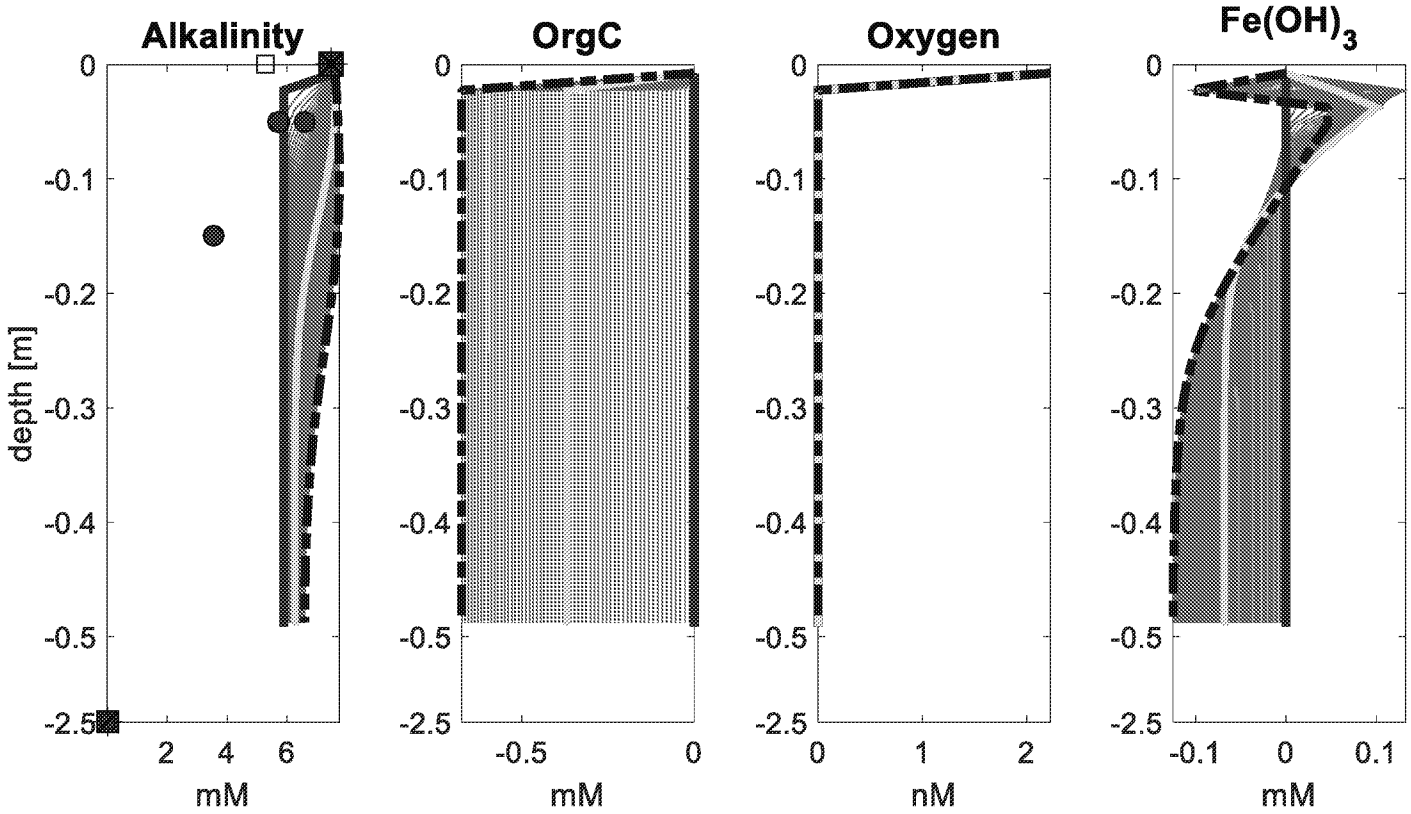
Alkalinity
OrgC
Oxygen
Fe(OH)3
depth [m]
0
-0.1
-0.2
-0.3
-0.4
-0.5
-2.5
2
4
6
-0.5
0
1
2
-0.1
0.1
mM
nM

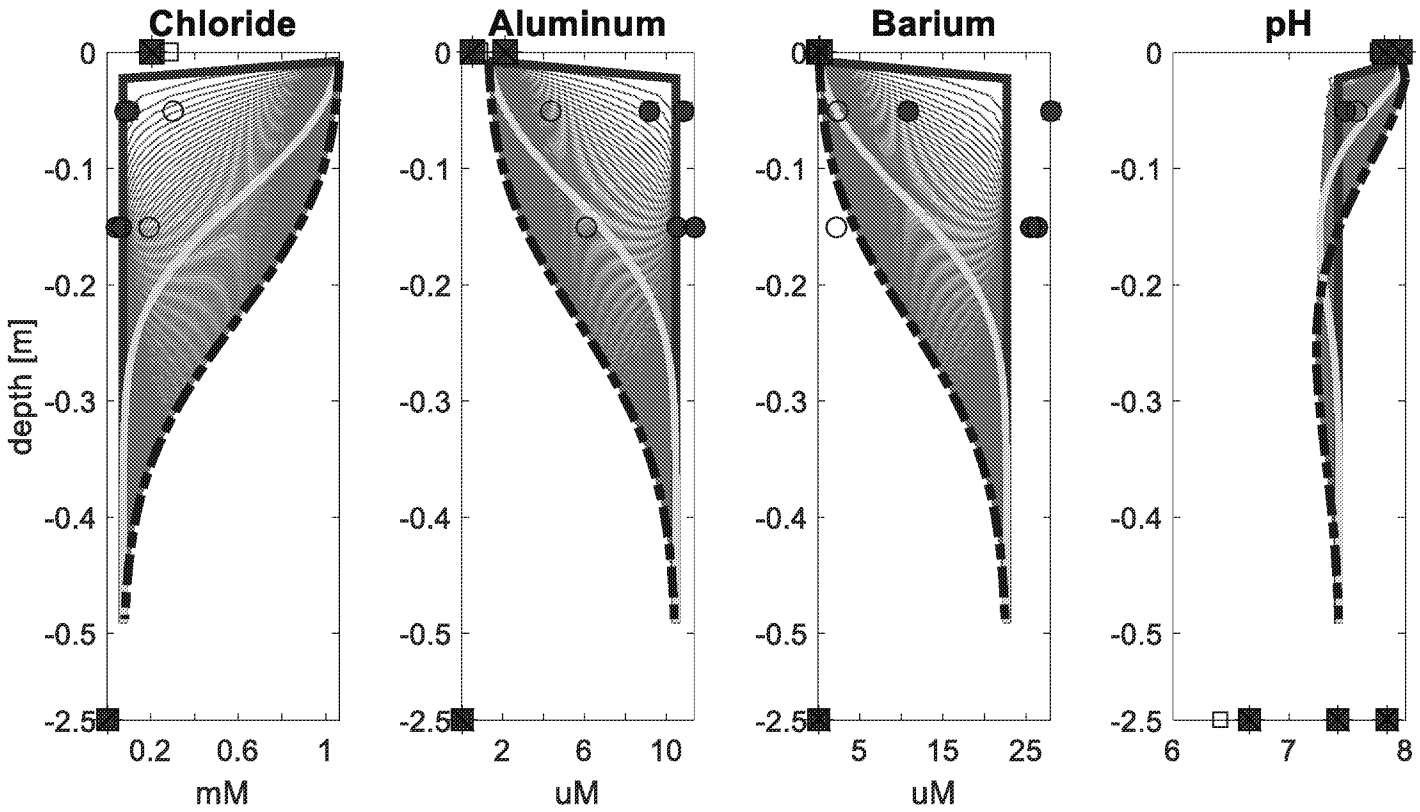
Chloride
Aluminum
Barium
pH
depth [m]
0
-0.1
-0.2
-0.3
-0.4
-0.5
-2.5
0.2
0.6
1
mM
2
6
10
uM
5
15
25
uM
6
7
8

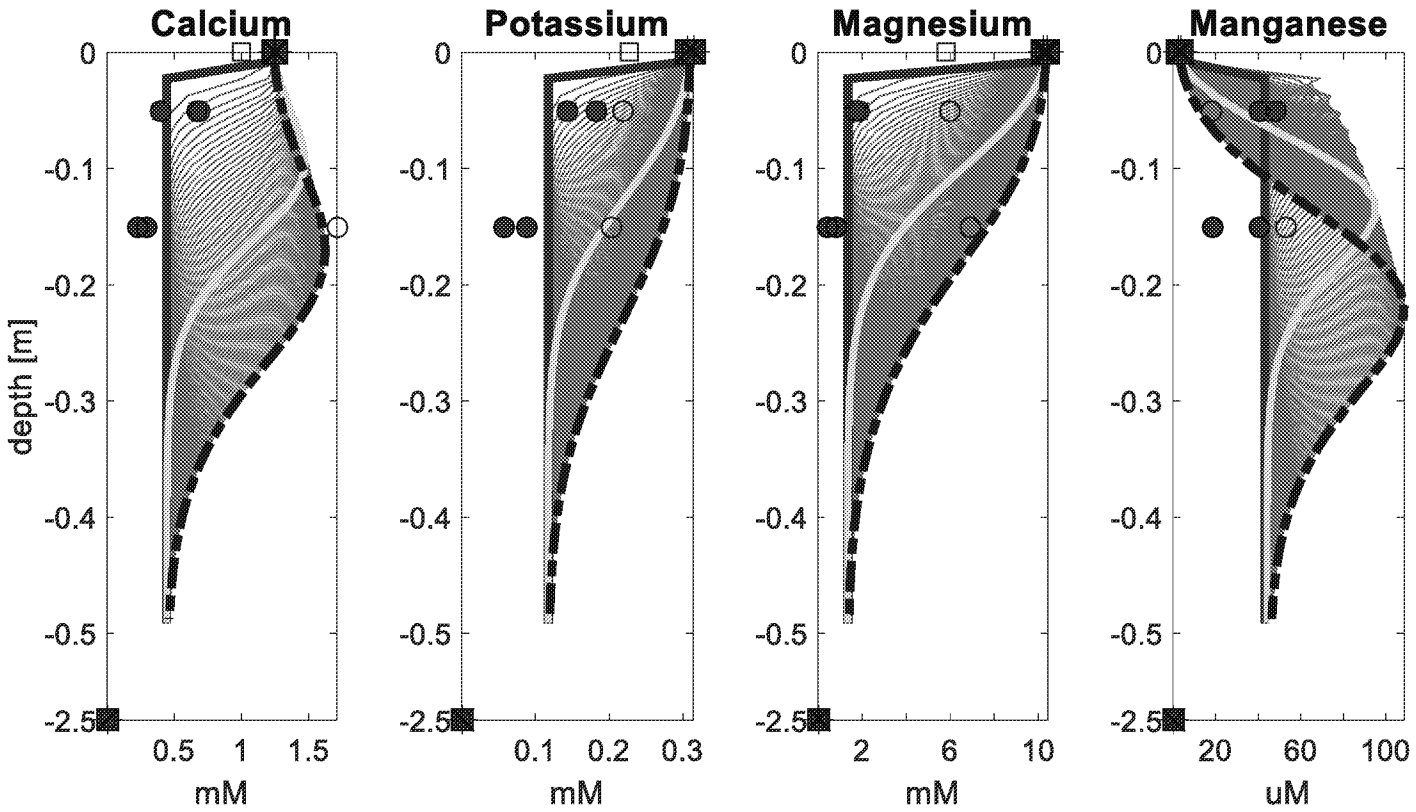
Calcium
Potassium
Magnesium
Manganese
depth [m]
0
-0.1
-0.2
-0.3
-0.4
-0.5
-2.5
0.5
1
1.5
mM
0.1
0.2
0.3
mM
2
6
10
mM
20
60
100
uM

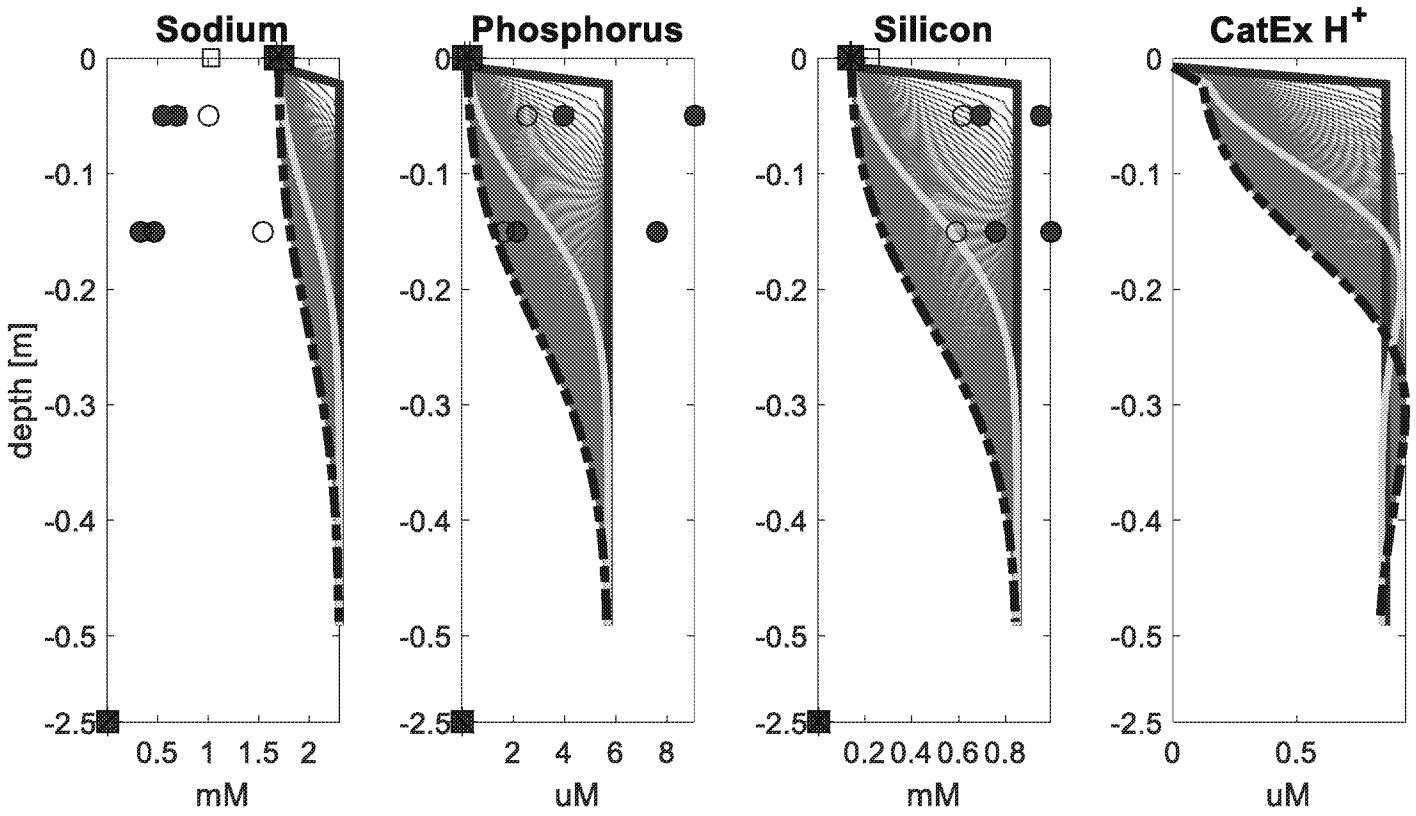
Sodium
Phosphorus
Silicon
CatEx H+
depth [m]
0
-0.1
-0.2
-0.3
-0.4
-0.5
-2.5
0.5 1 1.5 2
mM
2 4 6 8
uM
0.2 0.4 0.6 0.8
mM
0 0.5
uM

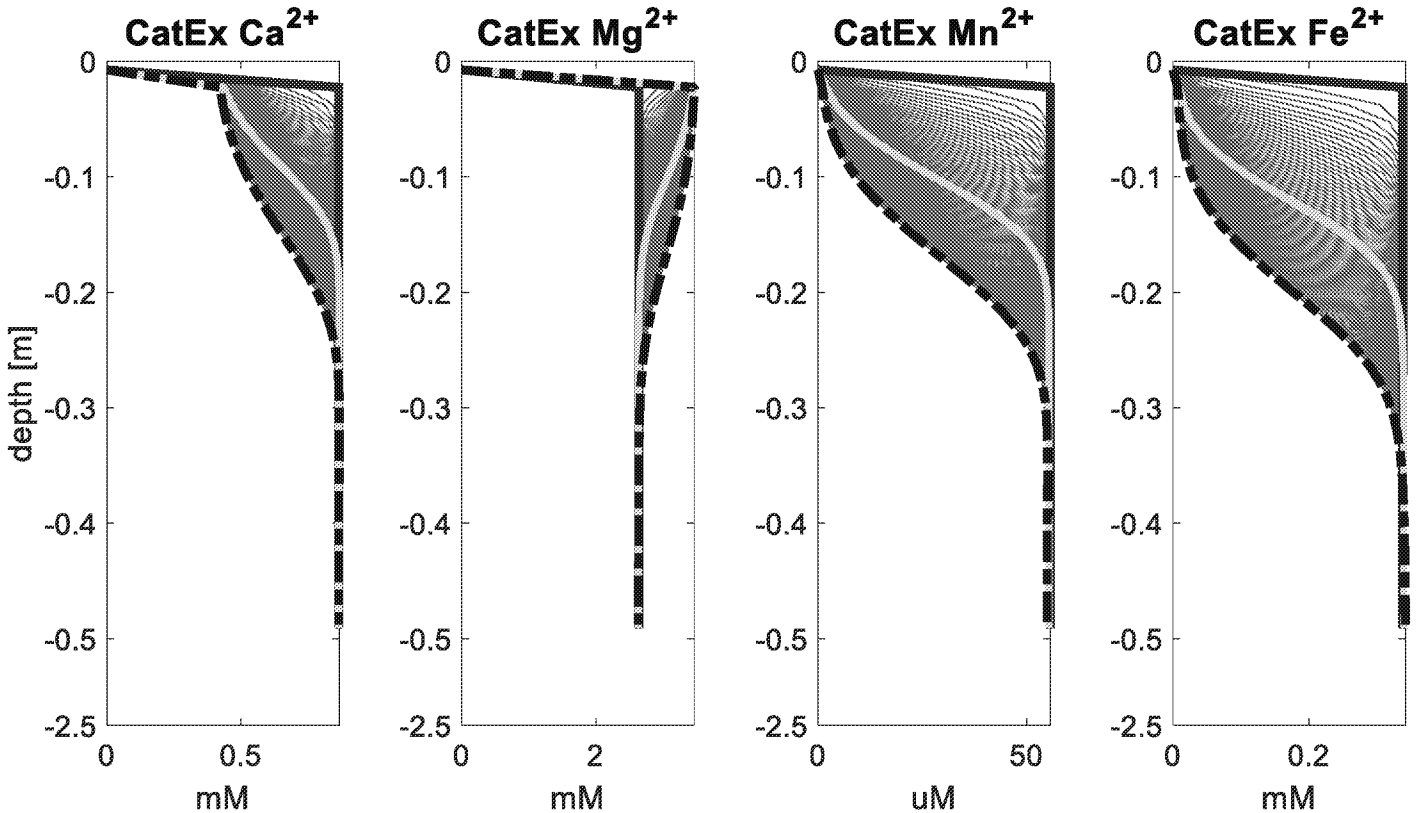

Figure 15. One dimensional model profiles for Simulation B. Initial model and field conditions (July) are shown by the solid line and final conditions (September) are shown by dashed lines. Simulation result for the halfway point of 30 days is shown by the bolded line within the thin daily time step lines. Porewater field data points represent the mean of the sample depth, with the upper data point at 5 cm to represent a 0-10 cm sample interval, and the lower points at 15 cm to represent a 10-20 cm sample interval. Initial surface water, porewater, and west groundwater field data are samples were collected on July 10, 2015 (closed circles/squares), and data used for calibration targets were collected on September 18, 2015 (open circles/squares). $Fe(OH)_3$ is shown as difference in concentration from initial conditions (simulation lines = result concentration-initial concentration).

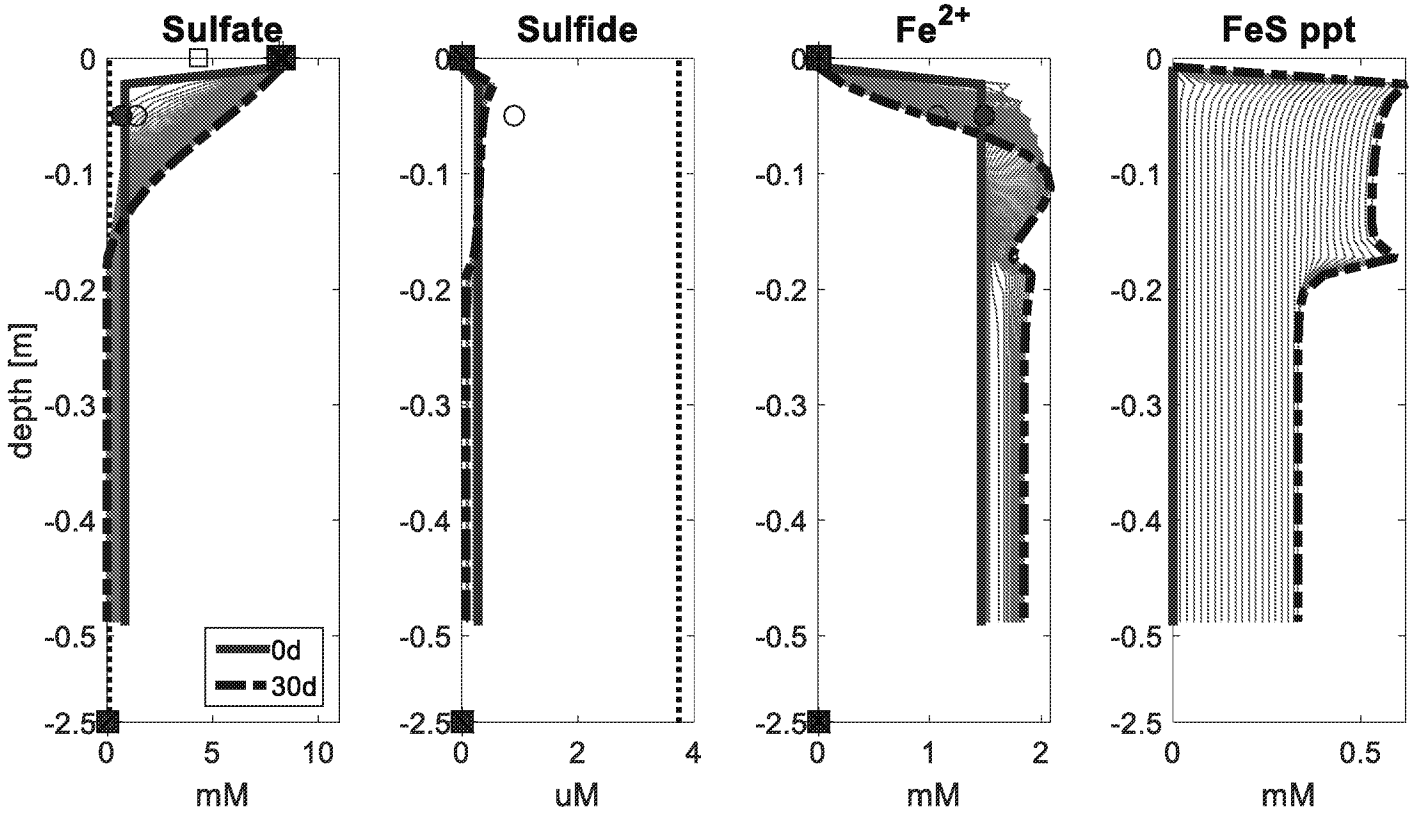
Sulfate
Sulfide
Fe2+
FeS ppt
depth [m]
0
-0.1
-0.2
-0.3
-0.4
-0.5
-2.5
0d
30d
0
5
10
mM
0
2
4
uM
0
1
2
mM
0
0.5
mM

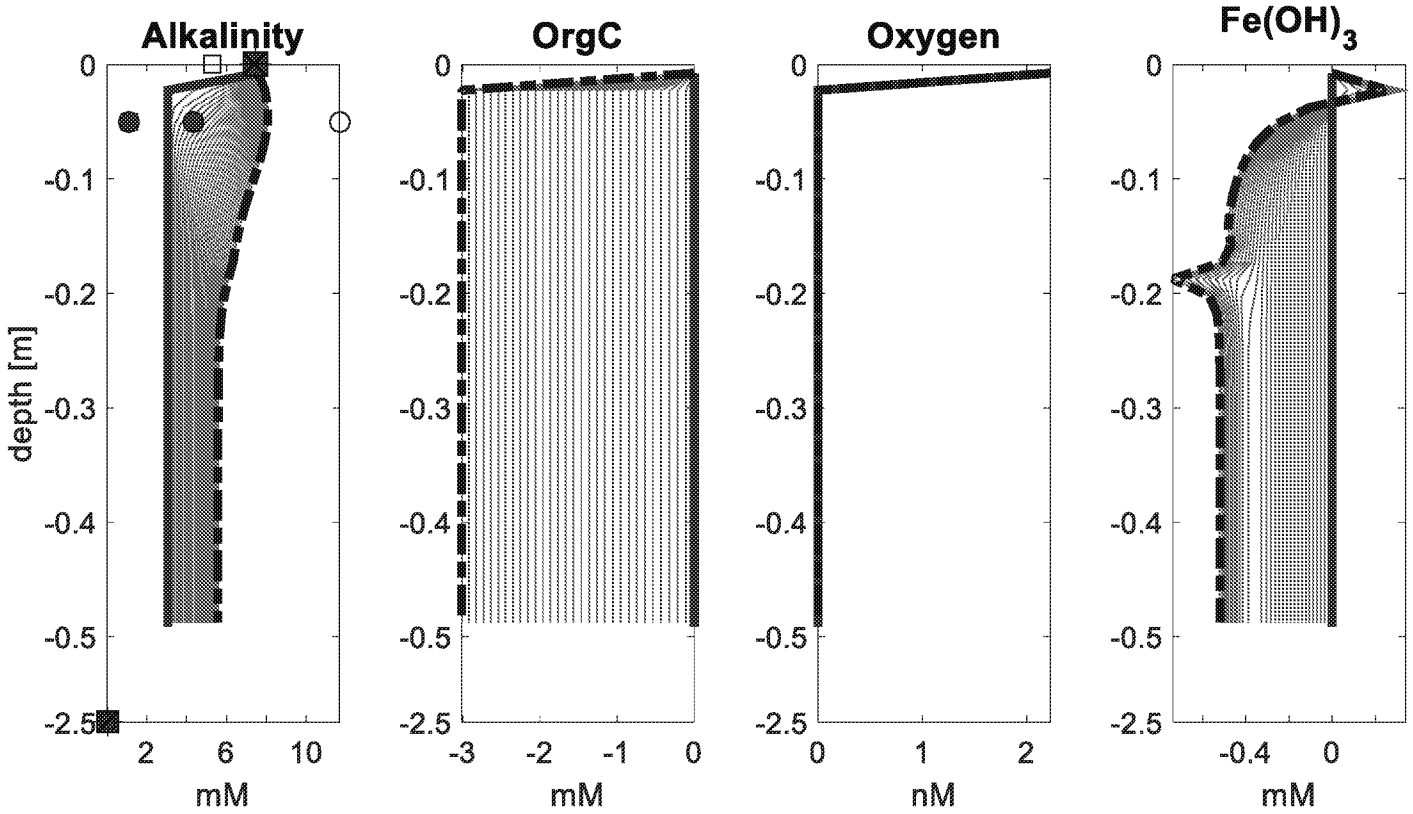
Alkalinity
OrgC
Oxygen
Fe(OH)3
depth [m]
0
-0.1
-0.2
-0.3
-0.4
-0.5
-2.5
2
6
10
-3
-2
-1
0
1
2
-0.4
mM
nM

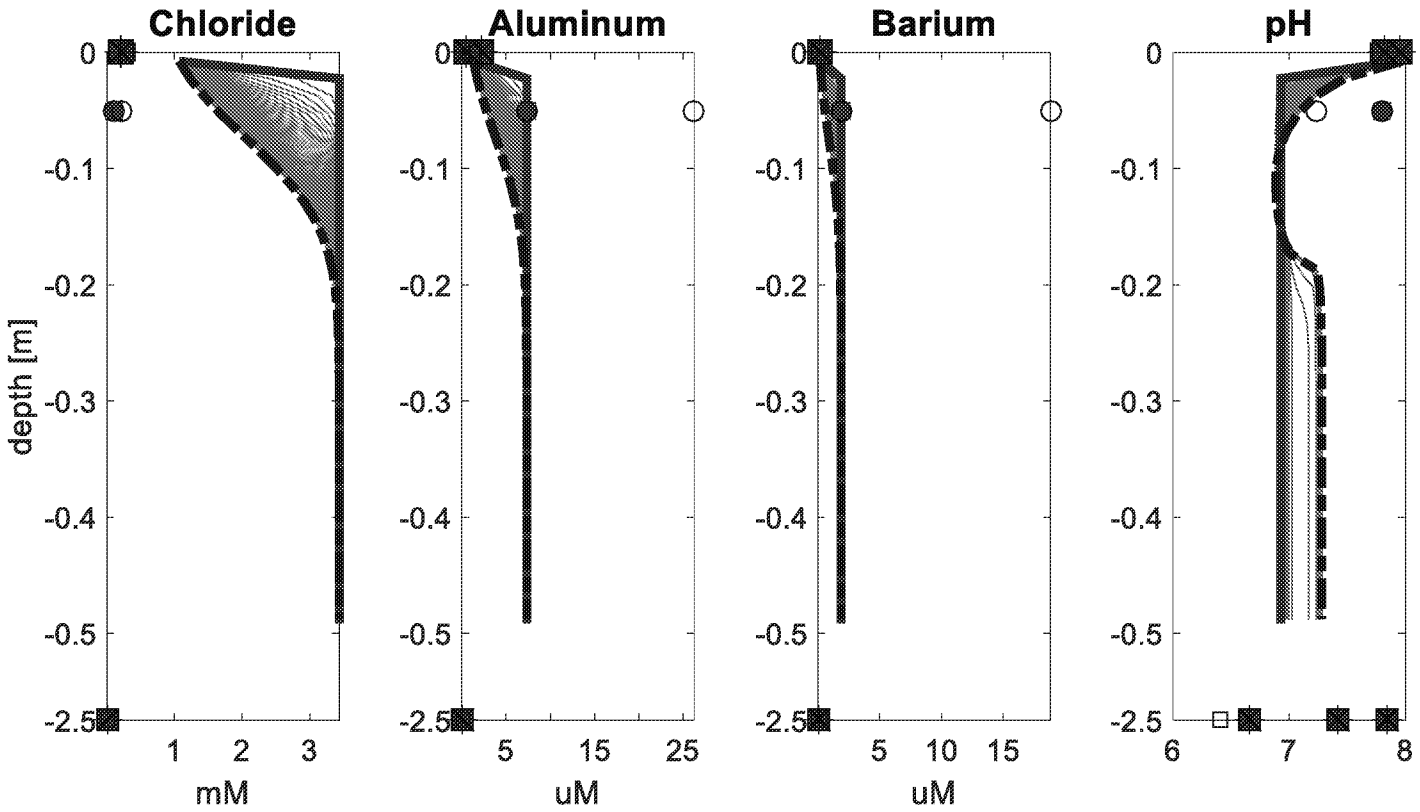
Chloride
Aluminum
Barium
pH
depth [m]
0
-0.1
-0.2
-0.3
-0.4
-0.5
-2.5
1
2
3
mM
5
15
25
uM
5
10
15
uM
6
7
8

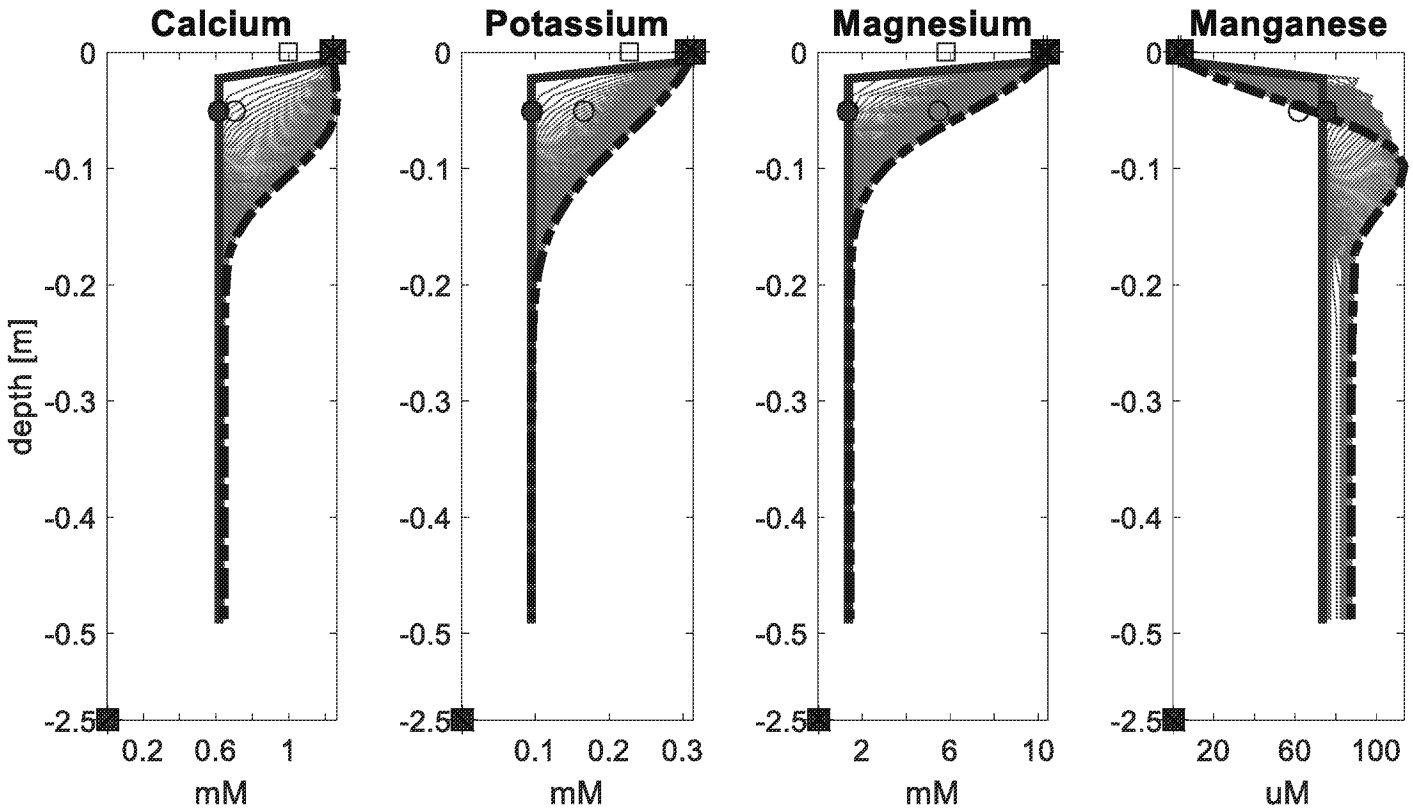
Calcium
Potassium
Magnesium
Manganese
depth [m]
0
-0.1
-0.2
-0.3
-0.4
-0.5
-2.5
0.2
0.6
1
0.1
0.2
0.3
2
6
10
20
60
100
mM
mM
mM
uM

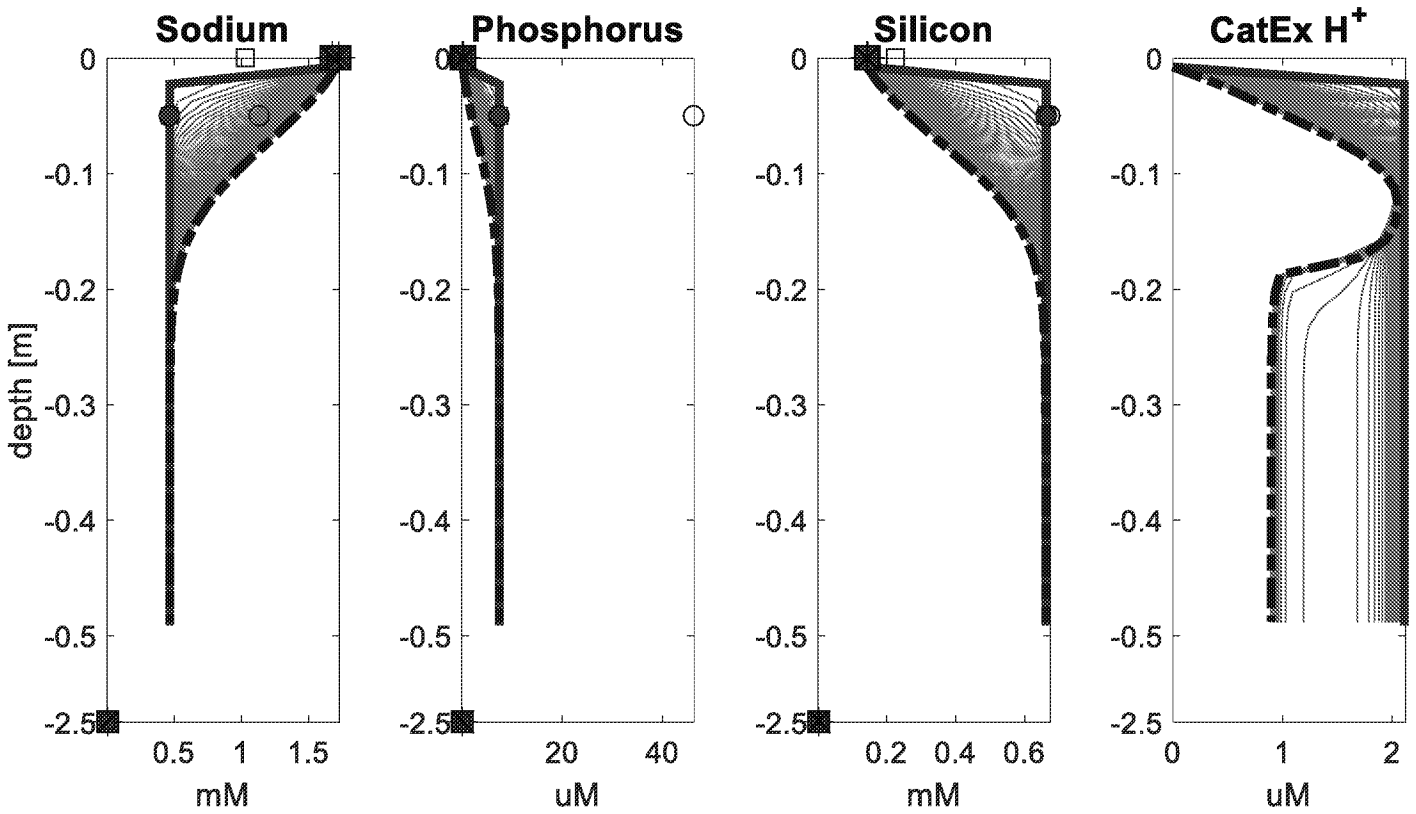
Sodium
Phosphorus
Silicon
CatEx H+
depth [m]
0
-0.1
-0.2
-0.3
-0.4
-0.5
-2.5
0.5
1
1.5
mM
20
40
uM
0.2
0.4
0.6
mM
0
1
2
uM

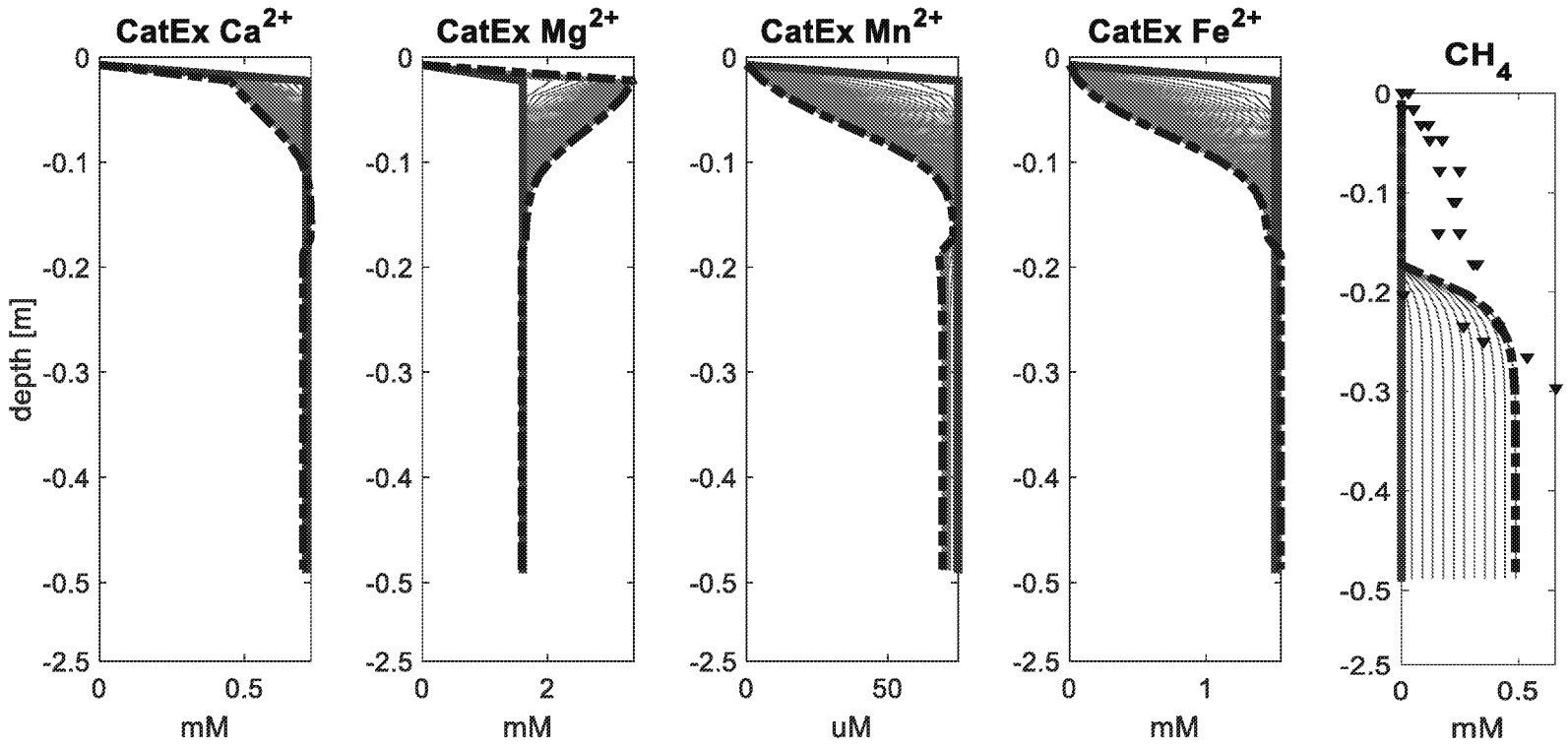

Figure 16. One dimensional model profiles for Simulation C. Simulation initial condition is indicated by the solid line, and simulation end profile is shown by the dashed line. Porewater field data points represent the mean of the sample depth, with the upper data point at 5 cm to represent a 0-10 cm sample interval, and the lower points at 15 cm to represent a 10-20 cm sample interval. Initial surface water, porewater, and west groundwater field data are samples were collected on July 10, 2015 (closed circles/squares), and data used for calibration targets were collected on August 13, 2015 (open circles/squares). Peeper data represents an equilibration time from August 13, 2015 through September 1, 2015, and are shown in black triangles.

10. References

Aiken, S.., 1986. The distinct morphology and germination of the grains of two species of wild rice (Zizania, Poaceae). *Canadian Field Naturalist*, 100, pp.237–240.

Anderson, G.C. & Woolworth, A.R., 1988. Through Dakota Eyes: Narrative Accounts of the Minnesota Indian War of 1862. *St. Paul: Minnesota Historical Society Press*.

Anderson, M.P., 1989. Hydrogeologic facies models to delineate large-scale spatial trends in glacial and glaciofluvial sediments. *Geological Society of America Bulletin*, 101(4), pp.501–511.

Armstrong, W., 1964. Oxygen Diffusion from the Roots of Some British Bog Plants. *Nature*, 204(4960), pp.801–802.

Associated Press, 2016. Mark Dayton proposes expanded wild rice rights for tribal members. *Pioneer Press*.

Bais, H.P. et al., 2004. How plants communicate using the underground information superhighway. *Trends in Plant Science*, 9(1), pp.26–32.

Bardini, L. et al., 2012. Nutrient cycling in bedform induced hyporheic zones. *Geochimica et Cosmochimica Acta*, 84, pp.47–61.

Bencala, K.E. & Walter, R.A., 1983. Simulation of solute transport in a mountain oil-and-riffle stream with a kinetic mass transfer model. *Water Resources Research*, 19(3), pp.718–724.

Berndt, M. & Bavin, T., 2009. Sulfate and mercury chemistry of the St. Louis River in Northeastern Minnesota: A Report to the Minerals Coordinating Committee. *Minnesota Department of Natural Resources, Division of Lands and Minerals*, pp.1–83.

Berner, R., 1964. Iron Sulfides Formed from Aqueous Solution at Low Temperatures and Atmospheric Pressure. *Journal of Geology*, 72(3), pp.293–306.

Berner, R.A., 1967. Thermodynamic stability of sedimentary iron sulfides. *American Journal of Science*, 265, pp.773–785.

Berthelin, J. et al., 1991. Iron Sulphide Accumulation in the Rhizosphere of Wetland Rice (Oryza sativa L.) as the Result of Microbial Activities. *Developments in Geochemistry*, 6, pp.453–468.

Bruijn, F.J. De, 2013. Molecular Microbial Ecology of the Rhizosphere: Volume 1 & 2. In John Wiley and Sons, pp. 1–3.

Van Cappellen, P. & Gaillard, J.-F., 1996. Biogeochemical dynamics in aquatic sediments. *Reviews in Mineralogy and Geochemistry*, 34(1).

Champ, D.R., Gulens, J. & Jackson, R.E., 1979. Oxidation–reduction sequences in ground water flow systems. *Canadian Journal of Earth Sciences*, 16(1), pp.12–23.

Chen, W.-F. & Liu, T.-K., 2005. Ion activity products of iron sulfides in groundwaters: Implications from the Choshui fan-delta, Western Taiwan. *Geochimica et Cosmochimica Acta*, 69(14), pp.3535–3544.

Claypool, G.E. & Kaplan, I.R., 1974. The Origin and Distribution of Methane in Marine Sediments. In *Natural Gases in Marine Sediments*. Boston, MA: Springer US, pp. 99–139.

Curtis, G.P., 2003. Comparison of approaches for simulating reactive solute transport

involving organic degradation reactions by multiple terminal electron acceptors. *Computers & Geosciences*, 29, pp.319–329.

D'Angelo, D.J. et al., 1993. Transient Storage in Appalachian and Cascade Mountain Streams as Related to Hydraulic Transient storage in Appalachian and Cascade mountain streams as related to hydraulic characteristics. *Source Journal of the North American Benthological Society J. N. Am. Benthol. Soc*, 12(123).

Dale, A.W. et al., 2008. Anaerobic oxidation of methane (AOM) in marine sediments from the Skagerrak (Denmark): II . Reaction-transport modeling. , 72, pp.2880–2894.

Davison, W., 1991. The solubility of iron sulphides in synthetic and natural waters at ambient temperature. *Aquatic Sciences*, 53(4), pp.309–329.

DeGonzague, B. et al., 1999. Dietary intake and body mass index of adults in 2 Ojibwe communities. *Journal of the American Dietetic Association*, 99(6), pp.710–716.

Detmers, J. et al., 2001. Diversity of sulfur isotope fractionations by sulfate-reducing prokaryotes. *Applied and environmental microbiology*, 67(2), pp.888–94.

Drewes, A.D. & Silbernagel, J., 2012. Uncovering the spatial dynamics of wild rice lakes, harvesters and management across Great Lakes landscapes for shared regional conservation. *Ecological Modelling*, 229, pp.97–107.

Emerson, S. & Hedges, J.I., 1988. Processes controlling the organic carbon content of open ocean sediments. *Paleoceanography*, 3(5), pp.621–634.

Froelich, P.N. et al., 1979. Early oxidation of organic matter in pelagic sediments of the eastern equatorial Atlantic: suboxic diagenesis. *Geochimica et Cosmochimica Acta*, 43(7), pp.1075–1090.

Gilbert, H., Herriman, D. & Chippewa of Lake Superior and the Mississippi, 1854. Treaty with the Chippewa.

Grayston, S.J., Vaughan, D. & Jones, D., 1997. Rhizosphere carbon flow in trees, in comparison with annual plants: the importance of root exudation and its impact on microbial activity and nutrient availability. *Applied Soil Ecology*, 5(1), pp.29–56.

Groffman, A.R. & Crossey, L.J., 1999. Transient redox regimes in a shallow alluvial aquifer. *Chemical Geology*, 161(4), pp.415–442.

Gwo, J.P. et al., 2001. HBGC123D: a high-performance computer model of coupled hydrogeological and biogeochemical processes. *Computers & Geosciences*, 27(10), pp.1231–1242.

Hammer, D., 1988. *Constructed Wetlands for Wastewater Treatment: Municipal, Industrial and Agricultural*, Lewis Publishers.

Hansel, C.M. et al., 2015. Dominance of sulfur-fueled iron oxide reduction in low-sulfate freshwater sediments. *The ISME journal*, 9(11), pp.1–13.

Harbaugh, A.W., 2005. MODFLOW-2005, The U.S. Geological Survey Modular Ground-Water Model—the Ground-Water Flow Process. In *Modeling techniques*. U.S. Geological Survey.

Harvey, J.W. & Bencala, K.E., 1993. The Effect of streambed topography on surface-subsurface water exchange in mountain catchments. *Water Resources Research*, 29(1), pp.89–98.

Harvey, J.W. & Wagner, B.J., 2000. Quantifying hydrologic interactions between streams

and their subsurface hyporheic zones. In *Streams and Groundwaters*. San Diego, CA: Academic Press, pp. 3–44.

Hayashi, M. & Rosenberry, D.O., 2002. Effects of Ground Water Exchange on the Hydrology and Ecology of Surface Water. *Groundwater*, 40(3), pp.306–316.

Healy, R.W. & Ronan, A.D., 1996. Documentation of computer program VS2DH for simulation of energy transport in variably saturated porous media -- modification of the U.S. Geological Survey's computer program VS2DT. Water-Resources Invenstigations Report 96-4230. *U.S. Geological Survey*.

Helgeson, C.H., 1978. Summary and critique of the thermodynamic properties of rock-forming minerals. *American Journal of Science*, 278, pp.1–229.

Henrichs, S.M. & Doyle, A.P., 1986. Decomposition of 14C-labeled organic substances in marine sediments'. *Limnol. Oceanogr*, 31(4), pp.765–778.

Hering, J.G. & Stumm, W., 1990. Oxidative and reductive dissolution of minerals. *Reviews in Mineralogy and Geochemistry*, 23(1).

Holmer, M. et al., 1998. Sulfate reduction in lake sediments inhabited by the isoetid macrophytes Littorella uniflora and Isoetes lacustris. *Aquatic Botany*, 60(4), pp.307–324.

Holmer, M.. & Storkholm, P.., 2001. Sulphate reduction and sulphur cycling in lake\rsediments: a review. *Freshwater Biology*, 46, pp.431–451.

Hunter, K.S., Wang, Y. & Cappellen, P. Van, 1998. Kinetic modeling of microbially-driven redox chemistry of subsurface environments : coupling transport , microbial metabolism and geochemistry. *Journal of Hydrology*, 209, pp.53–80.

Jacob, D.L. & Otte, M.L., 2003. Conflicting Processes in the Wetland Plant. *Ecology*, 3, pp.91–104.

Jakobsen, R. & Postma, D., 1996. Redox zonation : Equilibrium constraints on the Fe (III)/ SO4-reduction interface. *Geochimica et Cosmochimica Acta*, 60(17), pp.3169–3175.

Jakobsen, R. & Postma, D., 1999. Redox zoning , rates of sulfate reduction and interactions with Fe-reduction and methanogenesis in a shallow sandy aquifer , Rømø , Denmark. *Geochimica et Cosmochimica Acta*, 63(1), pp.137–151.

Jenks, A.E., 1900. *The wild rice gatherers of the upper lakes; a study in American primitive economics*, U.S. Government Printing Office.

Jin, Q. & Bethke, C.M., 2002. Kinetics of Electron Transfer through the Respiratory Chain. *Biophysical Journal*, 83(4), pp.1797–1808.

Jin, Q. & Bethke, C.M., 2005. Predicting the rate of microbial respiration in geochemical environments. *Geochimica et Cosmochimica Acta*, 69(5), pp.1133–1143.

Johnson, N.W., 2013. Response of rooting zone geochemistry to experimental manipulation of sulfate levels in Wild Rice mesocosms. *University of Minnesota Duluth*.

Kjerland, T., 2015. Wild Rice Monitoring Handbook. *The University of Minnesota Sea Grant Program. Publication #SH16*.

Koch, M.S., Mendelssohn, I.A. & McKee, K.L., 1990. Mechanism for the hydrogen sulfide-induced growth limitation in wetland macrophytes. *Limnology and Oceanography*, 35(2), pp.399–408.

Kosolapov, D.B. et al., 2004. Microbial processes of heavy metal removal from carbon-deficient effluents in constructed wetlands. *Engineering in Life Sciences*, 4(5), pp.403–411.

Kresic, N., 2007. *Hydrogeology and Groundwater Modeling, Second Edition - Neven Kresic - Google Books*, Taylor & Francis Group, LLC.

Kurtz, A.M. et al., 2007. The importance of subsurface geology for water source and vegetation communities in Cherokee Marsh, Wisconsin. *Wetlands*, 27(1), pp.189–202.

LaDuke, W., 2003. *Our Manoomin, Our Life*, Ponsford. White Earth Land Recovery Project.

LaDuke, W., 2005. *Recovering the Sacred*, Cambridge: South End Press.

Lamers, L.P.M. et al., 2002. Factors controlling the extent of eutrophication and toxicity in sulfate-polluted freshwater wetlands. *Limnology and Oceanography*, 47(2), pp.585–593.

Larowe, D.E. & Van Cappellen, P., 2011. Degradation of natural organic matter : A thermodynamic analysis. *Geochimica et Cosmochimica Acta*, 75(8), pp.2030–2042.

Lautz, L.K. & Siegel, D.I., 2006. Modeling surface and ground water mixing in the hyporheic zone using MODFLOW and MT3D. *Advances in Water Resources*, 29(11), pp.1618–1633.

Laverman, A.M. et al., 2012. Comparative survey of potential nitrate and sulfate reduction rates in aquatic sediments. *Geochimica et Cosmochimica Acta*, 77, pp.474–488.

Li, L. et al., 2010. Effects of physical and geochemical heterogeneities on mineral transformation and biomass accumulation during biostimulation experiments at Rifle , Colorado. *Journal of Contaminant Hydrology*, 112, pp.45–63.

Ludvigsen, L. et al., 1998. Anaerobic microbial redox processes in a landfill leachate contaminated aquifer (Grindsted, Denmark). *Journal of Contaminant Hydrology*, 33(3–4), pp.273–291.

Manger, G.E., 1963. Porosity and Bulk Density of Sedimentary Rocks : Contributions to Geochemistry, *U.S. Geological Survey*.

Mayer, K.. et al., 2001. Reactive transport modeling of processes controlling the distribution and natural attenuation of phenolic compounds in a deep sandstone aquifer. *Journal of Contaminant Hydrology*, 53(3), pp.341–368.

McGuire, J.T. et al., 2002. Evaluating behavior of oxygen, nitrate, and sulfate during recharge and quantifying reduction rates in a contaminated aquifer. *Environmental Science and Technology*, 36(12), pp.2693–2700.

Meeker, J.E., 1996. Wild-rice and sedimentation processes in a Lake Superior coastal wetland. *Wetlands*, 16(2), pp.219–231.

Morrice, J.A. et al., 1997. Alluvial characteristics, groundwater-surface water exchange and hydrological retention in headwater streams. *Hydrological Processes*, 11(3), pp.253–267.

Morse, J.W. et al., 1987. The chemistry of the hydrogen sulfide and iron sulfide systems in natural waters. *Earth-Science Reviews*, 24(1), pp.1–42.

Moyle, J.B., 1944. Wild rice in Minnesota. *The Journal of Wildlife Management*, 8(3),

pp.177–184.
MPCA, 2016. Draft Technical Support Document : Refinements to Minnesota's Sulfate Water Quality Standard to Protect Wild Rice. *Minnesota Pollution Control Agency. wq-s6-43v*, pp.1–97.
MPCA, 2015. Proposed approach for Minnesota's sulfate standard to protect wild rice. *Minnesota Pollution Control Agency, Report for the Minnesota Legislature*, pp.1–23.
Myrbo, A. et al. (a), Increase in nutrients, mercury, and methylmercury as a consequence of elevated sulfate reduction to sulfide in experimental wetland mesocosms. *In review*.
Myrbo, A. et al. (b), Sulfide generated by sulfate reduction is a primary controller of the occurrence of wild rice (Zizania palustris) in shallow aquatic ecosystems. *In review*.
Myrbo, A., 2013. Wild Rice Sulfate Standard Field Surveys 2011, 2012, 2013: Final Report. *University of Minnesota*.
Neori, A. et al., 2000. Bioactive chemicals and biological—biochemical activities and their functions in rhizospheres of wetland plants. *The Botanical Review*, 66(3), pp.350–378.
Ng, G.-H.C. et al., 2015. Reactive transport modeling of geochemical controls onsecondary water quality impacts at a crude oil spill site near Bemidji, MN. *Water Resources Research*, 51, pp.4156–4183.
Okabe, S., Nielsen, P.H. & Characklis, W.G., 1992. Factors Affecting Microbial Sulfate Reduct ion by Desulfovibrio desulfuricans in Continuous Culture: Limiting Nutrients and Sulfide Concentration. , 40, pp.725–734.
Pallud, C. & Van Cappellen, P., 2006. Kinetics of microbial sulfate reduction in estuarine sediments. *Geochimica et Cosmochimica Acta*, 70(5), pp.1148–1162.
Parkhurst, D.L. & Appelo, C.A.J., 1999. User's guide to PHREEQC (Version 2) - A computer program for speciation, batch-reaction, one-dimensional transport, and inverse geochemical calculations. Water-Resources Investigations Report 99-4259. *U.S. Department of the Interior, U.S. Geological Survey*.
Pastor, J. et al., 2017. Effects of sulfate and sulfide on the life cycle of Zizania palustris in hydroponic and mesocosm experiments. *Ecological Applications*, 27(1), pp.321–336.
Pollman, C. et al., 2017. The evolution of sulfide in shallow aquatic ecosystem sediments – an analysis of the roles of sulfate, organic carbon, iron and feedback constraints using structural equation modeling. *In review*.
Prommer, H., Barry, D.A. & Zheng, C., 2003. MODFLOW/MT3DMS-Based Reactive Multicomponent Transport Modeling. *Ground Water*, 41(2), pp.247–257.
Rickard, D. & Luther, G.W., 2007. Chemistry of Iron Sulfides. *Chemical Reviews 2*, 107, pp.514–562.
Roden, E.E., 2006. Geochemical and microbiological controls on dissimilatory iron reduction. *Comptes Rendus - Geoscience*, 338(6–7), pp.456–467.
Roden, E.E., 2012. Microbial iron-redox cycling in subsurface environments. *Biochemical Society transactions*, 40(6), pp.1249–56.
Rogosin, A., 1954. An Ecological History of Wild Rice. *MN Department of*

Conservation.
Rosenberry, D.O. & Labaugh, J.W., 2008. Field Techniques for Estimating Water Fluxes Between Surface Water and Ground Water Techniques and Methods 4 – D2. *U.S. Geological Survey*.
Runkel, R.L. & Kimball, B.A., 2002. Evaluating Remedial Alternatives for an Acid Mine Drainage Stream: Application of a Reactive Transport Model. *U.S. Geological Survey*.
Schäfer, D., Schäfer, W. & Kinzelbach, W., 1998. Simulation of reactive processes related to biodegradation in aquifers: 1. Structure of the three-dimensional reactive transport model. *Journal of Contaminant Hydrology*, 31(1), pp.167–186.
Schumacher, B.A., 2002. Methods for the Determination of Total Organic Carbon (TOC) In Soils and Sediments. *United States Environmental Protection Agency*.
Shotbolt, L., 2010. Pore water sampling from lake and estuary sediments using Rhizon samplers. *Journal of Paleolimnology*, 44(2), pp.695–700.
Smith, R.L. et al., 2013. Long-term groundwater contamination after source removal—The role of sorbed carbon and nitrogen on the rate of reoxygenation of a treated-wastewater plume on Cape Cod, MA, USA. *Chemical Geology*, 337, pp.38–47.
Sobolev, D. & Roden, E.E., 2002. Evidence for rapid microscale bacterial redox cycling of iron in circumneutral environments. *Antonie van Leeuwenhoek*, 81(1/4), pp.587–597.
Steenbergen, C., Sweerts, J. & Cappenberg, T., 1993. Microbial biogeochemical activities in lakes: stratification and eutrophication. In *Aquatic Microbiology: An Ecological Approach*. pp. 66–99.
Stonestrom, D. & Constantz, J., 2003. *Heat as a tool for studying the movement of ground water near streams - Geological Survey (U.S.) - Google Books*, U.S. Geological Survey, circular 1260.
Storey, R.G., Howard, K.W.F. & Williams, D.D., 2003. Factors controlling riffle-scale hyporheic exchange flows and their seasonal changes in a gaining stream: A three-dimensional groundwater flow model. *Water Resources Research*, 39(2).
Stream Solute Workshop, 1990. Concepts and Methods for Assessing Solute Dynamics in Stream Ecosystems. *Journal of the North American Benthological Society J. N. Am. Benthol. Soc*, 9(92).
Stumm, W. & Morgan, J., 1996. *Aquatic Chemistry: Chemical equilibria and rates in natural waters.*, New York, NY: Wiley and Sons.
Tarpgaard, I.H., Røy, H. & Jørgensen, B.B., 2011. Concurrent low- and high-affinity sulfate reduction kinetics in marine sediment. *Geochimica et Cosmochimica Acta*, 75(11), pp.2997–3010.
Teasdale, P.R., Batley, G.E. & Apte, S.C., 1995. Pore water sampling with sediment peepers. *Trends in Analytical Chemistry*, 14(6), pp.250–256.
U.S. EPA, 2001. *Methods for Collection, Storage and Manipulation of Sediments for Chemical and Toxicological Analyses: Technical Manual*, Washington, DC.
Vennum, T., 1988. *Wild Rice and the Ojibway People*, Minnesota Historical Society Press.
Walker, R. & Doerfler, J., 2007. Wild rice: the Minnesota Legislature, a distinctive crop,

GMOs, and Ojibwe perspectives. *University of Minnesota*.

Weber, K. a, Achenbach, L. a & Coates, J.D., 2006. Microorganisms pumping iron: anaerobic microbial iron oxidation and reduction. *Nature reviews. Microbiology*, 4(10), pp.752–764.

Weiss, J. V., Emerson, D. & Megonigal, J.P., 2004. Geochemical control of microbial Fe(III) reduction potential in wetlands: Comparison of the rhizosphere to non-rhizosphere soil. *FEMS Microbiology Ecology*, 48, pp.89–100.

Winter, T.C. et al., 1998. Ground Water. *U.S. Geological Survey Circular 1139*.

Wroblicky, G.J. et al., 1998. Seasonal variation in surface - subsurface water exchange and lateral hyporheic area of two stream - aquifer systems. *Water Resources Research*, 34(3), pp.317–328.

Yang, J.-X., Liu, Y. & Ye, Z.-H., 2012. Root-Induced Changes of pH, Eh, Fe(II) and Fractions of Pb and Zn in Rhizosphere Soils of Four Wetland Plants with Different Radial Oxygen Losses. *Pedosphere*, 22(4), pp.518–527.

Zarnetske, J.P. et al., 2012. Coupled transport and reaction kinetics control the nitrate source-sink function of hyporheic zones. *Water Resources Research*, 48(11).

Zheng, C. & Wang, P.P., 1999. MT3DMS: A Modular Three-Dimensional Multispecies Transport Model for Simulation of Advection, Dispersion, and Chemical Reactions of Contaminants in Groundwater Systems: Documentation and User's Guide, Contract Rep. SERDP-99-1. *U.S. Army Energy Resources and Development Center, Vicksburg, Miss*.